UNIVERSITA' DEGLI STUDI DI PADOVA

Sede Amministrativa: Università degli Studi di Padova
Dipartimento di Innovazione Meccanica e Gestionale

SCUOLA DI DOTTORATO DI RICERCA IN INGEGNERIA INDUSTRIALE
INDIRIZZO: INGEGNERIA DELLA PRODUZIONE INDUSTRIALE
CICLO XX

INVESTIGATION OF THERMAL, MECHANICAL AND MICROSTRUCTURAL PROPERTIES OF QUENCHENABLE HIGH STRENGTH STEELS IN HOT STAMPING OPERATIONS

Direttore della Scuola : Ch.mo Prof. Paolo F. Bariani
Supervisore : Ch.mo Prof. Paolo F. Bariani
Correlatore : Prof. Stefania Bruschi

Dottorando : Alberto Turetta

DATA CONSEGNA TESI
31 gennaio 2008

TABLE OF CONTENTS

PREFACE

First of all, I would like to thank Prof. Paolo F. Bariani that gave me the possibility to perform my PhD at DIMEG, and Stefania and Andrea for their valuable advices, suggestions and teachings.
I also acknowledge Mrs Merklein for having organized my stay at the LFT, University of Erlangen-Nuremberg, and Jurgen for his wholehearted hospitality and friendship that transformed this period into a really nice experience.

I express my grateful thanks to all my colleagues, for the friendly and bright atmosphere that was always present at DIMEG, and to the students that worked with me.

A big thank you to my wonderful family and, last but not least, to my Ultra High Strength Girlfriend Elena for her loving support.

ABSTRACT

Sheet metal working operations at elevated temperature have gained in the last years even more importance due to the possibility of producing parts characterized by high strength-to-mass ratio. In particular, the hot stamping of ultra high strength quenchenable steels is nowadays widely used in the automotive industry to produce body-in-white structural components with enhanced crash resistance and geometrical accuracy. The optimization of the process, where deformation takes place simultaneously with cooling, and of the final component performances requires the utilization of FE-based codes where the forming and quenching phases have to be represented by fully thermo-mechanical-metallurgical models. The accurate calibration of such models, in terms of material behaviour, tribology, heat transfer, phase transformation kinetics and formability, is therefore a strong requirement to gain reliable results from the numerical simulations and offer noticeable time and cost savings to product and process engineers.

The main target of this PhD thesis is the development of an innovative approach based on the design of integrated experimental procedures and modelling tools in order to accurately investigate and describe both the mechanical and microstructural material properties and the interface phenomena due to the thermal and mechanical events that occur during the industrial press hardening process.

To this aim, a new testing apparatus was developed to evaluate the influence of temperature and strain rate on the sheet metal elasto-plastic properties and to study the influence of applied stress and strain of the material phase transformation kinetics. Furthermore, an innovative experimental setup, based on the Nakazima concept, was designed and developed to evaluate sheet formability at elevated temperature by controlling the thermo-mechanical parameters of the test and reproducing the conditions that govern the microstructural evolution during press hardening. This equipment was utilized both to determine isothermal forming limit curves at high temperature and to perform a physical simulation of hot forming operations. Finally, a thermo-mechanical-metallurgical model was implemented in a commercial FE-code and accurately calibrated to perform fully coupled numerical simulations of the reference process.

The material investigated in this work is the Al-Si pre-coated quenchenable steel 22MnB5, well known with the commercial name of USIBOR 1500P®, and the developed approach proves to be suitable to proper evaluate high strength steels behaviour in terms of mechanical, thermal and microstructural properties, and to precisely calibrate coupled numerical models when they are applied to this innovative manufacturing technology.

The work presented in this thesis has been carried out at DIMEG labs, University of Padova, Italy, from January 2005 to December 2007 under the supervision of Prof. Paolo F. Bariani.

SOMMARIO

Negli ultimi anni le lavorazioni di lamiera ad elevate temperature hanno acquisito sempre più importanza grazie alla possibilità di produrre componenti caratterizzati da un elevato rapporto resistenza-peso. In particolare lo stampaggio a caldo di acciai alto resistenziali da tempra è oggigiorno ampiamente utilizzato nell'industria automobilistica per realizzare parti strutturali con più elevate resistenza agli urti e accuratezza geometrica. L'ottimizzazione delle prestazioni del processo, in cui le fasi di deformazione e tempra avvengono in contemporanea, e del prodotto finale richiede l'utilizzo di codici agli elementi finiti in cui le fasi di formatura e raffreddamento siano implementate in modelli termici, meccanici e metallurgici accoppiati. L'accurata calibrazione di tali modelli, in termini di comportamento reologico, tribologia, scambio termico, cinetica di trasformazione di fase e formabilità, rappresenta un requisito fondamentale per ottenere risultati affidabili dalle simulazioni numeriche e consentire agli ingegneri di processo e di prodotto di ottenere un sensibile risparmio di costi e tempi.

L'obiettivo principale di questa tesi di dottorato è lo sviluppo di un approccio innovativo basato sulla definizione di prove sperimentali e di modelli per l'analisi e la descrizione del comportamento meccanico e microstrutturale del materiale e dei fenomeni all'interfaccia che si presentano nelle condizioni meccaniche e termiche tipiche delle operazioni industriali di stampaggio a caldo.

Con questo obiettivo finale, è stata sviluppata una nuova attrezzatura di prova per valutare l'influenza di temperatura e velocità di deformazione sulle proprietà elasto-plastiche di lamiere metalliche e per studiare l'influenza di carichi e deformazioni applicati sulla cinetica di trasformazione di fase del materiale. Inoltre è stata progettata e messa a punto una nuova apparecchiatura sperimentale per valutare la formabilità di lamiere ad elevate temperature assicurando un controllo accurato dei parametri di prova termici e meccanici e riproducendo le condizioni che governano le trasformazioni microstrutturali durante le lavorazioni a caldo. Questa attrezzatura è stata utilizzata per determinare curve limite di formabilità isoterme ad elevata temperatura e, al tempo stesso, per effettuare una

simulazione fisica delle operazioni di formatura a caldo. Un modello accoppiato dal punto di vista termico, meccanico e metallurgico è stato accuratamente calibrato e implementato in un codice FE commerciale per effettuare simulazione del processo di riferimento.
Il materiale indagato in questo lavoro è l'acciaio da tempra 22MnB5, commercialmente noto col nome di USIBOR 1500 P®, e l'approccio sviluppato dimostra di essere adatto a studiare il comportamento di acciai alto resistenziali ad elevate temperature in termini di proprietà meccaniche, termiche e microstrutturali per poter calibrare modelli numerici accoppiati utilizzati nell'ottimizzazione di questa innovativa tecnologia di produzione.

Il lavoro presentato in questa tesi è stato svolto presso i laboratori del DIMEG, Università degli Studi di Padova, da Gennaio 2005 a Dicembre 2007, sotto la supervisione del Prof. Paolo F. Bariani.

CHAPTER 1
INTRODUCTION

In the last years the main targets of the automotive industries are represented by the reduction of fuel consumption and environmental impact, the increase of crash performance and safety and the increase of accuracy and quality of final components. These requirements force car manufacturers to a continuous search of new solutions, in direction of new products features and novel manufacturing processes. Different types of materials, both metallic and non-metallic, are used. Regarding metallic materials, aluminium alloys and different steels grades are the most common in body components and reinforcements beams and the introduction of ultra high strength quenchenable steels represents an innovative solution to increase the strength-to-mass ratio of sheet components. However, as the forming of such steels at room temperature is almost impossible, the utilization of sheet working operations at elevated temperature is increasing more and more. In the hot stamping or press hardening process the steel blank is heated up above austenitization, then transferred into the press where deformation takes place simultaneously with quenching in order to achieve a fully martensitic microstructure in the formed component at room temperature. Compared with traditional sheet metal forming operation, the proper design of hot stamping process chains requires a deep knowledge of both interface phenomena and material behaviour at high temperature. In particular, the choice of the most suitable process parameters of the forming and the cooling phases requires the utilization of FE-based codes where the process has to be represented by a fully thermo-mechanical-metallurgical model. Such a model has to be accurately calibrated and validated, by means of experimental techniques and numerical inverse analysis approaches, in order to obtain reliable results from the numerical simulations and achieve the desired mechanical and microstructural properties on final product.

1.1 The industrial problem

Sheet metal working operations at elevated temperatures have gained in the last few years even more importance due to the possibility of producing components characterized by high strength-to-mass ratio. Besides the worm forming of aluminium alloys, whose main target is to increase the material formability limits, the hot stamping of ultra high strength quenchenable steels is nowadays widely utilized in the automotive industry to produce components like bumpers and pillar with enhanced crash characteristic and geometrical accuracy due to reduced springback [1].

Weight and cost reduction in body-in-white components is mainly driven by the use of advanced sheet material in combination with optimized production technologies adapted to the particular material concept [2]. Matching exact mechanical properties of the intended steel grade against the critical forming mode in the stamping not only requires an added level of knowledge by steel suppliers and steel users, but also mandates an increased level of communication between them [3]. Cold forming of high and ultra high strength steels is limited due to reduced formability, high forces on tools, enhanced springback and wear phenomena and reduction of total elongation, see Figure 1.1.

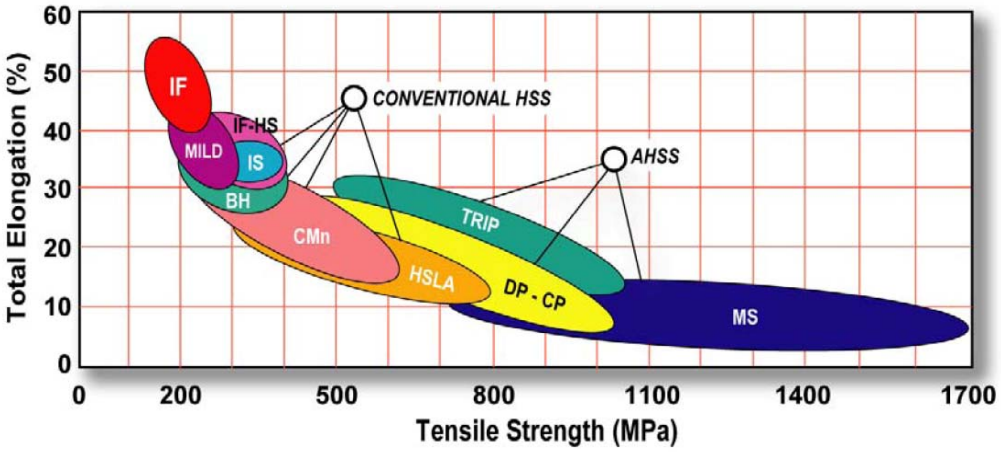

Figure 1.1 Relationship between tensile strength and total elongation for various type of steels [3].

The possibility of performing stamping operations at elevated temperatures offers the advantages of an enhanced formability together with a reduction of loads and springback phenomena. The press hardening is an innovative sheet metal forming technique showing an exceptional development and growth for different kinds of structural components; new hot-stampers appears on the market and several new lines are being built all over the world [4]. For example the total consumption of quenchenable steels for hot stamping was about 60000-80000t/year in Europe in 2003, and it will strongly increase up to 300000t/year in 2008-2009; a similar trend can be observed in North-America and Japan.
In the industrial process, the blank, which presents a ferritic\pearlitic microstructure in delivery conditions, is heated in the range between 850°C and 950°C and then it is rapidly transferred to the press where the whole deforming phase takes place in fully austenitic conditions [5]; the use of cooled dies assures a rapid cooling in order to obtain a martensitic microstructure in the component at room temperature, as shown in Figure 1.2.

Particular attention has to be paid to the factors influencing the part accuracy, the cycle time and the process stability when designing a hot stamping process to predict part feasibility and perform process layout.

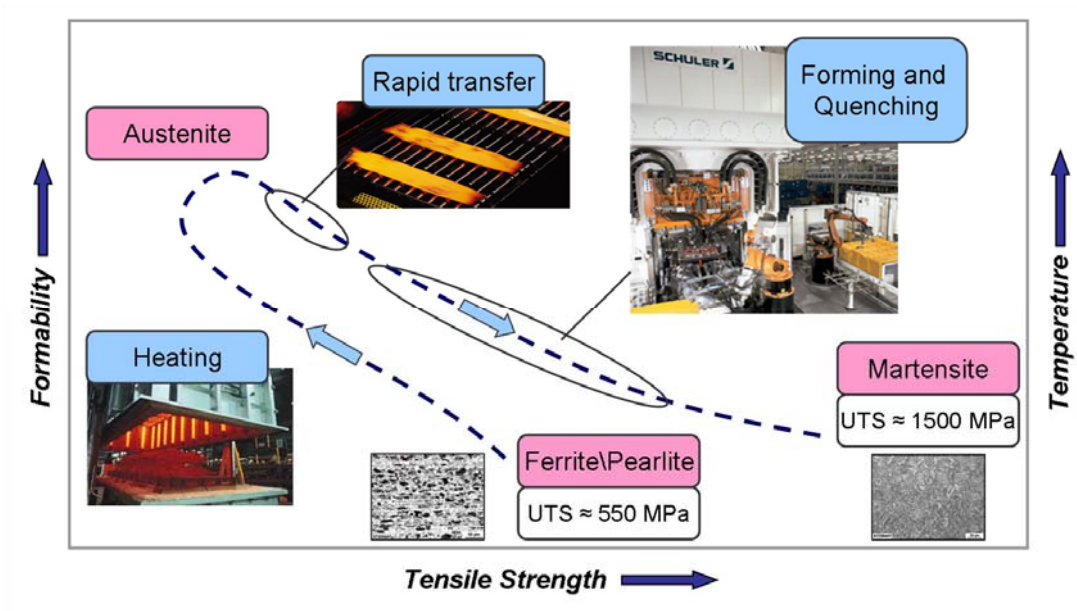

Figure 1.2 Thermo-mechanical cycle in the industrial hot stamping process.

Nevertheless, the simulation of hot forming and quenching of boron steels is still at a low development status in the automotive industry and relies in the experimental knowledge of few experts. Coupled thermo-mechanical-metallurgical models have to be implemented in the FE-codes to take into account all the thermal and mechanical events that material undergoes during the process [6]. The accurate calibration of these models, in terms of material behaviour, tribology, heat transfer, phase transformation kinetics and formability, is then a strong requirement to gain reliable result from the numerical simulation of the process. In particular, data about the elasto-plastic properties of boron steels as function of temperature and strain rate can be hardly found in scientific-technical literature, as well as the influence of applied stress and strain on the material transformation kinetics [7]. FE codes take into account material formability in sheet metal forming operations mainly using two approaches: the former is based on the on the availability of tools, like the forming limit curves, that verify if the calculated strains lie in the safe or unsafe region while the latter is based on the implementation of damage criteria to predict sheet fracture. The development and validation of these models are therefore fundamental achievements in order to perform numerical simulations with a great accuracy and offer noticeable time and cost savings to car designers.

1.2 Objective and organization of work

The main objective of this work is the design of innovative experimental procedures and the development of modelling tools to accurately investigate and describe the mechanical and microstructural properties of high strength quenchenable steels due to the thermal and mechanical events that occur during the industrial hot stamping process. The investigated material is the Al-Si pre-coated boron steel 22MnB5, produced by Arcelor™ with the commercial name of USIBOR 1500 P®

To fulfil this aim the following targets have been outlined:

- Determination of the optimum microstructural process window in terms of austenitization time and temperature.
- Design and setup of a new experimental apparatus to evaluate the influence of temperature and strain rate on the elasto-plastic material properties under the same conditions of the industrial process.
- Study of the influence of applied stress and strain on the material phase transformation kinetics.
- Design and setup of an experimental test to investigate the sheet formability and to determine Forming Limit Curves at elevated temperature.
- Description of the experimental and numerical tools used to calibrate and validate the FE model implemented to simulate hot forming operations.

This thesis has been divided into seven chapters. The first one contains a short introduction of the work and new trends in the automotive industry and a description of the hot stamping process. The collection of international scientific literature regarding press hardening and its numerical modelling is presented in the second chapter. In the third chapter a new experimental setup to study the elasto-plastic properties of sheet metal at elevated temperature is presented together with the rheological characterization of the 22MnB5 under the same conditions of the industrial process. The influence of applied stress and strain on the phase transformation kinetics is displayed in the forth chapter. The fifth chapter presents a new experimental apparatus developed to evaluate the material formability, perform physical simulation experiments and determine FLC in temperature. A thermo-mechanical-metallurgical model has been implemented in a commercial FE-code to perform fully coupled numerical simulations of the hot forming operations, and the main results regarding its calibration and validation are displayed in the sixth chapter. The final conclusions are presented in the last chapter.

CHAPTER 2
LITERATURE REVIEW

In the Introduction, it has been pointed out that the manufacturing technology based on sheet metal forming at elevated temperature proves today to have great potentiality of competitiveness in the automotive industry. The improvement of the quality and reliability of numerical simulations is the main prerequisite to optimize the hot stamping operations and obtain the desired mechanical and microstructural properties on final components.
When addressing to the hot stamping process, the FE simulations face many challenges such as the temperature and strain rate dependent material behaviour, the heat transfer at the workpiece-die interface and the coupled thermo-mechanical-metallurgical calculations. For an accurate description of these phenomena, it is therefore necessary to correctly understand and model all the aspects involved in hot forming operations, in order to determine experimentally material characteristics and thermal parameters and to model through an accurate mathematical transcription the coupling between the thermal, mechanical and metallurgical issues.
The literature review has thus been focused on the description of the hot stamping process in § 2.1 and on the state-of-the-art regarding the modelling and simulation of the hot forming operations in § 2.2. The inverse analysis theoretical principles used in this work for the heat transfer coefficient determination have been summarized in § 2.3. Finally the sheet metal formability evaluation at elevated temperature has been studied in § 2.4.

2.1 Hot stamping process description and technology

Nowadays, the demand of coupling performances with cost reduction and the respect of environment have represented the most challenging targets for the automotive industry, such as the increase of crash resistance and safety, the reduction of fuel consumption and emissions and the increase of accuracy and quality for easier, cheaper and more reliable joining and assembly of final components. These requirements force the car manufactures to a continuous research of new solutions, in direction of new product features and new manufacturing processes, leading the most significant evolution and innovation in sheet metal forming technologies [2, 8]. With regards to these aspects, the introduction of quenchenable high strength steels represents the solution to enhance the strength-to-mass ratio of body-in-white components, thus reducing the thickness of stamped parts, maintaining safety requirements and mechanical strength as well.

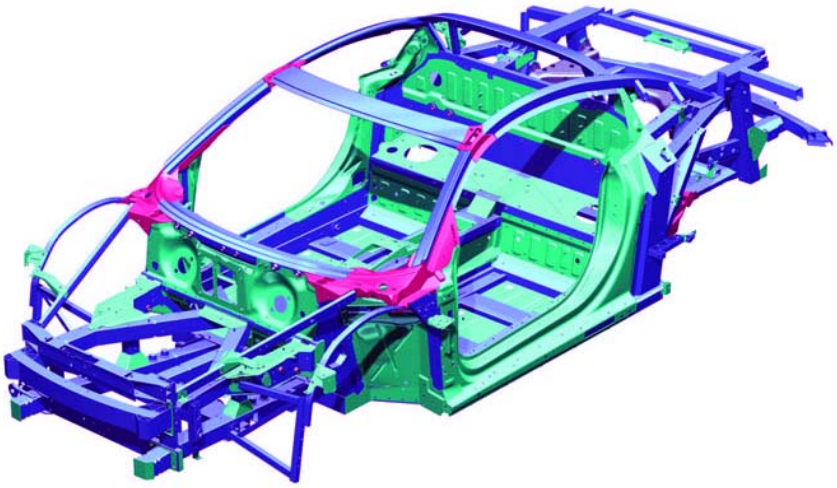

Figure 2.1 Range of application for hot stamped body-in-white components

However, the forming of such steels at room temperature is almost impossible due to the multi-phase microstructure, which is at the base of their strengthening and leads to unacceptable high loads and wear on tools and enhanced springback phenomena during forming, thus making traditional sheet metal forming technologies unsuitable. The possibility to perform stamping operations at elevated temperatures represents a solution of these problems and the hot stamping process proves to have a great potential to achieve improved service-life of tools, complex functional geometries of components and the required microstructure for highly resistant formed parts, due to the increased formability and reduced springback that these steels show at higher forming temperature.

Press hardening of ultra high strength boron steels is an non-isothermal sheet metal forming process, schematized in Figure 2.2, in which the forming and the quenching phases take place simultaneously.

The initial blank presents a ferritic/pearlitic microstructure in as delivery conditions, with limited mechanical properties and a tensile strength of about 400MPa and 600MPa. In the industrial process, the blank is heated in furnace in the range between 850°C and 950°C for several minutes in order to obtain a homogeneous austenitization of the sheet metal, then it is rapidly transferred to the press to avoid heat loss by means of robots or automated transfer lines. Afterwards deformation is performed in austenitic conditions and the use of continuous-cooled dies assure a rapid and controlled cooling in order to obtain a fully martensitic microstructure at room temperature, which guarantees strength levels above 1500MPa.

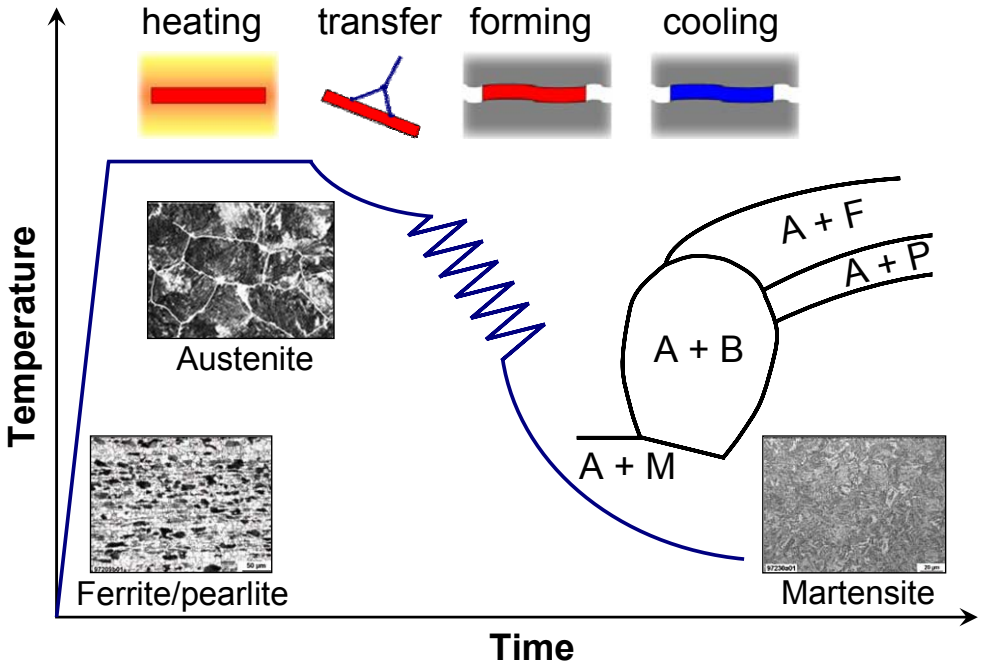

Figure 2.2 Hot stamping process

The total cycle time (transfer + forming + cooling into the die) requires approximately 15-25s and the formed component is removed from the dies at about 150°C. If the part leaves the stamping line too early, particular attention should be paid to avoid thermal distortion or uncompleted martensitic transformation [4]. Later on, the parts are usually drilled and trimmed through laser-cutting as well as conventional die-trimming.

The use of uncoated steels cal lead to an excessive oxidation and decarburization, even if inert atmosphere is utilized in the furnace because of the unavoidable contact with air during the transfer into the dieset. Due to these oxide scale layers, a surface finishing operation (e.g. shot blasting or sand blasting) has to be performed after the hot stamping, thus increasing process time and costs. In order to avoid these problems, Arcelor™ has developed an aluminium-silicon protective coating for the quenchenable boron steel 22MnB5, which is used as press hardening standard material in the automotive industry all over the world.

2.1.1 Base material properties and process design

The advantages of the hot stamping process are strictly linked to the high hardenability and extreme uniform microstructure offered by manganese-boron steels, leading to excellent behaviour under mechanical loading after quenching. Arcelor™ has developed

the well known boron micro-alloyed steel USIBOR 1500 P®, with the alloying composition 22MnB5 summarized in Table 2.1.

Table 2.1 Chemical composition of 22MnB5

C	Mn	Si	Cr	Ti	B
0.25	1.40	0.35	0.30	0.05	0.005

The USIBOR® mechanical properties before and after the quenching are reported in Table 2.2, according to the steel supplier indications.

Table 2.2 Tensile properties of 22MnB5 before and after quenching

22MnB5	Yield strength [MPa]	Tensile strength [MPa]	Elongation [%]
Precoated	370 - 490	~550	~21
Quenched	1200	1600	4.5

Mn and B are known to have a small influence on the strength after quenching, but they are essential to increase the hardenability, in fact according to the CCT curves of the material, see Figure 2.3, a minimum cooling rate of almost 30K/s after austenitization is necessary to obtain a fully martensitic microstructure at room temperature, avoiding the transformation of austenite into ferrite, pearlite and bainite during cooling.

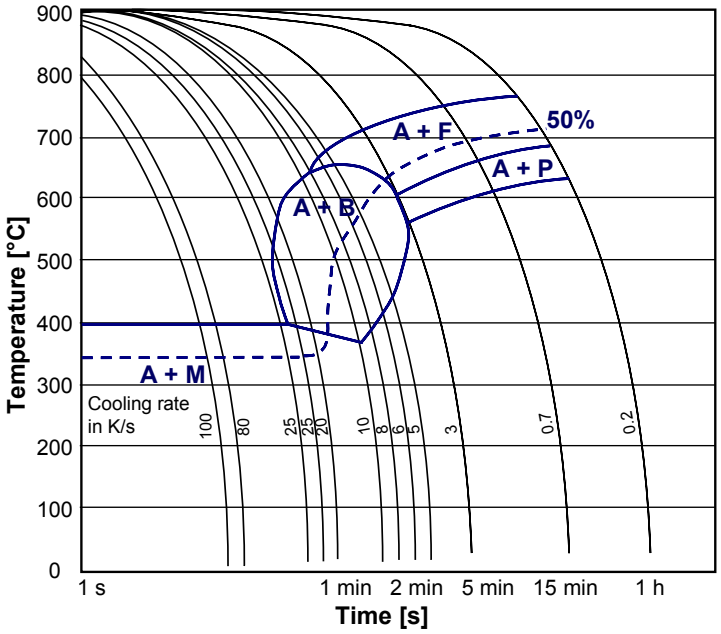

Figure 2.3 CCT diagram of USIBOR 1500 P® according to Arcelor [9]

The peculiarity of USIBOR 1500 P® is the Aluminium-Silicon coating layer which prevents the blank from oxidation at elevated temperature. This metallic coating has a thickness between 23μm and 32μm, see Figure 2.4, and during the heat treatment in the furnace it transforms into an alloyed layer made of Fe-Al-Si, strongly adherent on the substrate. The sheet has to be heated up to the austenitization temperature not faster than almost 12K/s in order to allow this alloying reaction and preserve the layer integrity [4].

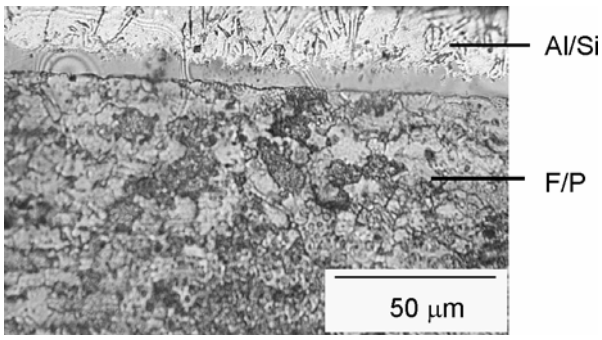

Figure 2.4 Micrograph of USIBOR 1500 P® Al-Si coating [10]

Other advantages of the USIBOR 1500 P® are the good spot weldability using conventional equipment, the increased paintability and corrosion resistance and the enhanced fatigue strength and impact resistance that can lead to a significant lightening potential in structural and safety components, such as B-pillars, fender beams, door reinforcements, middle posts etc. Furthermore, expensive protective post-coating like zinc painting are not necessary and the suppression of the furnace inert atmosphere and of the surface finishing operations leads to considerable time and money saving.

The proper design and optimization of the hot stamping involves a large number of parameters, regarding both the material and the process, that are strictly interrelated and that strongly affect the final component characteristics. In order to obtain the desired properties and quality on final parts, particular attention has to be paid to the factors that mostly influence the cycle time, the process parameters and their stability, in particular:

- the austenitization in the furnace should be performed with respect to the metallurgical transformation, in order to obtain a homogeneous austenitic microstructure, and to the intermetallic alloying reaction between the iron substrate and the Al-Si coating;

- the transfer time should be reduced as much as possible in order to limit the heat loss because at lower forming temperature the material formability is reduced and undesirable local phase transformations could occur;
- the forming phase should be fast enough to reduce the heat exchange between blank and dies during deformation, thus considering the influence of strain rate and temperature on the material rheological behaviour;
- the dies have to be designed to evacuate a big amount of heat by means of integrated cooling device in order to form and quench the blank at the same time, and obtain a fully martensitic microstructure at the end of the process, therefore the material phase transformation kinetics has to be taken into account.

2.2 Modelling and simulation of hot stamping

In the sheet metal forming industry, FE codes are widely used to predict and optimize manufacturing operations and to assess the forming feasibility of a part, reducing lead times and costs. At present, two main formulations are implemented in commercial codes: explicit and implicit approaches. Explicit formulations allow to reduce computation times and grant acceptable accuracy in the solution but may present instabilities in the analysis and exhibit significant limitations in the prediction of thermal aspects and microstructural evolution during hot stamping operations (e.g. Autoform, Pam-Stamp 2G). On the other hand, implicit codes (e.g. Forge, Marc, LS-Dyna, Abaqus) are characterized by higher accuracy in the results and, due to the non-linearity of the problem, they require long computation times that make them not suitable for industrial applications, furthermore reliable material and process data have to be evaluated more in detail [11, 12]. The introduction of temperature as an additional variable strongly influence the constitution of the finite element models and enhance their complexity compared to traditional sheet metal forming at room temperature [6, 13], as shown in Figure 2.5.

The main targets of press hardening simulations are the part geometry and the process parameters which guarantee a successful forming avoiding excessive wrinkling and thinning. In particular, the thickness distribution is used as input data in further crash simulations and the thermo-mechanical history of the material model is of great importance to capture the residual stress state that is responsible for the distortion of the final component [14].

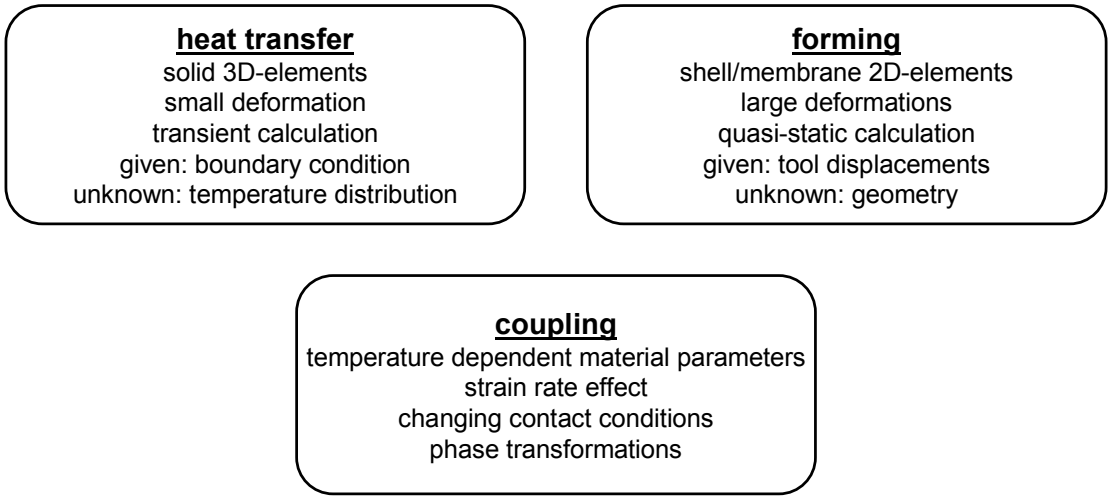

Figure 2.5 Main aspects of typical thermal and forming simulations and coupling to be realized in hot stamping modelling [5]

On the other hand, it is fundamental to accurately predict the final microstructure of the component early in the product development process, in order to obtain the desired characteristics on final parts in terms of mechanical properties and to ensure that the final microstructure is fully martensitic. The correct design of the forming and cooling phases requires the utilization of FE codes where the process has to be modelled through a fully coupled thermo-mechanical-metallurgical model. Therefore, also the austenite decomposition, the transformation induced plasticity and the influence of applied stress on the phase transformation kinetics have to implemented in the constitutive model.

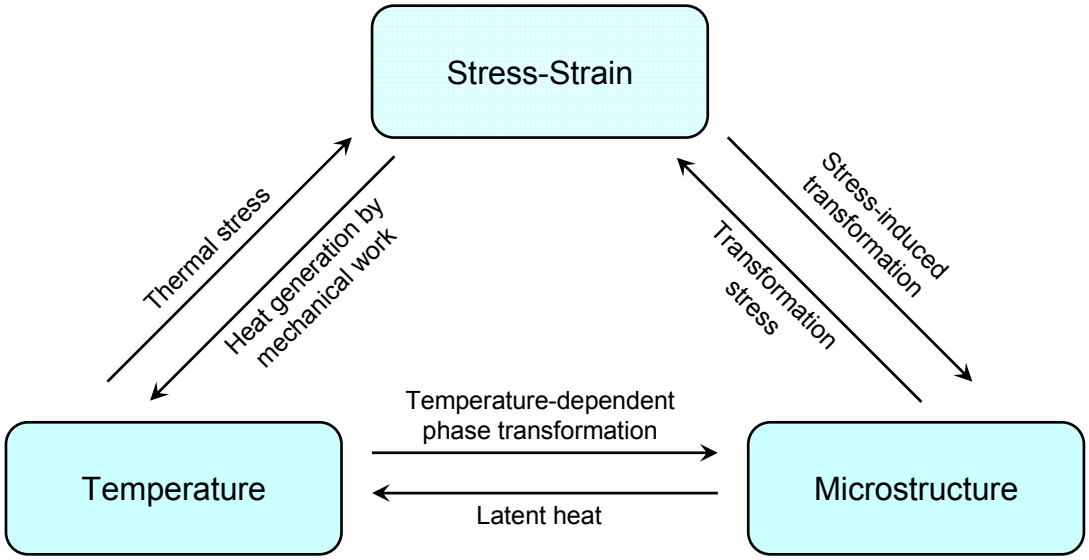

Figure 2.6 Coupling mechanisms during phase transformation [15]

The reliability of the numerical results depends not only on the models and the methods that are used, but also on the accuracy and applicability of the input data [16]. The material model and the related material properties data must be consistent with the conditions of the workpiece in the process of interest. The accurate calibration of such a model represents a strong requirement to gain reliable results from the FE simulations of the hot stamping process, and besides the parameters that are necessary for the simulation of conventional stamping, several material and process parameters and boundary conditions need to be additionally considered. In particular, data about the elasto-plastic properties of the material as function of temperature and strain rate, the sheet formability as well as the influence of applied stress and strain on the phase transformation kinetics have to be properly evaluated and implemented [17, 18]. Considering the complexity of the virtual model, several problems need to be solved to improve the simulation reliability and decrease input costs [19]:

- evaluation of which parameters have to be precisely modelled in order to improve the quality of numerical simulations;
- determination of which material characteristics need to be experimentally tested and which ones are not crucial for the numerical results;
- identification of the process parameters to be accurately considered already during the feasibility step in the die planning department.

An accurate and reliable analysis of the coupled thermo-mechanical-metallurgical process requires efficient simulation tools as well as good quality and relevant material data. The phenomena during hot stamping process can be divided into plastic deformation of blank, heat transfer between hot sheet and cold dies and phase transformation of sheet due to the cooling. Consequently, the simulation of the simultaneous forming and cooling should consider interactions between the mechanical and temperature field and the microstructure (Figure 2.7).

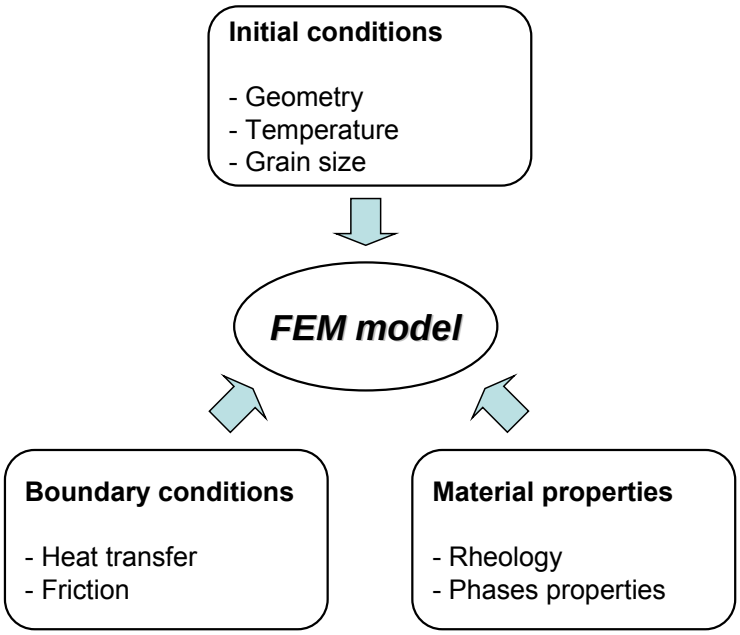

Figure 2.7 Thermo-mechanical-metallurgical FE model calibration

2.2.1 Thermo-mechanical properties

During hot stamping operations the blank is formed in the range between 850°C and 450°C, therefore the influence of temperature and strain rate has to be taken into account on the description of the material rheological behaviour, which has to be evaluated and modelled in this range.

Flow behaviour of metallic materials is the result of competitive balance between hardening and softening processes. When the dislocations annihilated by dynamic recovery equalize the dislocations generated by the work hardening, the flow curve attain a steady state [20].

In the empirical-analytical models, the flow stress is calculated as a function of the current process parameters by using an empirically derived equation [7]. These are strictly macroscale-length models and their formulation does not reflect any physical understanding of the phenomena that underlie the deformation process. The material constants do not have any physical meaning either since they are determined by fitting with experimental data [21, 22]. The following equations represents the oldest formulation of this kind of model, where the flow stress is determined as a function of a single variable, respectively the equivalent strain or strain rate in cold and hot conditions [23, 24]:

$$\sigma = k\varepsilon^{n} \tag{2.1}$$

and

$$\sigma = A - (A - B)e^{-\frac{\varepsilon}{\varepsilon_0}} \tag{2.2}$$

where σ is the equivalent stress and ε the equivalent strain.

The simultaneous dependence on equivalent strain ε, equivalent strain rate $\dot{\varepsilon}$ and temperature is expressed by the Norton-Hoff constitutive law:

$$\sigma = K\varepsilon^n \dot{\varepsilon}^m e^{\frac{\beta}{T}} \tag{2.3}$$

where K indicates the material consistency, n is the strain hardening coefficient and m represents the material strain rate dependency. The influence of the absolute temperature T is described through the exponential term $e^{\frac{\beta}{T}}$ where β is a constant material coefficient. To improve the fitting of this model the n and m coefficients can be described as functions of the temperature.

The most accurate representation of the flow curve in hot deformation conditions for FE-simulations id the Hansel-Spittel constitutive law:

$$\sigma_f = A \cdot e^{m_1 T} \cdot \varepsilon^{m_2} \cdot \dot{\varepsilon}^{m_3} \cdot e^{m_4/\varepsilon} \cdot (1+\varepsilon)^{m_5 T} \cdot e^{m_7 \varepsilon} \cdot \dot{\varepsilon}^{m_8 T} \cdot T^{m_9} \tag{2.4}$$

These models generally provide excellent mapping of the experimental stress-strain curves, however their extrapolation capabilities are usually poor outside the range of experiments used to generate and validate them and they are not very versatile. Nevertheless, the testing campaigns performed to identify constitutive material coefficients are not extensive, in fact it is only necessary to vary macroscopic parameters and these models are more used than other types because they make it easy to identify the coefficients, which can be easily implemented in FE codes.

To perform reliable thermo-mechanical coupled simulations also the Young's modulus and Poisson's ratio evolution with temperature should be implemented in the models [6].

2.2.2 Phase transformation kinetics

The complete description of the material transformation behaviour enables a prediction of the resulting material properties as a result of an accurate calculation of the volume fraction of the different phases. Cooling rates during quenching, and in particular the cooling phase of the hot forming process, are crucial in order to obtain the desired mechanical properties through a proper microstructure. The correct evaluation of the

phase transformation kinetics analysis is therefore essential to couple microstructural transformation and thermo-mechanical related phenomena.

Microstructural models describe the during- and post-deformation aspects of material response in terms of microstructure parameters. The phenomena covered by these models are dynamic and static phenomena, both of which are caused by deformation [25]. Some statistical models based on continuous curve transformation (CCT) permitting to point out the critical cooling rate for quenching depending on chemical composition and austenitization conditions have been proposed, but they are not accurate enough to be used to couple metallurgical and mechanical effect [26]. Phase transformations at constant temperature are investigated through the temperature-time-transformation (TTT) curves, indicating on a temperature vs. time logarithmic scale the starting and the ending transformation point at different constant temperatures.

According to the 22MnB5 CCT diagram (Figure 2.3), a minimum cooling rate of almost 27K/s has to be used to obtain a fully martensitic microstructure at the end of the hot stamping process. However, it has been shown that applied stress and strain can accelerate the austenite transformation [27, 28], thus a safety margin should be taken for this limit. Information about CCT and TTT diagrams of quenchenable boron steels can be found in the literature [29], but their correlation with the process parameters (e.g. stress and strain states) has not been investigated in depth yet and its evaluation represents a basic requirement to obtain reliable results from the numerical simulations of the hot stamping process.

2.2.2.1 Phase transformation modelling

The mathematical formulation for diffusion-controlled transformations is based on the nucleon-grain-growth theory. First publications about the kinetics of this kind diffusion-processes were made by Avrami [30]. The Avrami equation is widely used in the form:

$$\xi(t) = 1 - e^{-k(T)\eta(t)^{n(T)}} \tag{2.5}$$

where $\xi(t)$ is the volume fraction at the growing phase at time *t*, *n* is the Avrami coefficient depending on the germination mode and nuclei form, *k* is function of temperature and η is:

$$\eta(t) = \int_0^t q(u)du \tag{2.6}$$

where *q* represents the probability of a germ in the time unit to be active. This law is general enough to be utilized in both isothermal and anisothermal cases. It is possible to follow any cooling path and determine the correspondent transformed fraction by knowing *k, n* and *η.* The accessibility to experimental data necessary to determine those parameters force to a simplification of Avrami equation (2.5) and to deal with distinct approach to isothermal and anisothermal cases. In addition, the theoretical formulation of phase evolution was confirmed by experimental investigation of Johnson and Mehl [31].

The anisothermal kinetics theory is based on the subdivision of the thermal path in basic steps in order to reconstruct the anisothermal kinetics from the knowledge of isothermal one by applying the additivity principle, which is based on the theory advanced by Scheil [32] and can be mathematically stated as:

$$\int_0^t \frac{dt}{\tau(T)} = 1 \qquad (2.7)$$

where *dt* is the increment of time during continuous cooling and $\tau(T)$ represents the isothermal time required to initiate transformation at a specific temperature *T*. The additivity rule states that a transformation occurring while the temperature is changing can be considered as a series of isothermal events, with each increment of transformation being a function only of the fraction transformed and temperature.

The martensitic transformation requires a different mathematical approach, because it is very fast and without diffusion of carbon. The kinetics of this phase transformation is often modelled by the following equation, which was firstly formulated by Koistinen and Marburger [33]:

$$\xi(t) = 1 - e^{-\alpha(M_S - T)\kappa} \qquad (2.8)$$

where $\xi(t)$ is the volume fraction of martensite, *Ms* is the martensite-start temperature and α and *t* are material coefficients.

Some preliminary studies have been carried out in order to simulate the 22MnB5 phase transformation behaviour through the model expressed by the Johnson-Mehl-Avrami (2.6) and Koistinen-Marburger (2.8) equations, as shown in Figure 2.8, but further investigations are necessary to validate that model due to the lack of information about the 22MnB5 isotherm TTT diagram [34] and the influence of applied stresses on the material phase transformation kinetics.

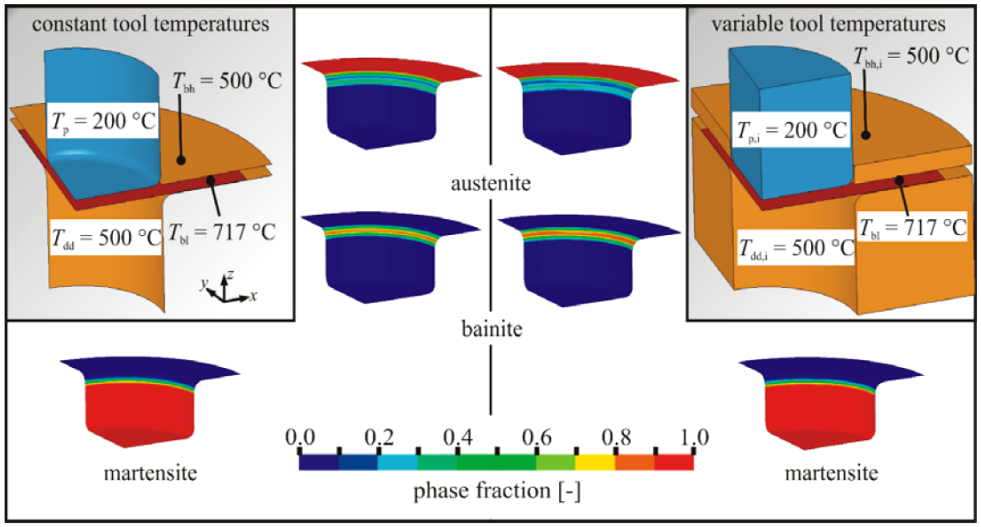

Figure 2.8 Resultant phase fraction of austenite, martensite and bainite after the cooling process simulation considering both elastic tools and heat transfer into the tools [34].

The martensitic transformation causes a release of latent heat of approximately 85kJ/kg, therefore this phenomena has to be taken into account for a correct simulation of the quenching phase.

2.2.2.2 Transformation plasticity

Solid state phase transformations do not only change the mechanical and thermal properties of the material, but result also in volumetric and deviatoric strains. If the phase transformation occurs without applied stress, the material response is purely volumetric and an increase in volume is observed due to the compactness differences between the parent and product phase. Transformation induced plasticity (TRIP) is an irreversible strain observed when metallurgical transformations occur under external stress that is lower than the yield stress of the parent phase. In technological applications, TRIP plays an important role in many problems, in particular for the understanding of residual stresses and distortions of the final component resulting from anisothermal forming operations.

Two mechanisms are usually considered to explain this phenomenon from a microstructural poi of view: the Magee mechanism [35] and the Greenwood-Johnson mechanism [36]. According to Magee, transformation plasticity is due to an orientation of the newly formed phase by the applied stress. This mechanism is particularly related to martensitic transformation during which martensite develops in the form of plates which generate high shearing in the austenitic phase. It is important to underline that if no

external stress is applied, this orientation is random and the resultant micro-stresses can be considered negligible. On the contrary, an applied load favours a particular orientation of martensitic plates with a consequent non nil resultant for micro-stresses [37]. According to Greenwood and Johnson transformation plasticity is due to the compactness difference between parent and product phase. Therefore, micro-stresses are introduced and generate plastic strains in the soft austenite when an applied deviatoric stress is applied. If no external load is applied, no transformation plasticity is observed, due to the nil volume average of the micro-plasticity [38].

It has been found that the linearity between applied load and final transformation plasticity surely exists only if the applied load is inferior to the half of the yield stress of austenite at the considered temperature, as shown in Figure 2.9.

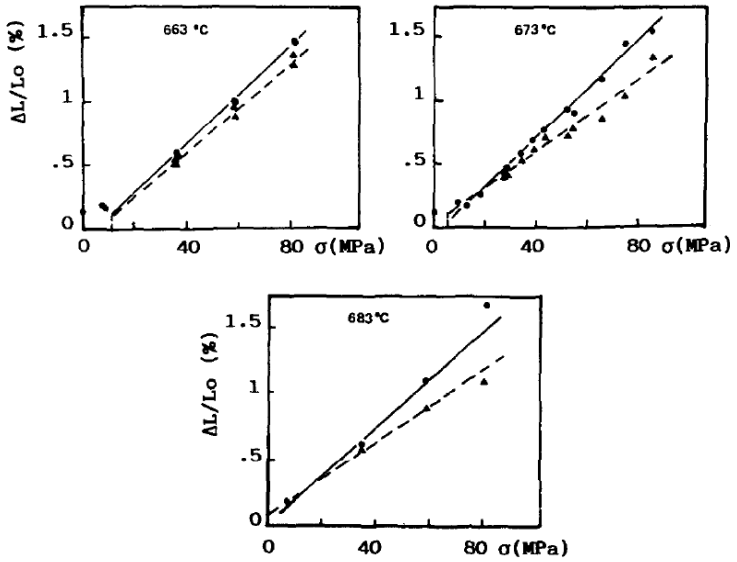

Figure 2.9 Transformation plasticity as function of applied load at three different temperatures [39]

More results can be found in the work published by Coret [15]. In addition, Taleb found that transformation plasticity strain increases for low fraction of transformed phase while a sort of saturation arises when about 70% of new phase is formed [38].

Åkerström developed a constitutive model taking into account austenite decomposition and transformation induced plasticity in order to increase the accuracy of numerical simulations of the hot stamping process [40], and Figure 2.10 shows some results regarding the validation of the implemented model.

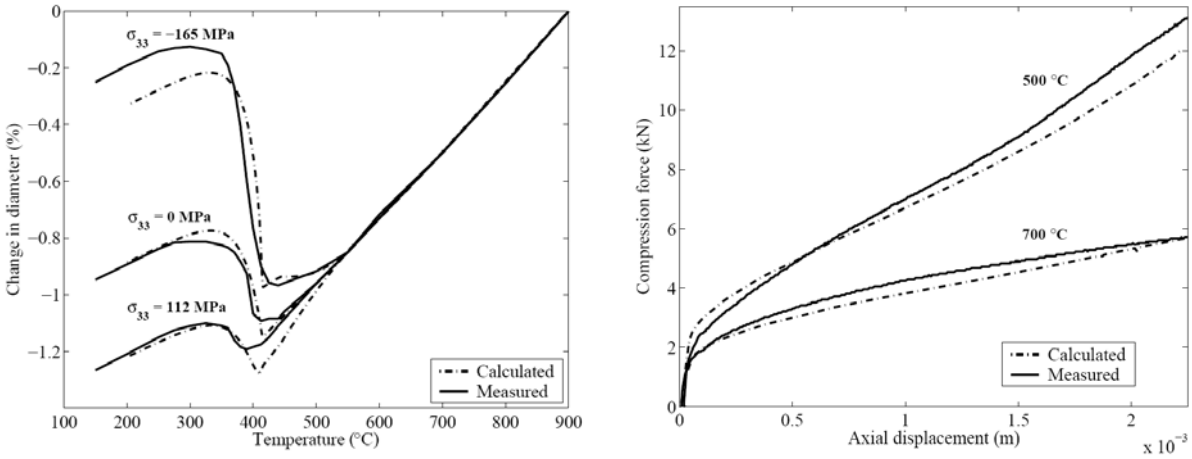

Figure 2.10 Change in diameter as function of temperature and axially applied force and compression force versus axial displacement at the isothermal temperatures of 500°C and 700°C [14]

In order to improve the predictive capabilities of these implemented models, additional experiments for different thermo-mechanical loading histories must be conducted because the mechanical data found in the literature are somewhat incomplete with respect to the temperature and strain range typical of the hot stamping process. Thus, there is a need for more studies of the mechanical response of individual phases [14].

2.2.3 Heat transfer

During the thermo-mechanical forming of the sheet in the hot stamping process, there is an extensive heat transfer between the hot blank and the water cooled dies. For the quality of the formed part it is important to guarantee a homogeneous martensitic microstructure in all the regions, therefore numerical simulations should model and predict with a great accuracy the physical mechanisms of heat transfer. When a gap is present between the sheet and the tools, the heat transmission is mainly driven by heat convection through the air. On the other hand, in case of zero clearance the heat transfer is led by the conduction and it strongly depends on the die-workpiece interface, temperature and contact pressure [41, 42].

Furthermore, during deformation most of the irreversible work done on the material is converted to heat and results in an increase of temperature. The component is part of a physical system and exchange heat with the environment and the temperature evolution in the system can be written as:

$$\underbrace{\rho c \frac{\partial T}{\partial t}}_{\substack{Temperature \\ evolution}} = \underbrace{div\left(k \cdot grad\left(T\right)\right)}_{Internalconduction} + \underbrace{\dot{W}}_{\substack{Internal \\ dissipation}} \quad (2.9)$$

In the area boundary the temperature evolution depends on the imposed temperature and radiation, conduction and convection exchange.

The radiation affect the area boundary with a flux exchange term Φ_r given by:

$$\Phi_r = \sigma\varepsilon\left(T^4 - T_0^4\right) \quad (2.10)$$

where ε is the material emissivity in its current conditions, σ is the Stefan constant, T_0 is the exterior area temperature and T the area boundary local temperature.

The area boundary is affected by the conduction and the convection with the flux exchange $\Phi_{conduction}$ and $\Phi_{convection}$ that can be expressed as:

$$\Phi_{conduction} = c\left(T - T_0\right) \quad (2.11)$$

$$\Phi_{convection} = h_c\left(T - T_0\right) \quad (2.12)$$

where c is the thermal conductivity of the material and h_c is the convection coefficient.

In a metal forming process, the physical system is composed of a workpiece, a set of dies and sometimes a lubricant. On a microscopic scale both the die and the workpiece reveal real surfaces which are not perfectly smooth, showing small peaks, asperities and valleys, as shown in Figure 2.11.

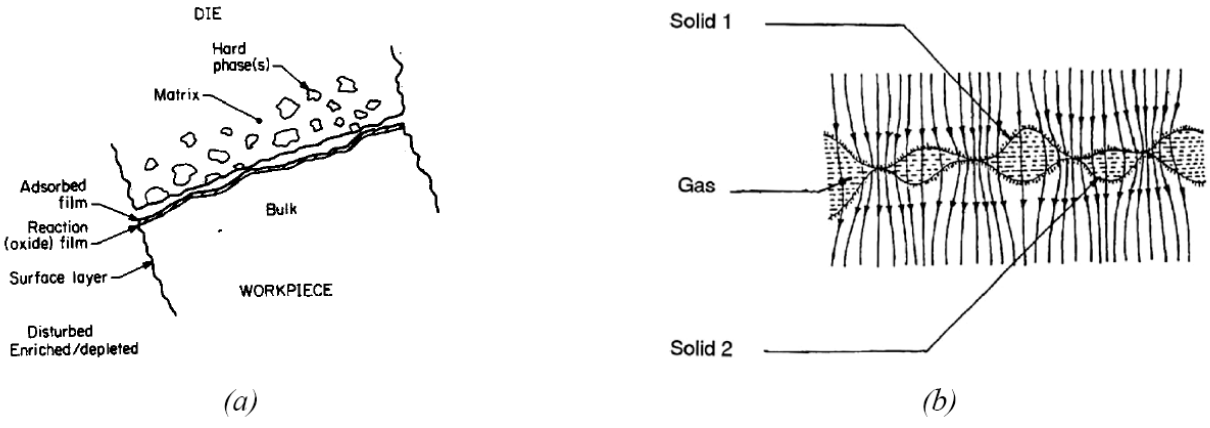

Figure 2.11 Die-workpiece interface on a micro-scale (a) [43] and heat flow through a joint (b) [44]

Due to the unevenness of the contact, the heat flux is altered and a temperature difference occurs at the interface of the two solids. This temperature difference is at the

base of the definition of thermal contact conductance *h*, generally known as heat transfer coefficient:

$$h = \frac{q}{T_{C1} - T_{C2}} \tag{2.13}$$

where T_{c1}-T_{c2} represents the temperature drop across the interface between two contact bodies and *q* is the heat flux, given by:

$$q = \frac{d}{dA}\left(\frac{dQ}{dt}\right) \tag{2.14}$$

The main parameters affecting the thermal contact conductance can be grouped into there classes [45]:

- process parameters: contact pressure, initial temperatures, contact time under pressure;
- interface conditions: lubrication, oxide scale, roughness, friction, surface cleaning, macro and micro geometry;
- material properties: type of contacting materials, rheological behaviour, thermal conductivity, heat capacity.

2.2.3.1 Heat transfer coefficient determination

Heat transfer coefficient between workpiece and dies becomes critical in order to simulate the hot forming operation and the subsequent cooling phase when a proper microstructure is required [5]. HTC values can be hardly found in the literature and there's no direct formulation to evaluate HTC. In recent years, thanks to the improvements in numerical methods and computer techniques, a growing interest in the evaluation of heat transfer has emerged, with the aim of providing numerical codes with a proper description of the process thermal boundary conditions. Several evaluation techniques can be performed to determine the value of *h* and the main research works related to the hot stamping process are reported.

The matching method consists on fitting the experimental temperature distribution to analytical or numerical solutions given by a thermo-mechanical model of the experiment for various values of *h*. The introduction of a model thus requires assumptions concerning material behaviour and values of thermal properties of specimens and dies that can lead, in case of inaccurate data, to a reduction of the relevance of the computed heat transfer coefficients.

Lechler et al. [1] studied the heat transfer coefficient evolution with contact pressure through an analytical approach based on the following equation:

$$\alpha = -\frac{c_p \rho V}{At} \ln\left(\frac{T(t) - T_\infty}{T_0 - T_\infty}\right) \tag{2.15}$$

where T_0 and $T(t)$ represent the initial and the actual temperature of the blank measured during the experiments and T_∞ indicates the temperature of the contact plates, which is assumed to be constant. Figure 2.12 shows some results for the USIBOR 1500 P® heat transfer coefficient evolution with respect to the applied contact pressure.

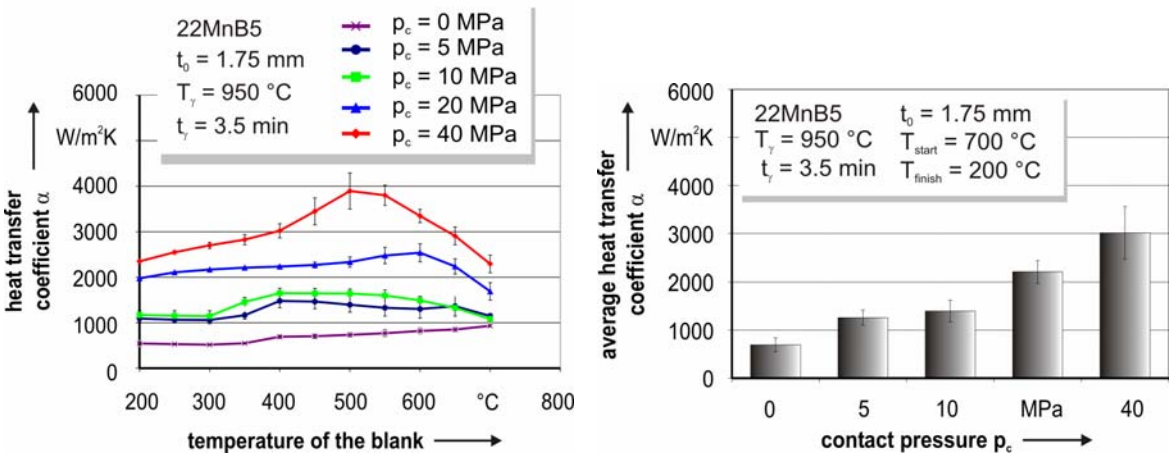

Figure 2.12 Heat transfer coefficient between workpiece and dies as function of the temperature and of the applied contact pressure [18]

The inverse analysis method is based on the solution of an inverse problem and may be applied to determine heat transfer coefficients under both steady-state and transient conditions. The main advantage of this approach is that the inverse analysis can be based on complex analytical and numerical models, making it possible to carry out experiments closer to the industrial conditions, however the drawbacks are the same outlined for the previous method, with a reduction in the relevance of the computed values in the case of inaccurate input data.

Geiger et al. [46] simulated with ABAQUS the cooling experiments with the USBOR 1500 P® in order to determine the heat transfer coefficients for different contact pressures through inverse analysis. Two interpolation points of the HTC were inserted in the simulation in order to interpolate linearly between the data points, as shown in Figure 2.13.

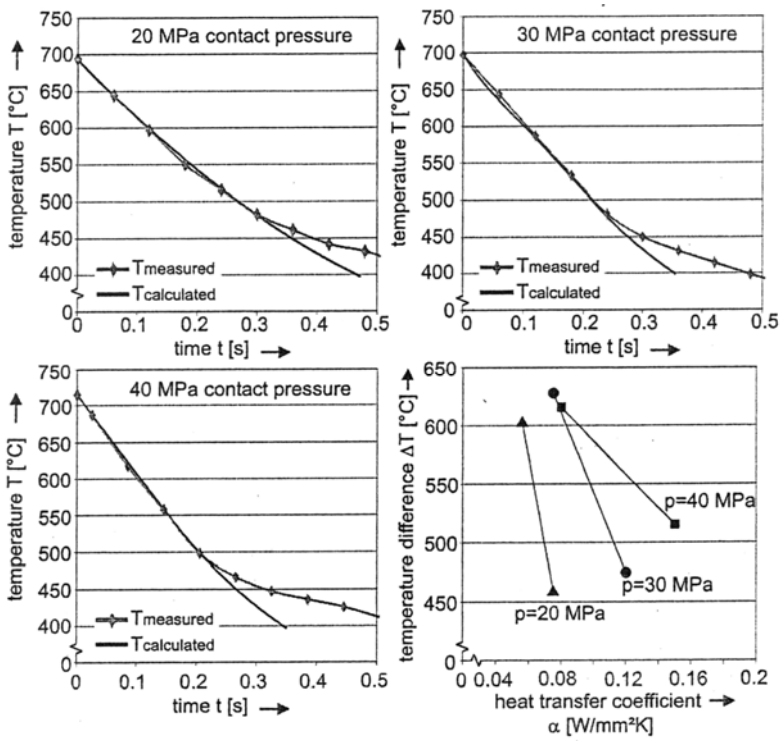

Figure 2.13 Comparison between the experimental and calculated curves with the determined heat transfer coefficients [46]

Forstner et al. [47] investigated the influence of temperature and contact pressure on the HTC in hot stamping operations through an inverse analysis performed with DEFORM 2D. In order to improve the accuracy of the prediction, the temperature dependence of HTC was implemented both as a constant and a variable value and the commercial software Calcsoft was also used for the inverse temperature modelling. The experimental setup and some results are presented in Figure 2.14.

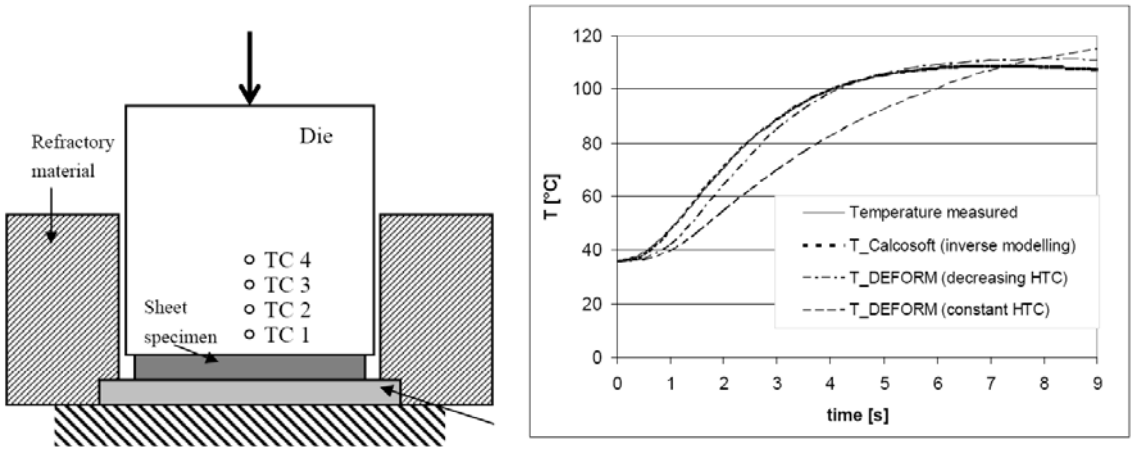

Figure 2.14 Experimental setup and comparison between the experimental and numerical curves of different HTC values [47]

2.3 Inverse analysis theoretical bases

In this work an inverse analysis technique will be used to determine the heat transfer coefficient, therefore its theoretical bases are briefly introduced.

A physical system can be described through a mathematical model able to express the system response M^C taking into account the boundary conditions. This direct model can be given as:

$$M^C = S(x) \tag{2.16}$$

where x represents the parameters describing the system under study and S is called forward operator.

On the contrary, the inverse analysis consists in determining the condition x leading a physical system to describe the experimental value M^{exp}, and can be expressed as the determination of:

$$x = S^{-1}(M^C) \text{ so that } M^C = M^{\exp} \tag{2.17}$$

The complexity of most direct models commonly adopted is sometime so elaborate that a simple inversion of the model results impossible, therefore regression methods are instead used, in order to predict an experimental state M^{exp} closer as possible to the predicted value M^C [48]. Only in the last years a systematic study for a general formulation and resolution of inverse problems has been performed involving several fields such as electronic [49], structural analysis [50], heat engineering [51, 52], geometrical optimization [53, 54] and rheological parameters identification [55, 56].

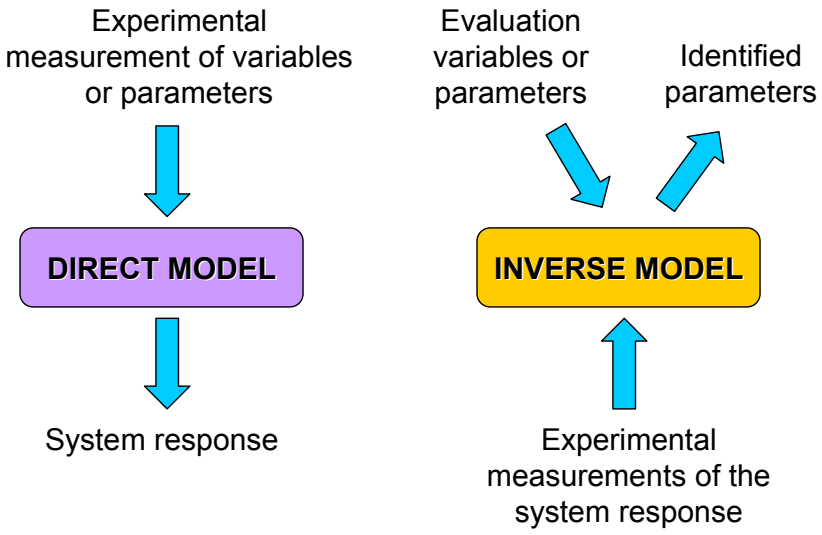

Figure 2.15 Comparison between forward and inverse problems

The inverse problem finds the model parameters given the values of the observables of the forward problem and it can be well conditioned if the following conditions are satisfied:

- For any *M* in the experimental space a solution exists.
- The solution is unique in the model parameters space.
- The inverse mapping $M \rightarrow x$ is continuous.

Otherwise, in bad-conditioned problems the existence, uniqueness and continuity of a solution are not all verified. Metal forming problems are generally bad-conditioned considering the model complexity and the typical number of variables.

The parameter identification method is based on the determination of the set of parameters *P* in order to minimize the difference between calculated values M^C of the observables and experimental values M^{exp} which are given by the equation:

$$M_i^{\exp} = M_i^C + \lambda_i \text{ with I = 1, 2, …, s} \tag{2.18}$$

where λ_i represents the gap between correspondent calculation and measurement including numerical approximation, measurement uncertainty and errors due to model assumptions and simplifications of the real process. The minimization of this difference basically consists of minimizing the gap λ_i by means of the cost function defined by:

$$Q\left(M^C(P), M^{\exp}\right) = \sum_{i=1}^{s} \lambda_i^2 = \sum_{i=1}^{s} \left(M_i^{\exp} - M_i^C\right)^2 \tag{2.19}$$

(2.19) is often expressed an the adimensional form;

$$Q = \sum_{i=1}^{s} \beta_i \left(M_i^{\exp} - M_i^C\right)^2 \tag{2.20}$$

where β_i are called weight coefficients and the following conditions have to be assured:

- Q must be semipositive defined (supposing $\beta_i > 0$)
- Q = 0 if and only if $M^C = M^{exp}$

When the optimization is based on multiple objectives it is necessary to define a multi-criteria cost function:

$$Q = \sum_{k=1}^{nobs} \sum_{i=1}^{s} \beta_i \left(M_i^{k^{\exp}} - M_i^{k^C}\right)^2 \tag{2.21}$$

where *nobs* is the number of observable quantities taken into account and $M_i^{k^{\exp}}$ refers to the i-th experimental value of the k-th observable quantity. (2.21) permits to consider, during deformation, the influence of different optimizing parameters on different experimental values.

A more general form of the cost function employs a statistical approach [49] where the optimization problem is lead to the determination of the parameters which maximize the prediction probability of the experimentally evaluated measure. For a Gaussian distribution, the cost function depends on the mean value of the experimental measure $\tilde{m}\left(M_i^{k^{\exp}}\right)$, which are supposed to be equal to the calculated ones $M_i^{k^C}$, and the quadratic deviation of measurement errors $\sigma_i^{k^2}$.

The cost function can be expressed as:

$$Q = \sum_{k=1}^{nobs}\sum_{i=1}^{s}\lambda_i^k\left[\bar{m}_i - M_i^{k^C}\right]^2 + \sum_{j=i}^{r}\gamma_j\left[P_j - \bar{P}_i\right]^2 \tag{2.22}$$

where $\lambda_i^k = 1/\sigma_i^{k^2}$ with k=1,2,…,nobs and $\gamma_j = 1/\sigma_{pj}^2$

Several methods can be used for the minimization problem [57-59] and the Gauss-Newton method, used in this investigation, will be described more in detail.

The Gauss-Newton method introduces a linearization of the non-linear expression of terms representing the computed observables M_i^C neglecting the second order derivative. This method is based on the first order Taylor series expansion of Q in the quadratic form:

$$\frac{dQ}{dP}(P+\Delta P) = \frac{dQ}{dP}(P) + \frac{d^2Q}{dP^2}(P)\cdot\Delta P + \theta\left(\Delta P^2\right) \tag{2.23}$$

An extreme of the Q function is obtained imposing:

$$\frac{dQ}{dP}(P+\Delta P) = 0 \tag{2.24}$$

and neglecting terms grater than first order the equation (2.23) can be expressed as a linear system:

$$\begin{cases} A\cdot\Delta P + B = 0 \\ A = \dfrac{d^2Q}{dP^2}(P) \\ B = \dfrac{dQ}{dP}(P) \end{cases} \tag{2.24}$$

where:

$$B_k = \frac{dQ(P)}{dP_k} = 2\sum_{i=1}^{s}\beta_i\left(M_i^C - M_i^{\exp}\right)S_{ik} \tag{2.25}$$

$$A_{jk} = \frac{d^2 Q(P)}{dP_j dP_k} = 2\sum_{i=1}^{s} \beta_i \left(M_i^C - M_i^{\exp}\right) \frac{d^2 M_i^c}{dP_j dP_k} + 2\sum_{i=1}^{s} \beta_i \frac{dM_i^c}{dP_j} S_{jk} \quad (2.26)$$

$$S_{jk} = \frac{dM_i^C}{dP_k} \quad (2.27)$$

and *S* is called sensibility matrix.

The peculiarity of this method consists in neglecting the second order derivatives of the calculated observables of the direct model in (2.26) which becomes:

$$A_{jk} = \frac{d^2 Q(P)}{dP_j dP_k} \cong 2\sum_{i=1}^{s} \beta_i \frac{dM_i^C}{dP_j} S_{ik}$$

The solution of the linear system (2.24) leads thus to the determination of the components of the matrix *S*.

The sensitivity matrix allows to determine the matrix *A* and the gradient *B* of the linear system (2.24). It is therefore necessary to calculate the derivatives of M^C respect to each parameter to be determined and the sensitivity analysis may be performed [60]:

- by finite differences;
- by means of analytic direct calculation;
- with the formulation of a conjugate problem;
- with a semi-analytical evaluation.

2.4 Formability

The formability of sheet metal depends on both material characteristics (e.g. anisotropy and microstructure) and on forming process conditions (e.g. temperature, friction, strain rate and strain path). Sheet metal formability is generally estimated using several tests (e.g. uni-axial and bi-axial tests, bulging test, FLC, LDH, flange insertion test, etc). Each type of test has some advantages and some disadvantages in its application both at room and at elevate temperature.

The concept of the forming limit curve has been introduced by Keller [61] and Goodwin [62] in order to represents comprehensively sheet metal formability and it has been widely used both in factories and research laboratories as one of the criteria for optimizing stamping processes and in the design of dies. Such curves indicate both the principal strains at diffuse or localized instability for different strain paths.

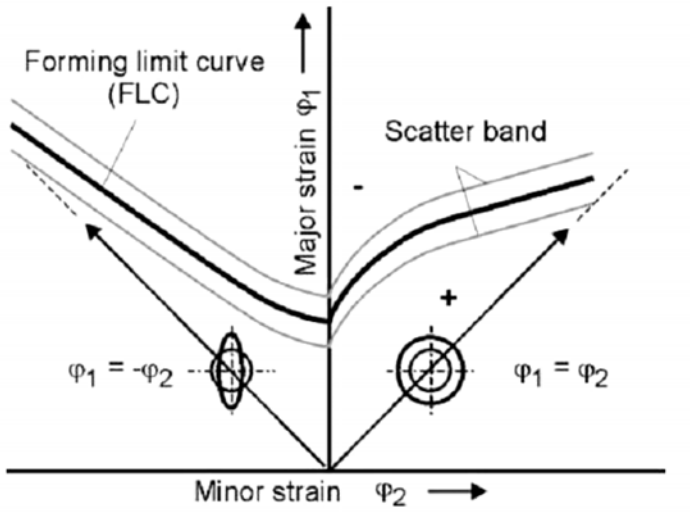

Figure 2.16 Standard forming limit curve including scatter band

At room temperature two main methods are generally used to obtain limit curves, the Marciniak and the Nakazima, and they effectively constitute the state-of-the-art. The main differences between these tests is the shape of the punch which is respectively flat and hemispherical. The Nakazima setup is simpler to perform but a special lubrication system (e.g. oil, Teflon foil, elastic pad, etc.) has to be used to reduce friction, while the Marciniak test is equipped with carrier blanks to prevent the contact between the punch and the tested specimen, thus reducing the difficulties caused by friction. Specimens of various width are used to determine a complete FLC [63].

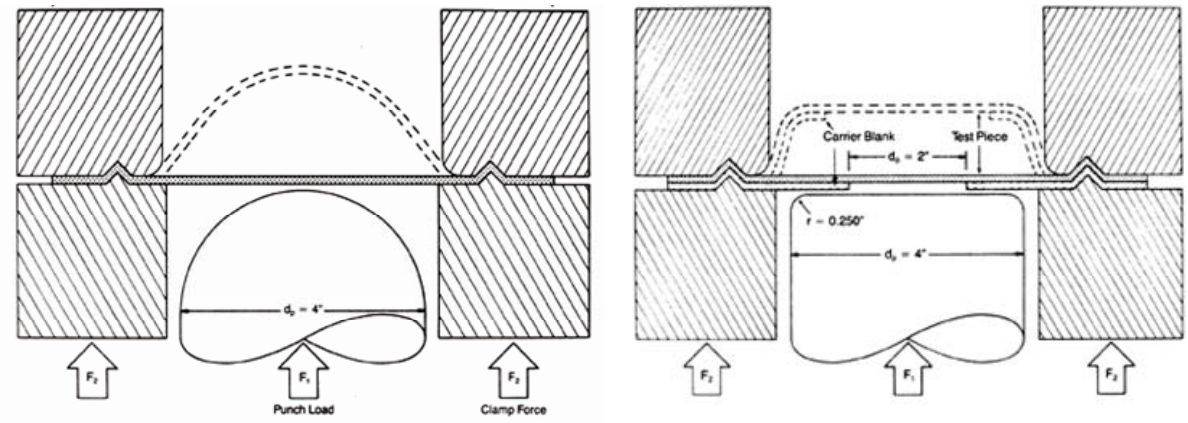

Figure 2.17 Typical Nakazima (a) and Marciniak (b) setups

Because of the complexity of the experimental determination of FLC, several theoretical calculating models have been proposed on the basis of the classical or modified Swift and Hill instability criteria [64, 65] to calculate the limit strains: diffuse necking, localised necking, initial non-homogeneity, linear perturbation analysis, etc [66]. The mathematical model proposed by Marciniak and Kuczynski (M-K) model is based on the assumption that the strain localisation, in the case of biaxial straining, appears in the region of a geometric non-homogeneity of the sheet metal, see Figure 2.18.

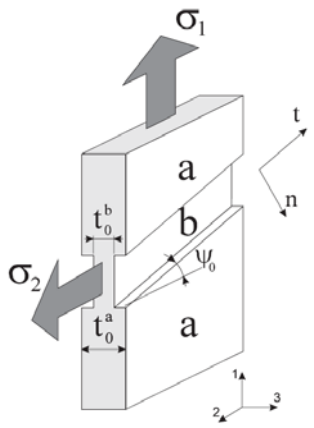

Figure 2.18 Geometrical model of the Marciniak-Kuczynski theory

However, the limit strains calculated according to the M-K model (using the Von Mises or Hill's yield criteria) are overestimated in the domain of biaxial straining and underestimated in the domain of plane straining [67]. Therefore the shape and position of the FLCs are strongly influenced by the expression of the yield criterion used in the model and the determination of yield locus requires great efforts compared to standardised tests and no internationally standardized procedure is established [68]. It has been found that FLC is affected by many factors such as r-value, material imperfection, yield criteria, grain size, etc [69]. This complexity has made the existing approaches of predicting FLCs often unsatisfactory. The limitations in the theoretical predictions of FLC mainly lie in its many assumptions, some of which are not justifiable or lack of proper experimental verification [70].

In recent years, the principle of continuum damage mechanics (Figure 2.19), plastic mechanics of porous material, and microscopic materials science combined with the FE methods have also been introduced in the theoretical prediction of the FLCs [71]. These results have significantly enriched and improved the understanding and application of the

FLC. However, there is not a general model that can be successfully applied at elevated temperature, furthermore, the calculation for predicting the FLC are still too complex and thus limited in practical applications. In fact, industrial applications such as sheet stamping require a simple, accurate and rapid approach to evaluate FLC.

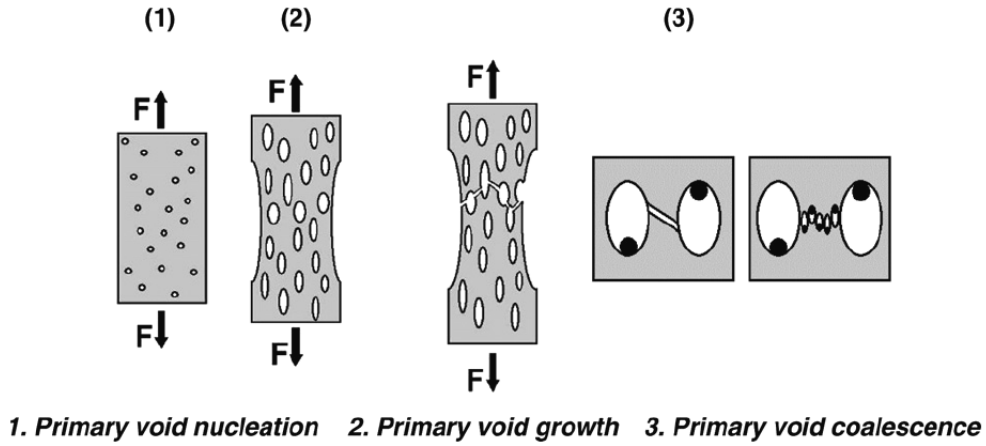

Figure 2.19 Ductile damage process of structural steels [72]

The quality and reliability of FLCs are fundamental in the use of FE analysis software in the product development and process optimization phases [73] and are gaining in significance more and more within the last years. The FE numerical strain distribution is generally compared to the material FLC in order to predict sheet failure and verify if the calculated strains lie in the safe or unsafe region [74].

Until now, FLC has been usually determined using line mesh methods based on circular or linear pattern applied to the surface of the non-deformed specimen. Deformation of this pattern is evaluated with the help of magnifying glasses, microscopes and flexible measurement strips. Experimental methodology using grid selection and classification in the proximity of the neck and strain measurement in the neck region is often time consuming and this method is limited by the contour sharpness of the deformed pattern and the measurement accuracy of the evaluation (Figure 2.20).

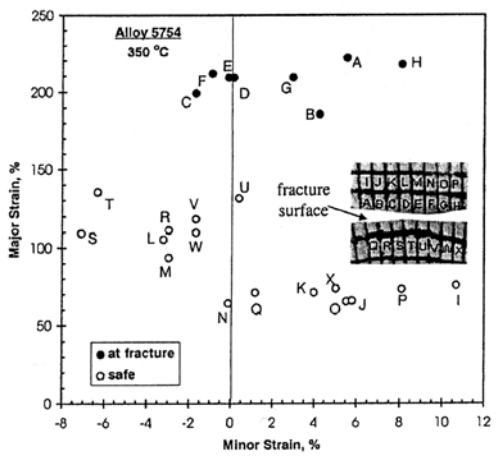

Figure 2.20 Typical discontinuity in the FLC determination through grid analysis

The characteristics of sheet metal materials must be determined as quick as possible in order to meet today's industrial requirements. The introduction of the optical measurement systems based on the stochastic marking approach (e.g. GOM-ARAMIS™), represents a solution to these problems, leading the advantages of reduced effort and comfortable handling [75]. The use of two CCD cameras combines the advantages of photogrammetry and of the object grating method, significantly reducing time and costs for the FLC determination.

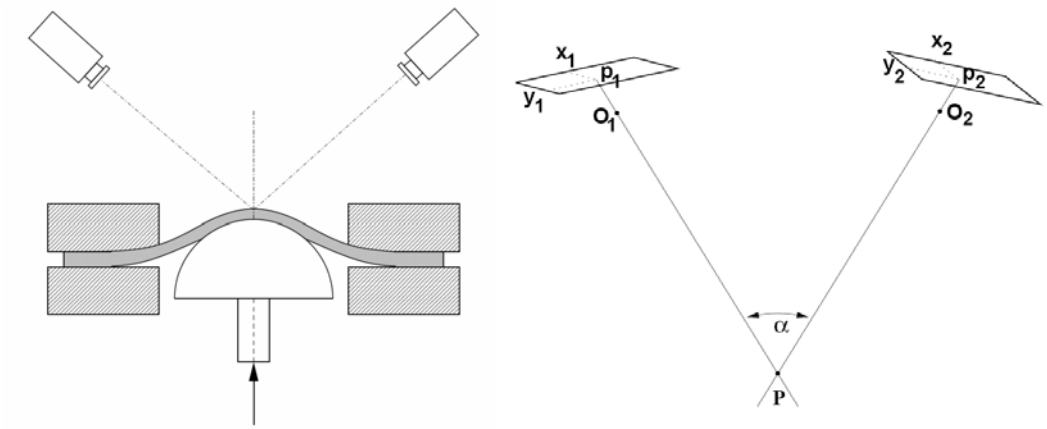

Figure 2.21 Schematic setup of Nakazima test with the arrangement of the CCT camera and photogrammetric model

The reproducibility of FLCs depends on its determination and the experimental device, and many evaluation criteria have been proposed such as cracking, definite necking or

diffuse necking. In the ISO 12004 [76] the failure criterion is defined as the onset of localized necking, which corresponds to a load instability and it is difficult to detect. Geiger et al. [77] have developed a new analysis method to detect the onset of necking in order to avoid misinterpretations and get more stable and reliable FLCs. It is based on the first derivation of the major strain as function of its coordinate and the rapid increase of this function indicates the existence of a load instability.

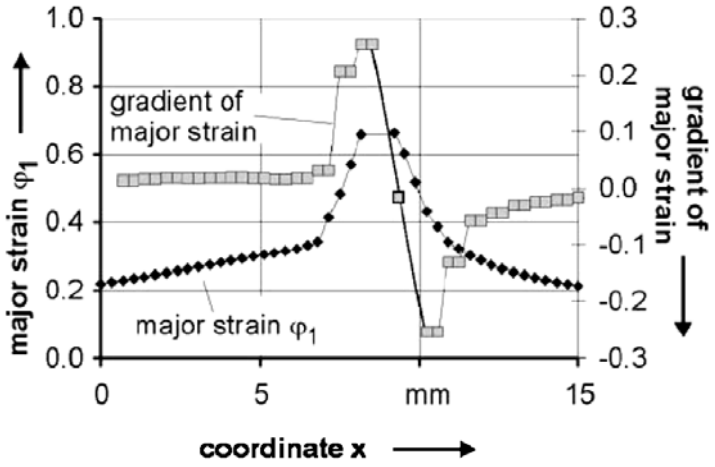

Figure 2.22 Gradient of major strain as an indicator for the onset of necking according to Geiger et al. [77]

A new version of the ISO 12004 has been presented under the protection of the German group of the IDDRG in order to harmonize the execution of experimental tests and its analysis [78]. The procedures and mathematical methods elucidated in the "ISO-12004 Proposal Version 15-8-2005" have been implemented in the ARAMIS™ software in order evaluate the forming limit state and determine the FLC. This procedure can be considered the state-of-the-art in the evaluation of FLC at room temperature.

The application of FLCs shows an insufficient accuracy when applied at elevated temperature due to the complex material behaviour and the interface conditions during the tests. Hora et al. [79] have proposed a new method for the failure prediction in sheet metal forming processes at elevated temperature based on forming limit diagrams with temperature dependency as a additional variable (FLC-T). In case of press hardening the temperature influence is introduced through strain and strain-rate dependant hardening curves modelled with the Zener-Hollomon law and a direct FEM prediction similar to the M-K failure criterions is used. The thinning of the sheet indicates the failure, although it is generally predicted with some delay and the numerical results show a strong sensitivity to

the thermal conditions, therefore further effort has to be invested for the validation of this method.

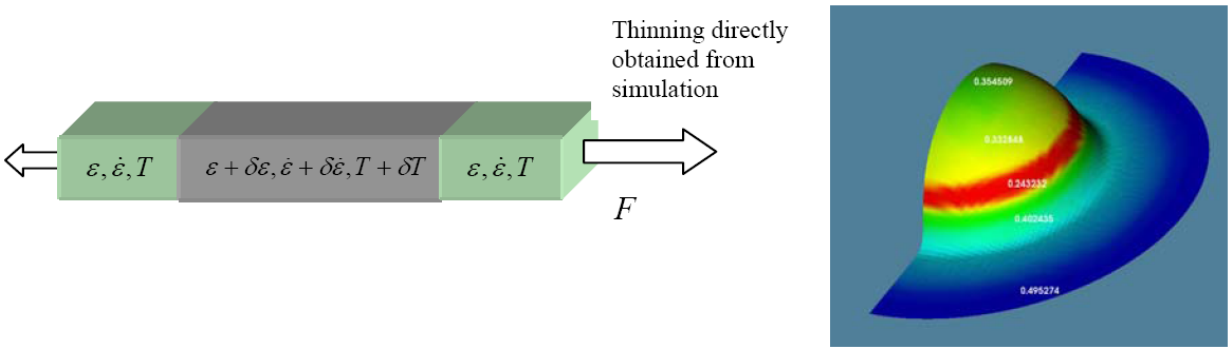

Figure 2.23 Quasi M-K criterion model developed by Hora et al. [79]

Dahan et al. [80] have developed a new experimental apparatus to perform experimental hot stamping tests. Specimens are heated in a furnace, afterwards they are moved to the Nakazima setup and deformed by means of the punch movement. A grid is etched on the specimen and the strain distribution is measured by means of *a posteriori* analysis using a patter recognising systems. The analysis scheme to determine the critical strain values is based on the Bragard method, which uses the extrema of the second derivative of the major strain to determine the critical major strain value and thus one point of the FLC through a polynomial function, as shown in Figure 2.24.

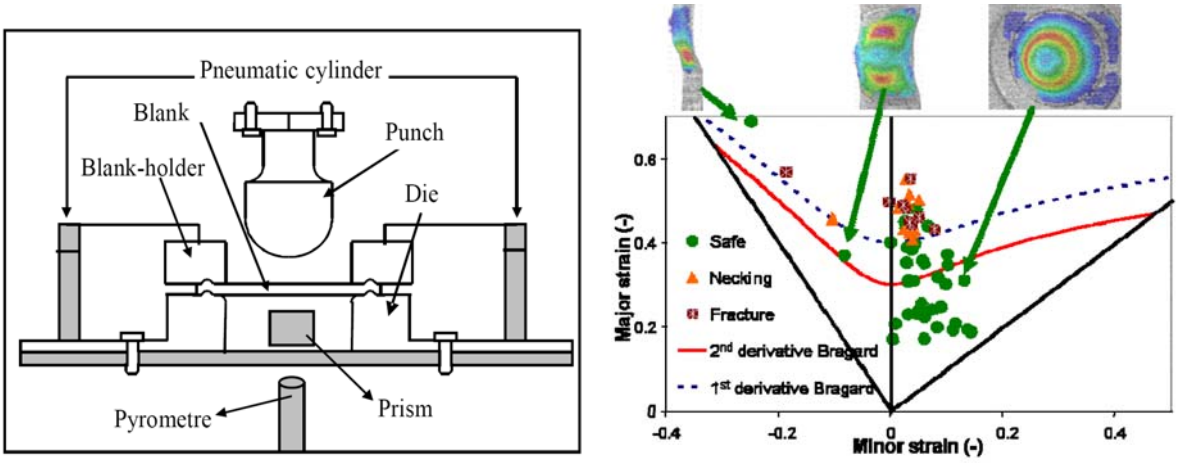

Figure 2.24 Experimental setup for the Nakazima hot stamping tests and USIBOR 1500 P® FLC determination trough the Bragard method [81]

A new experimental setup has been developed at the Chair of Manufacturing Technology at the University of Erlangen-Nuremberg to determine FLC at elevated temperature according to the significative characteristics of the hot stamping process [10], although no significative results have been published yet regarding the FLC of quenchenable high strength steels.

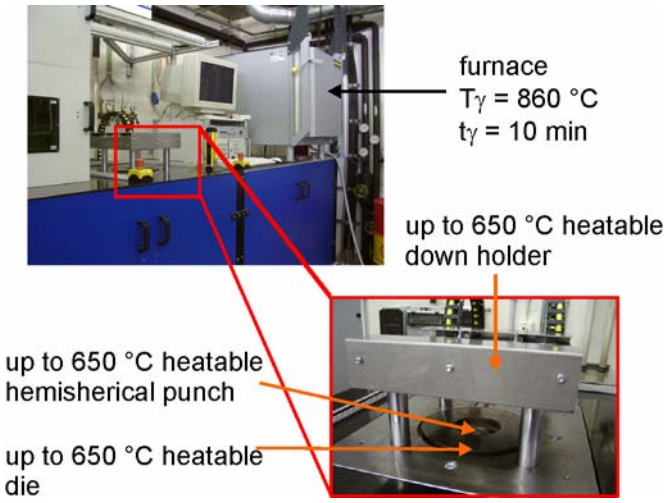

Figure 2.25 Experimental setup for the determination of FLC at elevated temperature [10]

Experimental investigations on the formability of quenchenable high strength steels at high temperature require the development of new testing procedures and experimental techniques that physically reproduce the conditions typical of the hot forming process and permit an accurate control of the thermal, mechanical and microstructural phenomena that occur during the tests, in order to properly describe the material limit strains in FE simulations and virtual process prototyping techniques when they are applied to hot stamping process.

CHAPTER 3
THERMO-MECHANICAL PROPERTIES

FE simulations are even more important in the optimization of the hot stamping process and the precise calibration of the numerical models is a strong requirement to obtain reliable results, nevertheless accurate data about the material behaviour can be hardly found in the scientific-technical literature.

Some investigations have been carried out to overcome this lack, and in § 3.1 the determination of the optimum process windows in terms of austenitization time and temperature is described. Furthermore, a new experimental apparatus which has been developed to study the rheological properties in the same thermo-mechanical conditions of the industrial process is shown in § 3.2.1. In the scope of this work the aluminium/silicon-based pre-coated high strength steel 22MnB5 has been investigated and the results regarding the flow curve in temperature, § 3.2, the plastic anisotropic evolution, § 3.3, and the influence of testing temperature on the Young's modulus and yield strength evolution, § 3.4, are afterward presented.

3.1 Microstructural process window

In the industrial hot stamping process the sheet is heated in the furnace in order to obtain a complete austenitization of the blank. One of the main issue is to guarantee a completely homogeneous microstructure after the austenitization: for this reason both the most suitable austenitization temperature and related holding time were determined in preliminary heating tests. This information could help in designing the thermal cycle the specimen had to be subjected during further experimental analysis.

The investigated material was the quenchenable high strength steel 22MnB5 with a thickness of 1.5mm; the sheet presented an aluminium/silicon-based coating to prevent oxidation and decarburization at elevated temperature. The tests were performed through the Gleeble 3800 thermo-mechanical simulator in order to obtained the desired thermal profile in the middle of the specimens. Figure 3.1 shows the temperature vs. time diagram of the testing procedure setup: samples were heated up at 10K/s to the austenitization temperature, held at this temperature and afterward the specimen were quenched by means of an air jet. The austenitization parameters are displayed in Table 3.1.

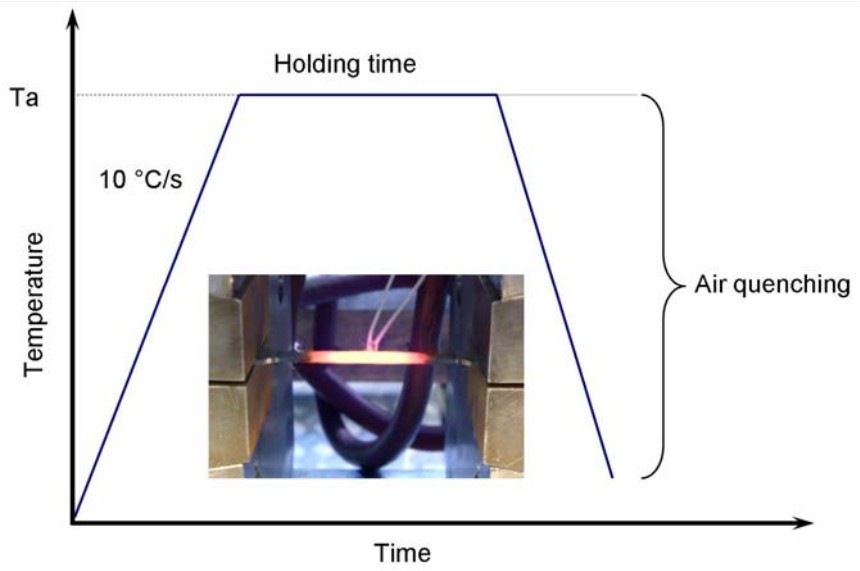

Figure 3.1 Thermal profile of the experimental austenitization tests

Table 3.1 Austenitization times and temperatures

Austenitization temperature [°C]	*Holding time [s]*			
850	*60*	*120*	*300*	*600*
900	*60*	*120*	*300*	*600*
950	*60*	*120*	*300*	*600*

Considering the resulting microstructure, an austenitization temperature of 850°C was not high enough to avoid the presence of non-transformed ferrite at room temperature as shown in Figure 3.2 (a), whereas a temperature of at least 900°C was necessary to obtain a complete austenitization together with a fully martensitic microstructure as displayed in Figure 3.2 (b).

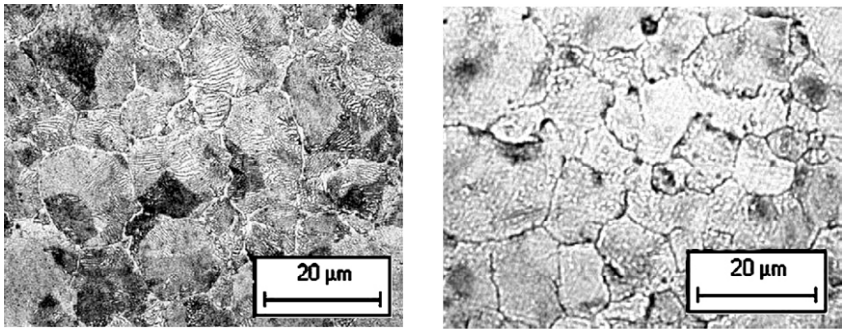

Figure 3.2 Micrographs of austenitized specimens after 5min at 850°C (a) and after 5min at 900°C (b)

The McQuaid-Ehn procedure was used to determine the influence of the testing parameters on the former austenite grain size of quenched specimens. An holding time of 5min assured an homogeneous austenitization in the gauge length of the specimen without a significant grain coarsening as shown in Figure 3.3.

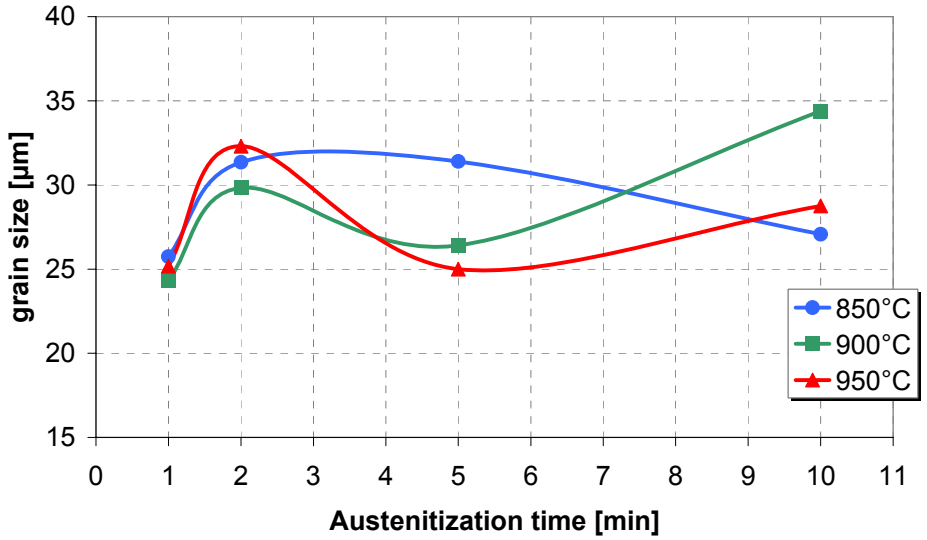

Figure 3.3 Austenitic grain size of quenched specimens after different austenitization times and temperatures

Several cooling tests were performed in order to determine the characteristic features of the CCT curves of the material. Different cooling rates were applied to the samples after an austenitization at 900°C for 5min, while monitoring the onset and the completion of the phase transformations by means of a radial dilatometer installed in the Gleeble machine (see the variation in sheet width vs. temperature as recorded through the dilatometer in Figure 3.4). The temperature of martensite start, that corresponds to the lower acceptable limit of the forming phase in the industrial process, was found to be 380°C. The martensite finish temperature was recognized to be about 300°C and this value has to be taken into account for the proper determination of the cooling time of stamped components into the water-cooled dies at the end of the hot stamping process.

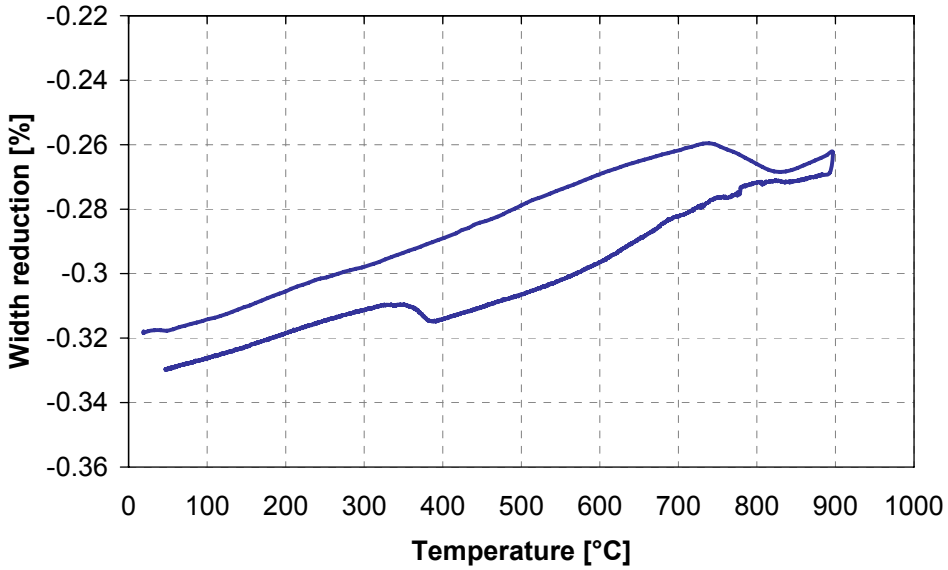

Figure 3.4 Dilatometer curve with a cooling rate of 50 K/s

Hardness measurements at room temperature were performed on the specimens used for the cooling tests in order to determine the resultant percentage of martensite, which is proportional to the hardness value. The trend displayed in Figure 3.5 allows to identify the critical cooling rate to avoid bainitic\ferritic transformation, that was recognized to be about 30K/s, as suggested by the steel supplier.

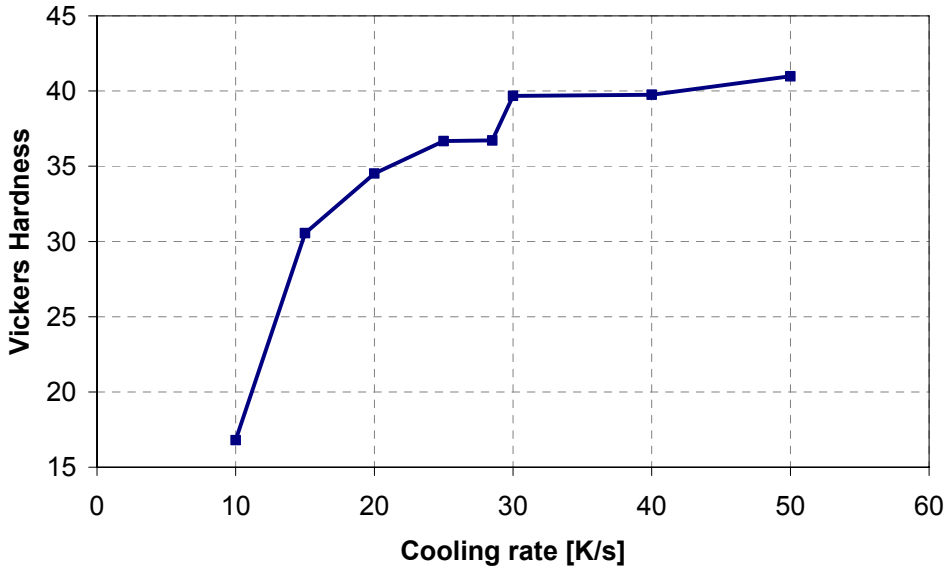

Figure 3.5 Vickers hardness at room temperature for different cooling rates

3.2 Flow curves in temperature

Data about the elasto-plastic properties of the sheet metal as function of temperature and strain rate can be hardly found in the literature, as well as the influence of applied stress and strain on the material phase transformation kinetics. To overcome this lack, a new experimental apparatus has been developed at the Chair of Manufacturing Technology at the University of Padova and an experimental campaign has been performed to evaluate the mechanical and microstructural properties of the 22MnB5.

3.2.1 Experimental apparatus

A new setup has been designed to reproduce the same thermo-mechanical conditions of the industrial press hardening process in a controlled experimental environment in order to study the rheological behaviour of sheet metal at elevated temperature. The apparatus consists of a 50kN MTS™ hydraulic testing machine, equipped with an inductive heating system connected to a 30kW high frequency power supply and with the ARAMIS-GOM™ optical measurement system, capable to detect the strain field during deformation, see Figure 3.6.

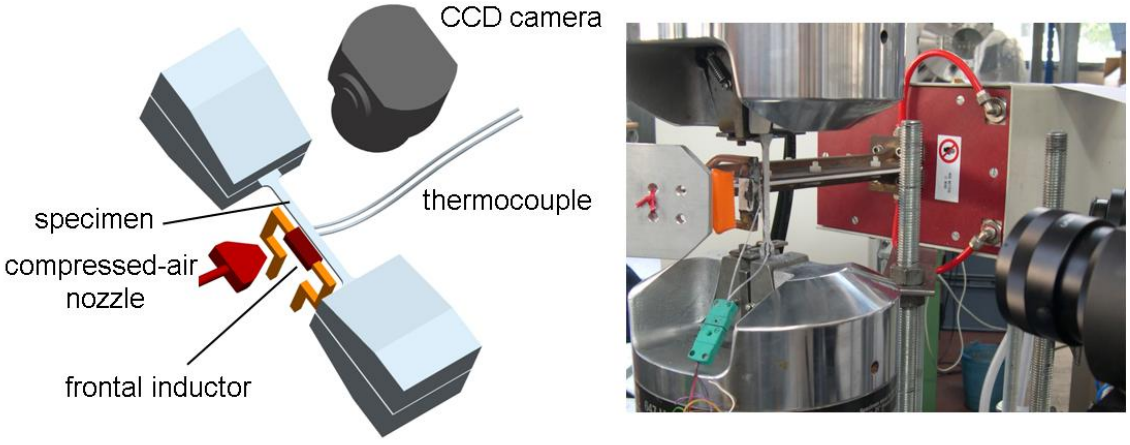

Figure 3.6 The new experimental setup developed at the University of Padova

The frontal inductor, which shape has been previously optimized through an infrared analysis in order to obtain an uniform thermal distribution in the gage length, can heat the sheet specimen up to 1200°C; the temperature evolution is measured by means of a K-thermocouple spot-welded in the centre of the specimen. Cooling rates up to 100K/s are

assured by using a compressed air jet, which pressure and intensity can be regulated by means of a pressure reducing valve.

The inductor is moved by means of a brushless motor, Figure 3.7, that can guarantee the correct positioning of the frontal coil in order to obtain the proper temperature distribution in the gage length of the specimen at the beginning of the test. This equipment also adjusts the vertical position of the inductor during the deformation phase to maintain the heated zone of the sheet centred with respect to the thermocouple position and to guarantee a constant and uniform thermal profile in the area of interest. The relative position of the inductor is kept under control during the test by means of a potentiometer connected to the support.

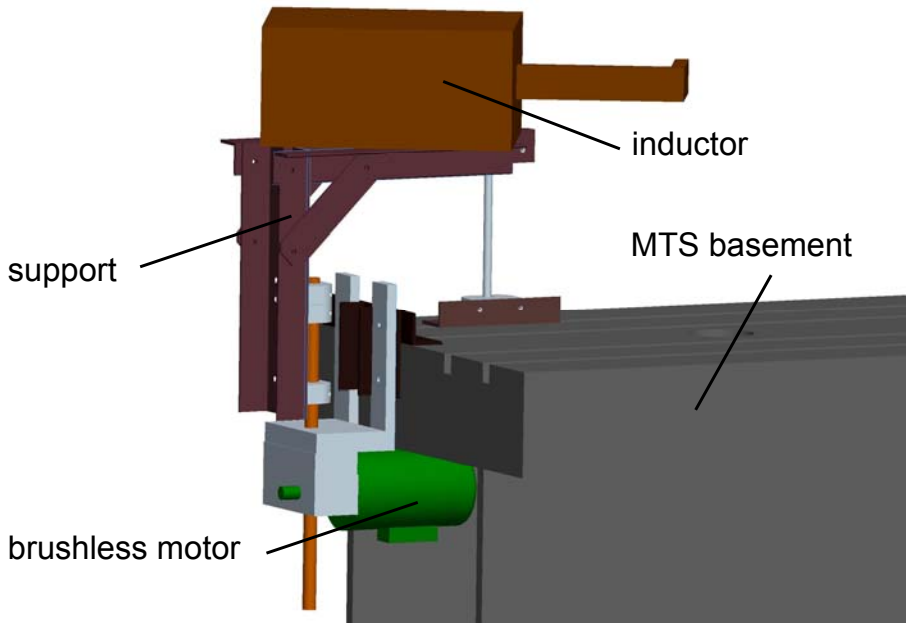

Figure 3.7 Inductor positioning system

The ARAMIS™ optical system is equipped with a 12Hz CCD camera placed in front of the specimen, on which an appropriate stochastic pattern is created in order to resist during deformation at elevated temperature and assure an accurate strain field measurement in the gauge lenth. In Figure 3.8 it is possible to notice the stochastic pattern sprayed on the surface of the tensile specimen and the corresponding major strain distribution measured by the ARAMIS™ system.

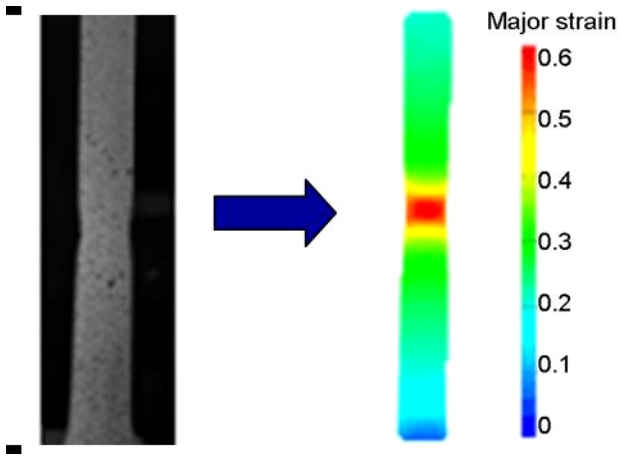

Figure 3.8 Stochastic pattern and ARAMIS™ strain field measurement

One of the big advantages of the ARAMIS™ system is the possibility to measure the strain distribution during deformation with a non-contact approach, nevertheless the maximum frame rate of 12Hz representes a limitation during high speed tests. The system has been therefore equipped with an external high speed camera to increase the acquisition rate in order to perform accurate measurement during tests at higher strain rate of $1s^{-1}$. A PIKE - AVT™ camera is connected to a National Instrument™ Compact Vision System CVS-1455 through a firewire cable and can acquire up to 60 frame per second.

Figure 3.9 AVT™ PIKE camera connected to the National Instrument™ CVS-1455

All the different devices and sensors are connected to a National Instrument™ CompactRIO, which is a control and acquisition system powered by reconfigurable I/O

FPGA technology. A dedicated LABVIEW™ program guarantees the achievement of the imposed thermal profile by adjusting the inductive power through a PID controller, synchronizes the tensile test together with the external camera image acquisition and with the vertical positioning of the inductor and saves all the acquired data (e.g. images, temperature profiles, inductor vertical position, load and stroke values) into a database for further elaborations.

3.2.1.1 Tensile test optimization

The stroke speed of the MTS hydraulic testing machine is set in order to obtain the desired average strain rate in tensile tests and it is generally kept as a constant value during all the deformation phase. The optical system allows to determine the true strain and strain rate evolution measured in this testing condition; Figure 3.10 shows the quasi-exponential major strain vs. stroke curve obtained when the velocity of the stroke is set equal to a constant value of 1.5mm/s to obtain an average strain rate of $0.1s^{-1}$.

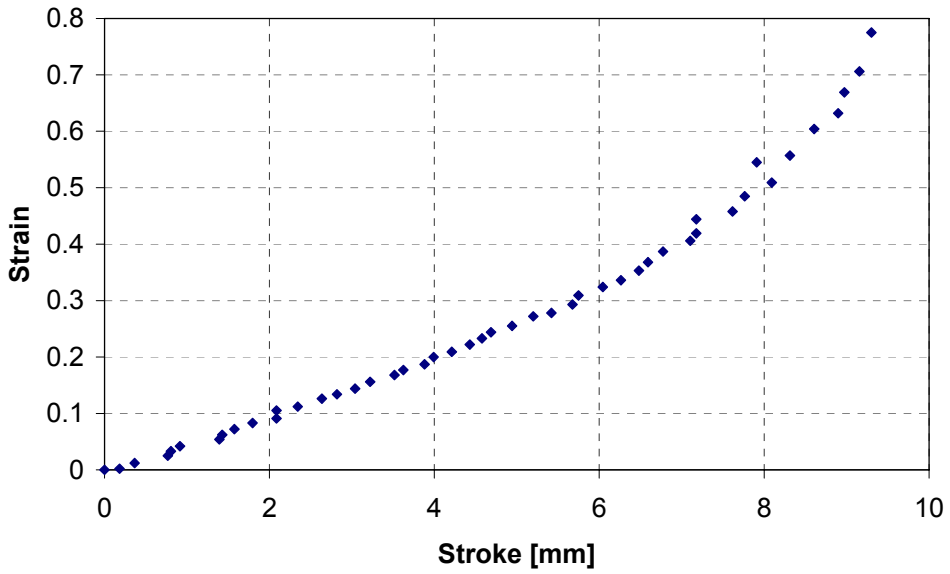

Figure 3.10 Typical major strain evolution during tensile tests with constant stroke speed

In Figure 3.11 it is possible to notice how the strain rate actually changes during the entire deformation, in fact it is lower than the imposed value at the beginning of the test and it rapidly increases after the onset of necking, thus contradicting the initial strain rate constancy assumption.

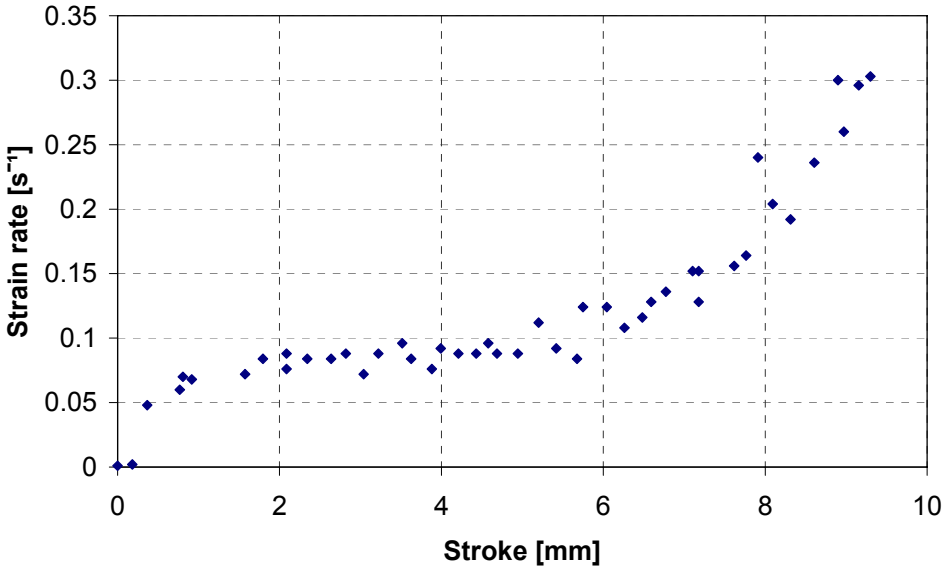

Figure 3.11 Typical strain rate evolution during tensile tests with constant stroke speed

In order to avoid this phenomenon and obtain an almost constant strain rate during the entire tensile test, the stroke speed was modified for all the different strain rate values (e.g. 0.01, 0.1 and $1s^{-1}$) through a trial-and-error approach by increasing the velocity in the first part of the tensile test and by reducing it at the end. The result obtained for the $0.1s^{-1}$ testing procedure optimization is shown in Figure 3.12.

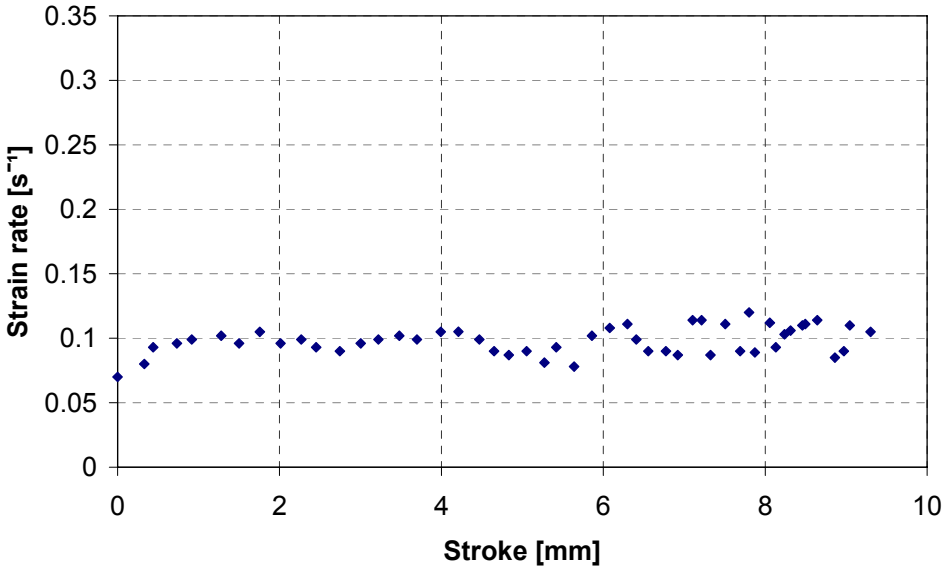

Figure 3.12 Strain rate evolution with the modified testing procedure ($0.1s^{-1}$)

3.2.2 Experiments and results

Uniaxial tensile tests were performed by means of the new apparatus in order to determine the influence of cooling rate, temperature and strain rate on the flow curves of the 22MnB5 under the typical conditions of the industrial hot stamping process. The specimen geometry was chosen according to the recommendation of ISO 10130.

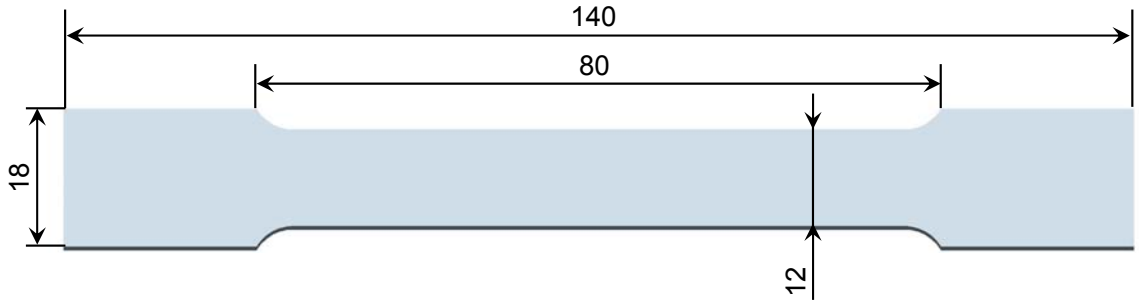

Figure 3.13 Tensile test specimen geometry

The same thermo-mechanical cycle that material undergoes during press hardening operations was therefore reproduced by means of the new experimental setup. The specimens were austenitized at 950°C for 3min, afterwards two different cooling rates equal to 30K/s and 50K/s were applied until the desired temperature *Ti* was reached as shown in Figure 3.14; isothermal tensile tests were afterwards performed at different temperatures and strain rates as summarized in Table 3.2. The stroke speed were set according to procedure described in the previous paragraph in order obtain a constant strain rate during the entire deformation. At least two test runs were carried out for each test condition to assure the repeatability of the results.

Table 3.2 Experimental parameters used for the tensile tests

Deformation temperature [°C]	*Strain rate [s^{-1}]*		
500	*0.01*	*0.1*	*1*
650	*0.01*	*0.1*	*1*
800	*0.01*	*0.1*	*1*

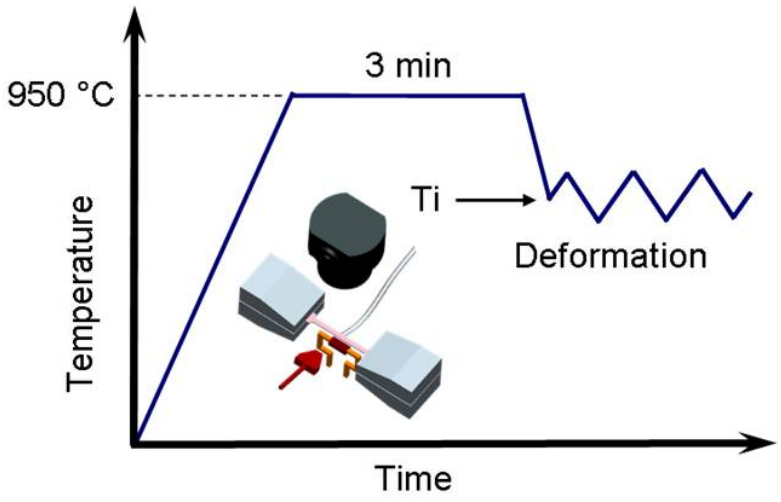

Figure 3.14 Thermo-mechanical cycle of the tensile tests

In order to increase the accuracy in the analysis of the acquired data, several stage points were taken in the transversal section of the specimen in correspondence of the uniform temperature distribution area. The major strain path was exported, values corresponding to the different points were averaged and finally the flow curve was calculated for each stage by correlating the averaged major strain to the MTS load values according to following equation:

$$\sigma = \frac{F}{w_0 \cdot t_0 \cdot e^{-\varepsilon}} \tag{3.1}$$

where F is the axial force, w_0 and t_0 the initial width and thickness of the specimen, ε the averaged logarithmic strain previously calculated and σ the resulting true stress.

The investigated steel 22MnB5 shows a similar behaviour at both cooling rates of 30K/s and 50K/s and exhibits a strong temperature dependency as shown in Figure 3.15. The strain rate also influence the material strength that strongly increases with enhancing strain rate and decreasing temperature, while the influence of the cooling rate is significant only at lower temperatures and velocities where microstructural phase transformation may occur during deformation, drastically changing the slope of the curve, Figure 3.16-17.

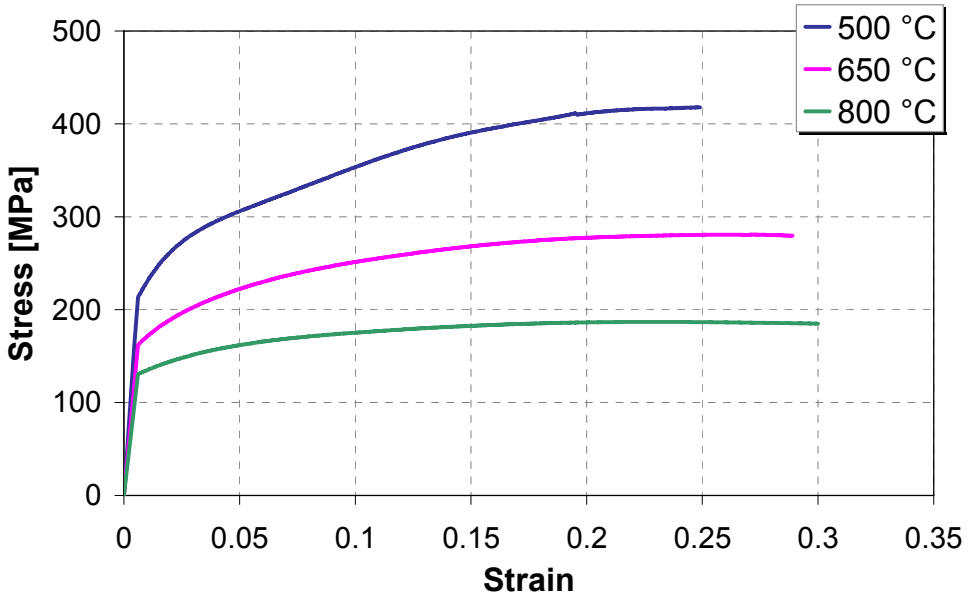

Figure 3.15 22MnB5 temperature sensitivity (strain rate of $1s^{-1}$ and cooling rate of 50K/s)

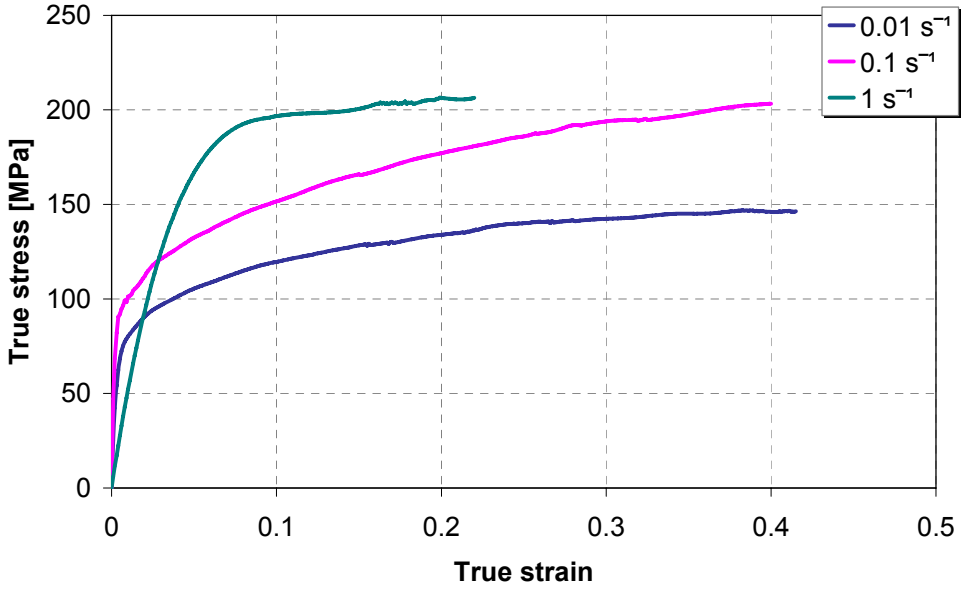

Figure 3.16 22MnB5 strain rate sensitivity (temperature of 800°C and cooling rate of 30K/s)

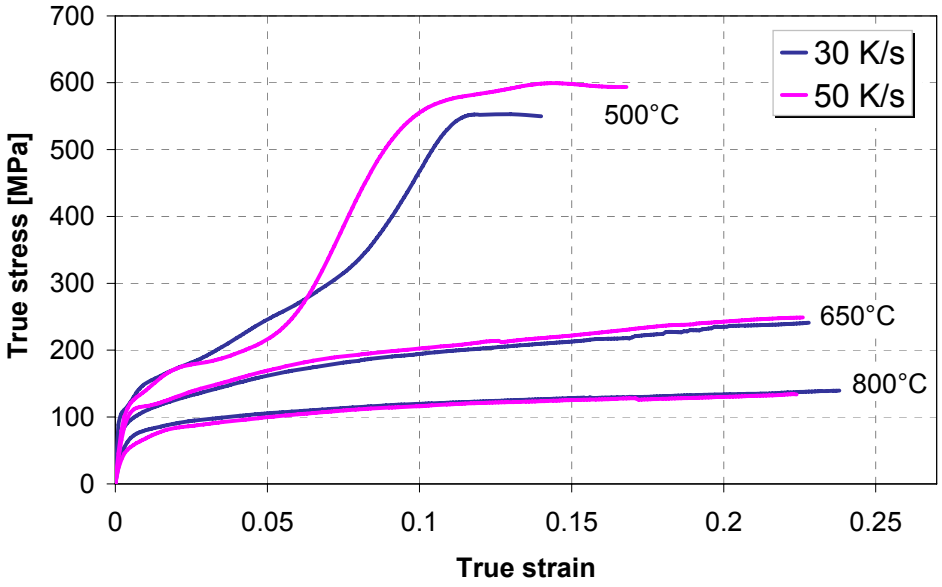

Figure 3.17 22MnB5 sensitivity to the cooling rate (strain rate of $1s^{-1}$)

3.3 Plastic anisotropy evolution

Recently, many models and yield criteria for anisotropic material have been proposed and implemented in FE codes for numerical simulations of sheet metal forming processes, so the quality of computational results is strongly influenced by the accuracy of the variables implemented to describe the material behaviour. Anisotropy is one important mechanical property influencing sheet metal forming operation and it is a result of the crystallographic structure acquired during the thermo-mechanical processing of the blank. A new analysis procedure was developed and the experimental apparatus described in § 3.2.1 was used to evaluate the influence of testing parameters on the plastic anisotropic coefficients of the hot stamping steel 22MnB5.

3.3.1 Analysis procedure

An official guideline to determine anisotropic coefficients at elevated temperatures still not exists, therefore a new procedure has been developed to increase the accuracy in the analysis of the data acquired by the ARAMIS™ optical measurement system. Several stage points were taken in correspondence of the transverse section of the specimen, Y axis in Figure 3.18, then the mayor and the minor strain paths were exported and values corresponding to the different points were averaged.

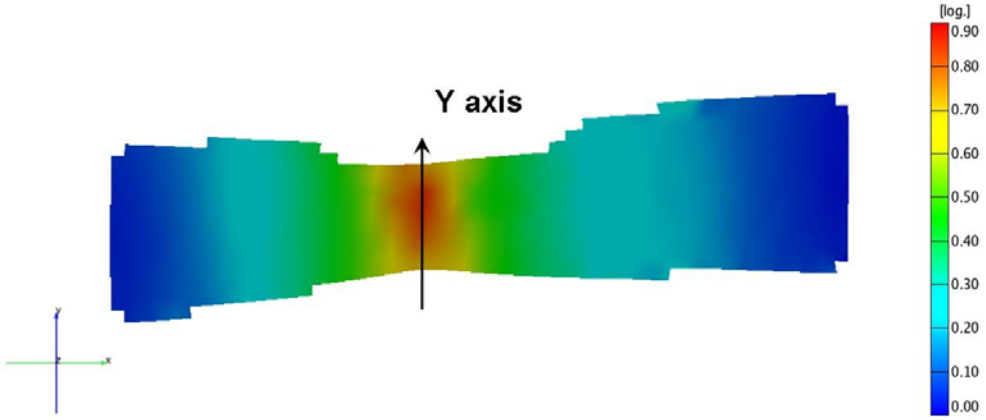

Figure 3.18 True strain field measured through the ARAMIS™ optical system

Normal anisotropy *r* was calculated for each stage according (3.2) where ε_1 is the longitudinal true strain, ε_2 the true strain in width direction and ε_3 the true strain in thickness direction, calculated by assuming the volume constancy during plastic deformation.

$$r = \frac{\varepsilon_2}{\varepsilon_3} = -\frac{\varepsilon_2}{\varepsilon_1 + \varepsilon_2} \tag{3.2}$$

A common trend was noticed in the evolution of normal anisotropy during the entire tensile test: the values considerably fluctuated in correspondence of the initial part of the tensile curve, then they approached nearly a constant value. Plastic anisotropy was therefore calculated averaging the data in that one characterized by uniform deformation before the onset of necking, corresponding the reaching of the maximum force value, as shown in Figure 3.19.

The *r*-values were determined for tensile specimens cut at 0°, 45° and 90° with respect to the rolling direction of the sheet in order to investigate the material anisotropic behaviour. The coefficients of the normal anisotropy $\bar{r}_n$ and the planar anisotropy Δr were therefore calculated according to the following equations:

$$\bar{r}_n = \frac{1}{4}(r_0 + r_{90} + 2r_{45}) \tag{3.3}$$

$$\Delta r = \frac{1}{2}(r_0 + r_{90} - 2r_{45}) \tag{3.4}$$

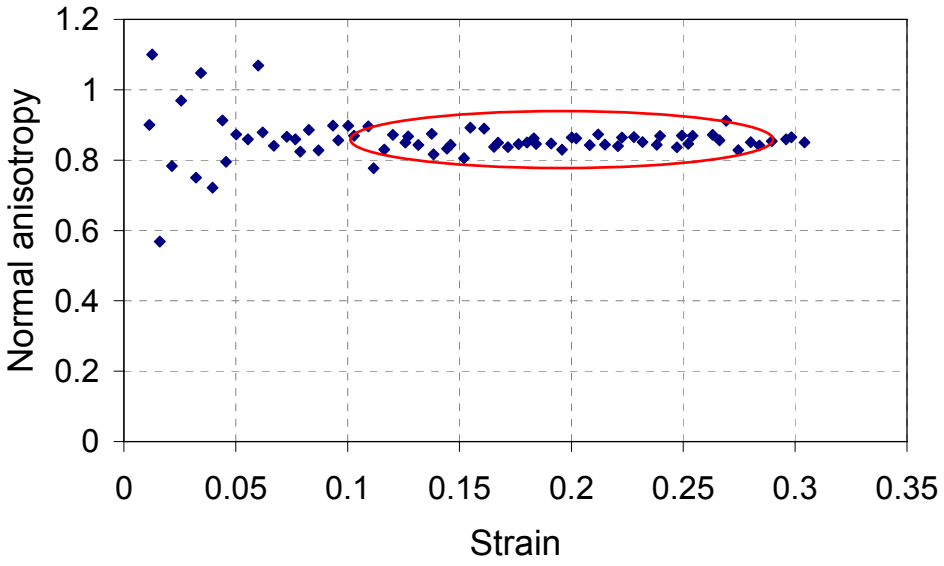

Figure 3.19 Independency of the normal anisotropy r from the true strain (deformation at 800°C – 0.01s^{-1})

3.3.2 Results and discussion

Uniaxial tensile tests were performed by means of the new setup in order to evaluate the influence of cooling rate, temperature and strain rate on the plastic anisotropy evolution of the 22MnB5. The tensile specimens were austenitized at 950°C for 3min, chilled down at the desired temperature with cooling rate of 30K/s and 50K/s and deformed at constant strain rate. The testing parameters are given in the following Table 3.3

Table 3.3 Experimental parameters used for the tensile tests

Deformation temperature [°C]	*Strain rate [s^{-1}]*		
500	*0.01*	*0.1*	*1*
650	*0.01*	*0.1*	*1*
800	*0.01*	*0.1*	*1*

In Figure 3.20 it is possible to notice the normal anisotropy evolution for specimens cut at 0°, 45° and 90° with respect to the rolling direction of the sheet during deformation at 0.1s^{-1} and 800°C.

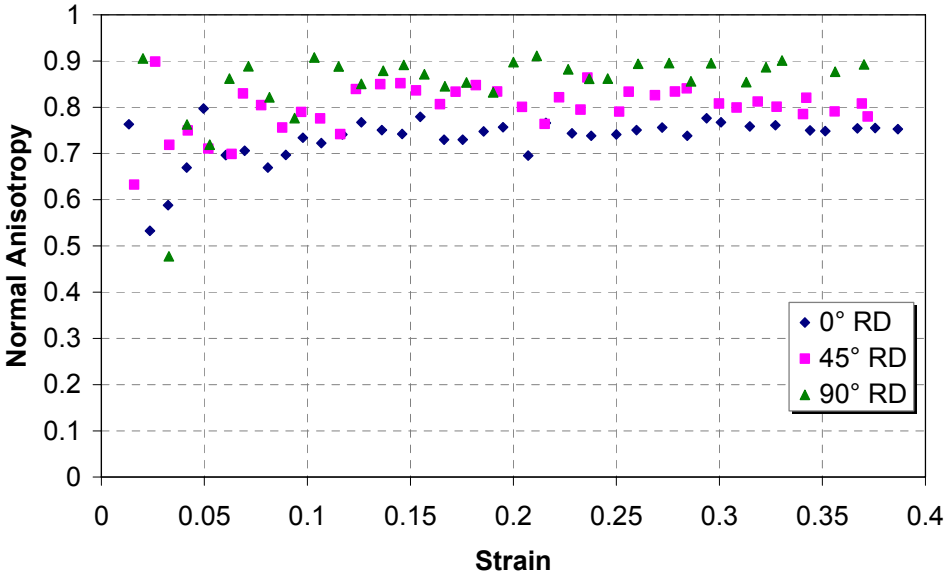

Figure 3.20 Average normal anisotropy sensitivity to temperature and strain rate (cooling rate of 30K/s)

The normal anisotropy in dependency of the rolling direction was determined for each test condition in order to determine the average normal anisotropy $\bar{r}_n$ and planar anisotropy Δr through the above described procedure; the obtained results are shown in the following figures with their standard deviation.

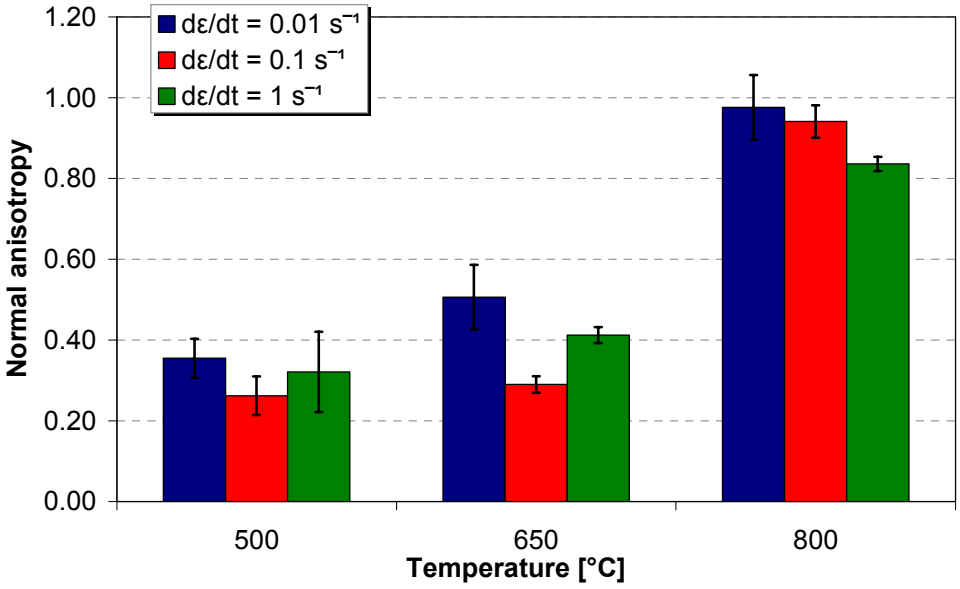

Figure 3.21 Average normal anisotropy sensitivity to temperature and strain rate (cooling rate of 50K/s)

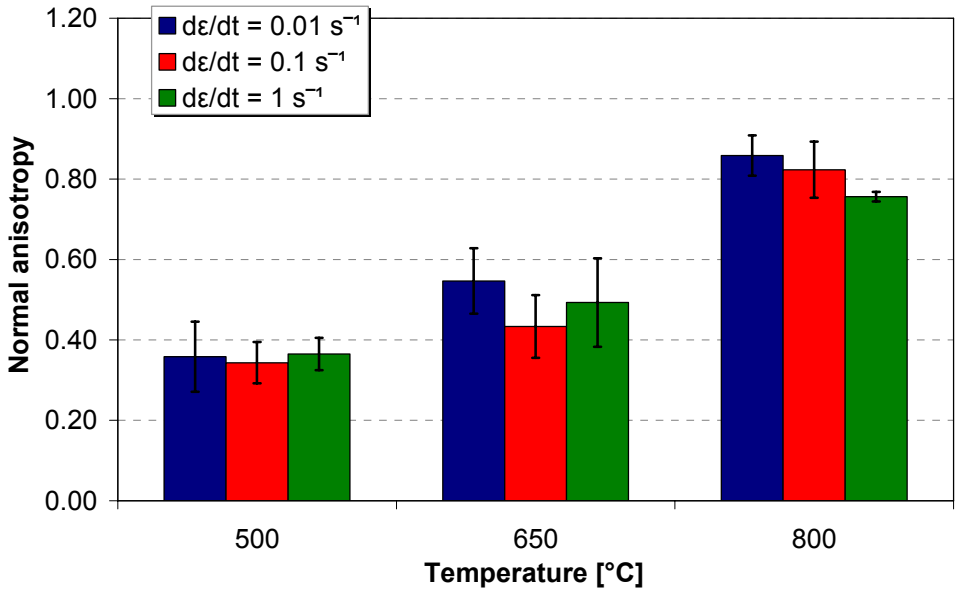

Figure 3.22 Average normal anisotropy sensitivity to temperature and strain rate (cooling rate of 30K/s)

The average normal anisotropy was strongly affected by the deformation temperature, in fact at 800°C the material showed an almost isotropic behaviour, while the anisotropic tendency increased with decreasing temperature. Normal anisotropy sensitivity to strain rate was less pronounced and the influence of microstructural evolution should be considered for a better comprehension of this phenomenon because of the possible bainitic phase transformation during deformation at lower strain rates. The material exhibited a similar trend with both cooling rates of 30K/s and 50K/s.

The planar anisotropy was approximately equal to zero in all testing condition, as shown in Tables 3.4 and 3.5, because the crystallographic grain orientation due to the sheet rolling practically disappeared after austenitization.

Table 3.4 Influence of temperature and strain rate on planar anisotropy with a cooling rate of 30K/s

30 K/s		*Temperature [°C]*		
		500	*650*	*800*
Strain rate [s^{-1}]	*0.01*	*0.13*	*-0.07*	*0.05*
	0.1	*-0.02*	*0.06*	*0.06*
	1	*-0.06*	*0.14*	*0.02*

Table 3.5 Influence of temperature and strain rate on planar anisotropy with a cooling rate of 50K/s

50 K/s		*Temperature [°C]*		
		500	*650*	*800*
Strain rate [s^{-1}]	*0.01*	*0.13*	*-0.11*	*-0.06*
	0.1	*0.10*	*0.03*	*-0.07*
	1	*0.01*	*0.01*	*-0.12*

Considering these results, the forming of the blank in the industrial process should be performed as soon as possible after austenitization in order to avoid the sheet cooling and to form the component at the highest temperature, combining the advantages of lower loads on tools and increased formability. In fact the higher normal anisotropy at elevated temperature allows deeper parts to be drawn due to the greater resistance to thinning and strength in the through-thickness direction, and may reduce the chance of wrinkling or ripples in the component. In addition the disappearance of planar anisotropy after austenitization strongly reduces the importance of the orientation of the sheet with respect to the die or the part to be formed and decreases asymmetric forming and earing.

3.4 Elastic properties

The experimental device described in § 3.2.1 was modified in order to evaluate the influence of testing temperature on the 22MnB5 elastic properties by means of an axial extensometer.

3.4.1 Testing procedure

The apparatus previously described was modified to study the Young's modulus and yield strength evolution of sheet metal at elevated temperature through the data analysis of extensometer measurements. In this new configuration, the optical system was replaced by an air-cooled MTS 632.52 high temperature axial extensometer, appropriately adapted to reduce the distance between the extension rods to 11mm in order to obtain a gage length with a uniform temperature distribution, as shown in Figure 3.23.

The 22MnB5 specimens were austenitized at 900°C for 3 minutes, afterward a cooling rate of 50K/s was applied and tensile tests were performed at constant temperature in the range between 900°C and 20°C.

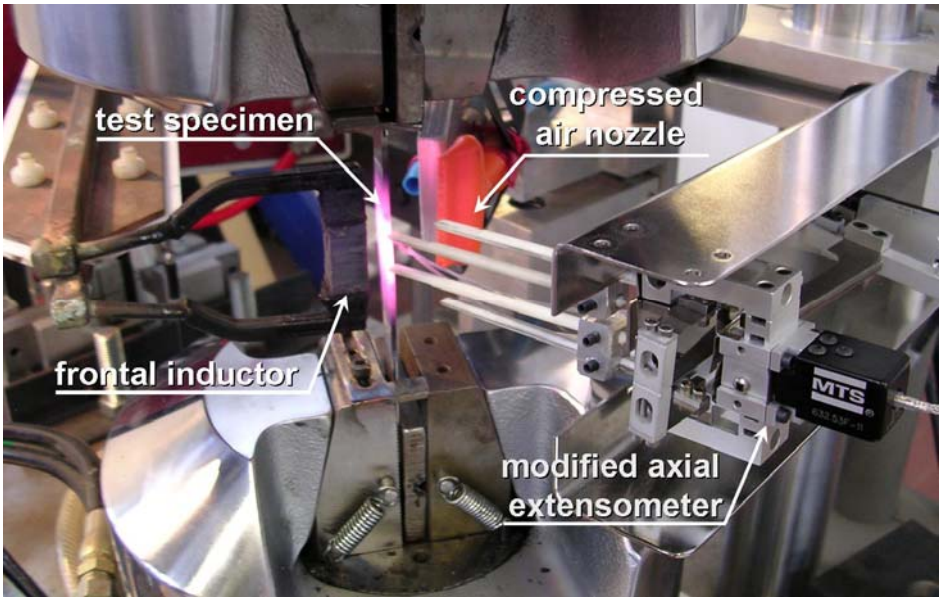

Figure 3.23 Experimental apparatus with the modified axial extensometer

3.4.2 Results

The extensometric measurements were elaborated according to the ASTM guideline [82]. The Young's modulus was calculated as the slope of the first part of the tensile curve, as displayed in Figure 3.24 for the test performed at 500°C, while the yield strength was determined by means of the 0.2% offset method.

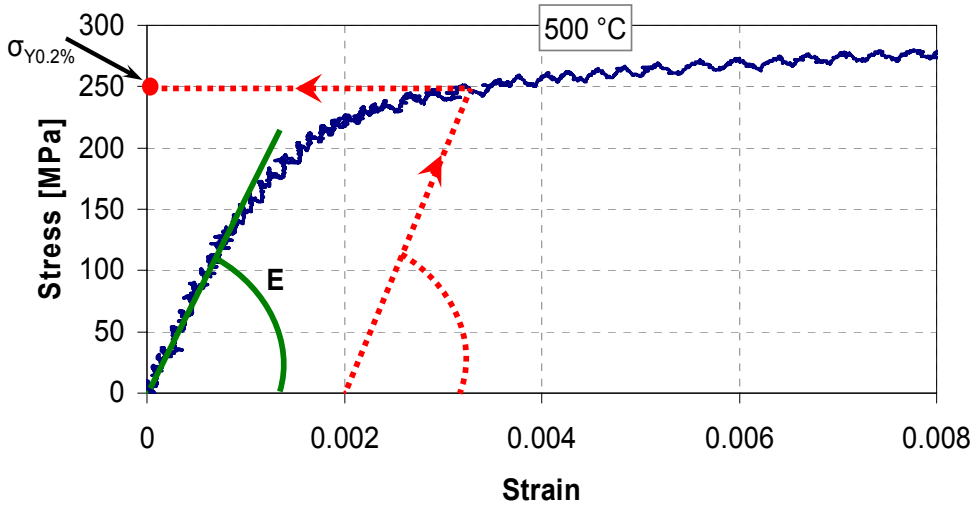

Figure 3.24 Young's modulus and yield strength $\sigma_{Y0.2\%}$ analysis procedure

Tensile tests were performed with steps of 100°C from room temperature up to 900°C and the extensometric results at different temperatures are reported in the following figures, divided in the two ranges 20-400°C and 500-900°C.

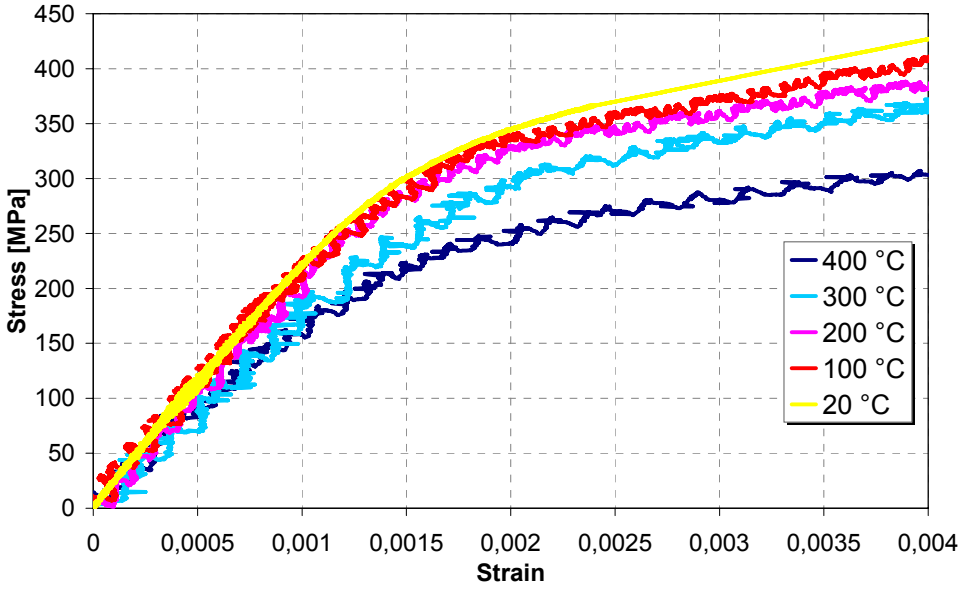

Figure 3.25 Extensometric results in the range 20-400°C

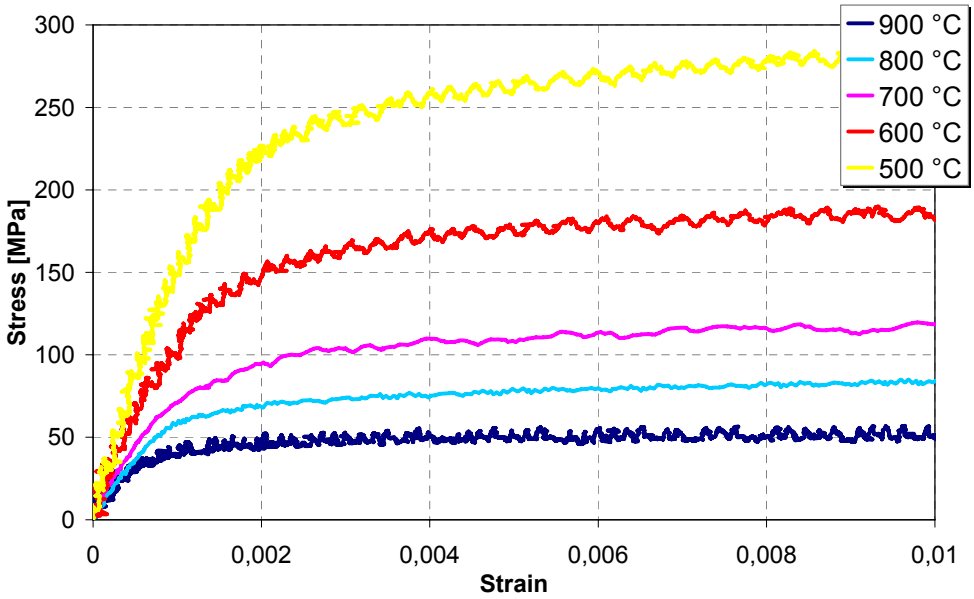

Figure 3.26 Extensometric results in the range 500-900°C

Table 3.6 shows the Young's modulus and yield strength evolution with temperature of the high strength steels 22MnB5 after austenitization. The testing temperature has a strong influence on the elastic properties of the material which drastically decrease with enhancing deformation temperature, see Figure 3.27 and Figure 3.28, and the lower elastic modulus values allow to reduce springback phenomena and therefore increase the accuracy of stamped components in hot forming operations.

Table 3.6 Elastic modulus and yield strength evolution with temperature

Temperature [°C]	***20***	***100***	***200***	***300***	***400***	***500***	***600***	***700***	***800***	***900***
Young's modulus [GPa]	*212*	*205*	*200*	*164*	*158*	*140*	*95*	*62*	*55*	*45*
Yield strength $_{0.2\%}$ [MPa]	*370*	*362*	*350*	*338*	*295*	*254*	*167*	*95*	*72*	*46*

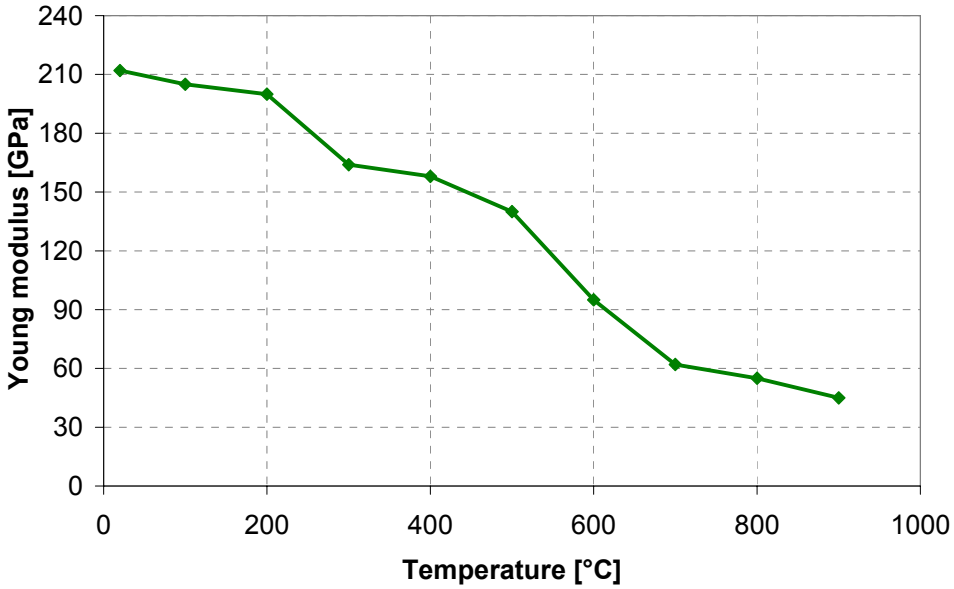

Figure 3.27 Young's modulus evolution with temperature

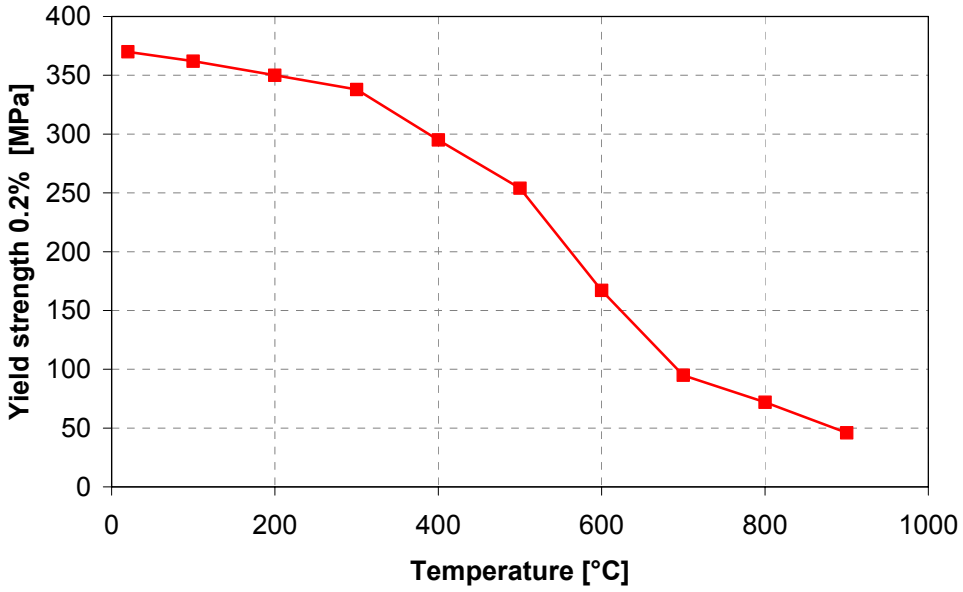

Figure 3.28 Yield strength $\sigma_{Y0.2\%}$ evolution with temperature

3.5 Conclusions

In hot stamping operations an accurate evaluation of the influence of process parameters on the properties of final sheet components is fundamental to the design and optimization of the forming process.

22MnB5 optimum process window and phase transformation data were identified through thermal tests reproducing the industrial conditions. A new experimental apparatus equipped with an inductive heating was developed to study the material rheological behaviour in the same thermo-mechanical conditions of the industrial hot stamping process. Uniaxial tensile test were therefore performed at different temperatures and strain rates, so material flow curves were determined together with the anisotropic coefficients evolutions through the optical measurement system ARAMIS™. The material exhibits a strong sensitivity to temperature and strain rate while the cooling rate after austenitization modifies the rheological behaviour only when phase transformations occurs during deformation. The material is almost isotropic at 800°C, while the normal anisotropy decreases with decreasing temperature and the planar anisotropy practically disappears after austenitization. An extensometric analysis was also carried out to evaluate the Young's modulus and yield strength evolution with temperature.

CHAPTER 4
PHASE TRANSFORMATION KINETICS

Press hardening is a non-isothermal process where deformation takes place simultaneously with quenching, therefore particular attention has to be paid to the evaluation of the influence of applied stress and strain on the phase transformation kinetics in order to gain more reliable results from the numerical simulations of the hot stamping operations.

The new experimental apparatus, described in the previous chapter, was used to determine the 22MnB5 transformation plasticity of phases occurring from austenitization to room temperature by means of extensometric analyses, as displayed in § 4.1. The influence of applied stress and strain on the microstructural transformation kinetics of the material was also investigated and the results regarding the shift of the TTT curves for the ferritic and bainitic transformation are presented in § 4.2.

4.1 Transformation plasticity

The transformation plasticity strain is a plastic strain which arises when a phase transformation occurs in presence of an applied load, even if this load is lower than the yield strength of the weaker phase [38]. A permanent strain can appear during phase transformation due to the differences in the phases specific volumes [83] and this phenomenon can become more and more relevant when thermal stresses are superimposed. From this standpoint, it can be deduced that transformation plasticity appears each time the stress which arises can be considered external with reference to the growing-up phase.

The 22MnB5 transformation plasticity strain has been therefore evaluated in order to be implemented in the thermo-mechanical-metallurgical FE models and to increase the accuracy of the hot forming numerical simulations.

4.1.1 Testing procedure

The testing procedure suggested by Taleb [38] was adapted to the new experimental equipment configuration, described in § 3.4.1, in order to accurately evaluate the transformation plasticity strain for each phase transformation occurring to 22MnB5 from austenitization to room temperature. All the tests were carried out on the new apparatus capable to perform coupled thermal and mechanical cycles and to assure an accurate control of all testing parameters, during the tests the phase transformation starting and ending where monitored through the modified axial extensometer.

The procedure consists of two cycles. In the firs cycle, a free dilatometric test is performed on the tensile specimen, which is austenitized at 900°C, held in temperature for 3min and then cooled down until room temperature; the cooling rate is chosen according to the CCT curves to obtain the desired microstructure. Then the transformation plasticity test is performed by superimposing a mechanical cycle to the thermal one, by applying a load just before the onset of the phase transformation to investigate, see Figure 4.1. At the end, metallographic analyses are performed to be sure that the desired transformation is achieved and to check the effectiveness of the applied thermal cycle.

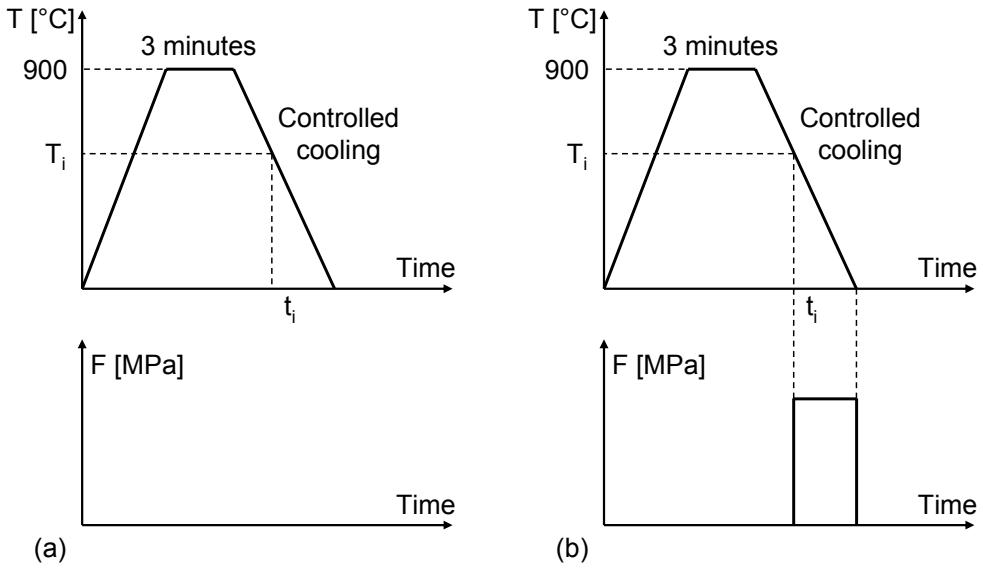

Figure 4.1 Testing procedure: free dilatometric test (a) and transformation plasticity test (b)

The total strain can be calculated as:

$$\varepsilon^{tot} = \varepsilon^{th} + \varepsilon^{el} + \varepsilon^{p} + \varepsilon^{tp} + \varepsilon^{vp} \tag{4.1}$$

where ε^{tot} is the total strain, while ε^{th}, ε^{el}, ε^{p}, ε^{tp}, ε^{vp} are, respectively, the thermal, elastic, plastic, transformation plasticity and viscoplastic components of the strain.

Some assumption permit to simplify the calculation by neglecting some contributions in (4.1). If the applied stress external to the growing-up phase is lower than the yield stress of the weaker phase present at the beginning of the structural transformation, it can be supposed that the classic plastic strain ε^{p} is negligible. As regards ε^{vp}, it seems important to underline that viscoplasticity is a very complex phenomenon which depends both from the temperature at which the load is applied and on its duration; moreover its contribution

can be difficulty quantified. However viscoplastic strain can also be neglected if the stress is applied in the range where creep phenomena are less significant.

Finally the transformation plasticity strain can be estimated as:

$$\varepsilon^{tp} = \varepsilon^{tot} - \varepsilon^{th} - \varepsilon^{el} \tag{4.2}$$

where ε^{tot} and ε^{th} are deduced from the dilatometric tests, while ε^{el} can be calculated through the Hooke's law. The model expressing the transformation plasticity strain as function of the applied load is:

$$\varepsilon^{tp} = k \cdot g(Z) \cdot \sigma \tag{4.3}$$

where k is called the transformation plasticity coefficient, σ is the applied stress and Z the volume proportion of the product phase. (4.3) can be written as follows where the function $g(Z)$ is equal to 1 when the transformation is complete:

$$k = \frac{\varepsilon^{tp}}{g(Z) \cdot \sigma} \tag{4.4}$$

Z can be estimated as:

$$Z = \frac{\varepsilon^{th} - \alpha_1 \left(T - T^{\alpha}\right) + \Delta\varepsilon_{12}^{T^{\alpha}}}{\left(\alpha_2 - \alpha_1\right) \cdot \left(T - T^{\alpha}\right) + \Delta\varepsilon_{12}^{T^{\alpha}}} \tag{4.5}$$

for diffusive transformation (ferrite, pearlite and bainite) and as:

$$Z = 1 - e^{\left[c\left(M_s - T\right)\right]} \tag{4.6}$$

for non-diffusive transformation (martensite).

In (4.5) and (4.6) α_1, α_2 and $\Delta\varepsilon_{12}^{T^{\alpha}}$ are deduced from the free dilatometric tests while c is a kinetic parameter whose value can be considered equal to 0.011 [84]. α_1 is the thermal dilatation for the γ phase, α_2 is the thermal dilatation coefficient for the α phase, $\Delta\varepsilon_{12}^{T^{\alpha}}$ is the difference between thermal strain of α and γ phases at the reference temperature T^{α} = 25°C and ε^{th} is the thermal strain. When austenite transform in the mixture phases ferrite+pearlite, Z is calculated as the sum of the two volume proportion.

(4.5) can be equivalently written as:

$$\varepsilon^{th} = \alpha\left(T - T^{\alpha}\right) + \left(1 - Z\right)\Delta\varepsilon_{12} \tag{4.7}$$

where:

$$\alpha = Z\alpha_2 + (1 - Z)\alpha_1 \tag{4.8}$$

$$\Delta\alpha_{12} = \left(\alpha_{\alpha} - \alpha_{\gamma}\right)\Delta T - \Delta\varepsilon_{12}^{25°C} \tag{4.9}$$

It is important to underline that the definition of the plasticity coefficients previously described is valid only for mono-axial tests, in case of multi-axial loads this definition has to be modified [85].
In the following paragraphs, the experiments carried out to determine the transformation plasticity of phases in which 22MnB5 can transform during cooling from austenitization conditions will be described and main results will be discussed.

4.1.2 Ferrite + pearlite

The tests were performed on new specimen of 22MnB5 prepared following the ISO 10130 recommendations. The cooling rate was chosen in order to maximize the percentage of ferrite+pearlite at room temperature, according to the CCT curves of the material (Figure 2.3). The parameters characterizing the thermal cycle are summarized in Table 4.1.

Table 4.1 Thermal cycle parameters

Heating rate [K/s]	*Austenitization temp. [°C]*	*Soaking time [s]*	*Cooling rate [K/s]*
10	*900*	*180*	*1.5*

The occurring of phase transformation can be observed in Figure 4.2. During the heating phase the dilatation of the specimen and the transformation from α-iron and γ-iron could be seen.

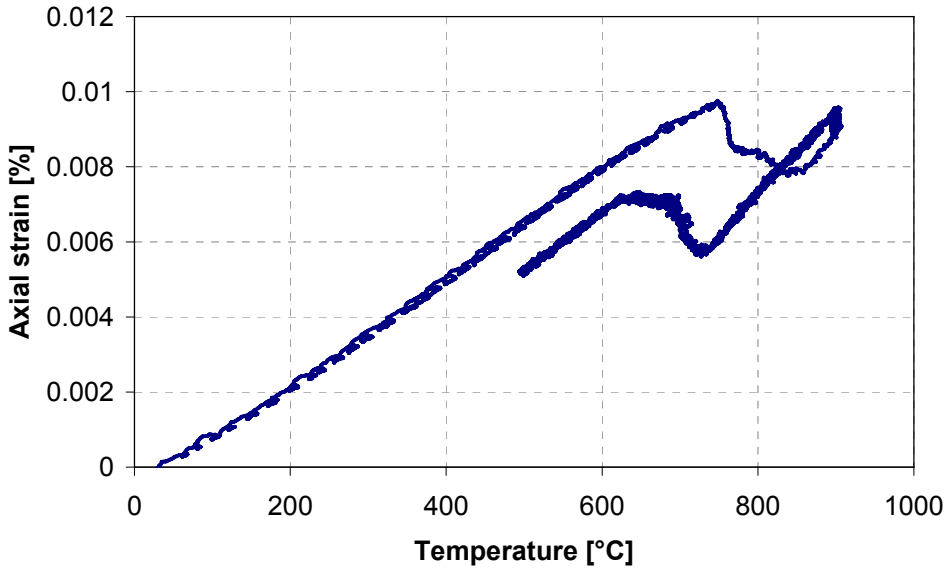

Figure 4.2 Stress-free curve

Then cooling was characterized by changes in the specimen dimension and the ferritic phase transformation was evidenced by a variation of the axial strain as the ferritic specific volume is different than the austenitic one. Some important information were obtained from Figure 4.2, such as the temperature at which ferrite started growing up and the temperature of the transformation end. Also the field characterizing the presence of γ-iron was determined. These data are reported in the following table:

Table 4.2 Relevant thermal parameters

Ac_1 [°C]	Ac_2 [°C]	F_S [°C]	F_F [°C]	α_α [$°C^{-1}$]	α_γ [$°C^{-1}$]	$\Delta\varepsilon_{12}$
752	835	727	629	$1.45 \cdot 10^{-5}$	$2.28 \cdot 10^{-5}$	0.0011

where Ac_1 and Ac_3 identify the start and the end of γ transformation, F_S and F_F the limits of the ferritic\pearlitic transformation and $\Delta\varepsilon_{12}$ is the thermal strain due to the different microstructure.

4.1.2.1 Determination of transformation plasticity

The thermal cycle previously described was used in the tests with the applied stress; the procedure followed in the experiments was:

- Heating from room temperature up to 900°C with heating rate of 10K/s
- Soaking at 900°C for 3min
- Cooling from 900°C with a cooling rate of 1.5K/s
- Constant load application during cooling starting from 750°C

The applied elastic stresses are summarized in Table 4.3

Table 4.3 Levels of applied stress during tests

Test	1	2	3	4
Stress [MPa]	12.5	25	37.5	50

The corresponding load to be applied were easily calculated as the section dimensions of the specimen were known. It has to be remarked that the stress was applied before the onset of phase transformation in order to avoid any influence on the kinetics of phase transformation during loading. In Appendix A the curves representing axial strain as function of temperature obtained from the tests with applied stress are shown.

The calculation of the transformation plasticity strain was carried out starting from the results obtained from the modified axial dilatometer and following the procedure indicated in [38]. For all test conditions the strain vs. temperature were cut and aligned at 740°C, differences arising in the calculated strain were mainly due to the elastic component of the strain and the creep deformation, see Figure 4.3.

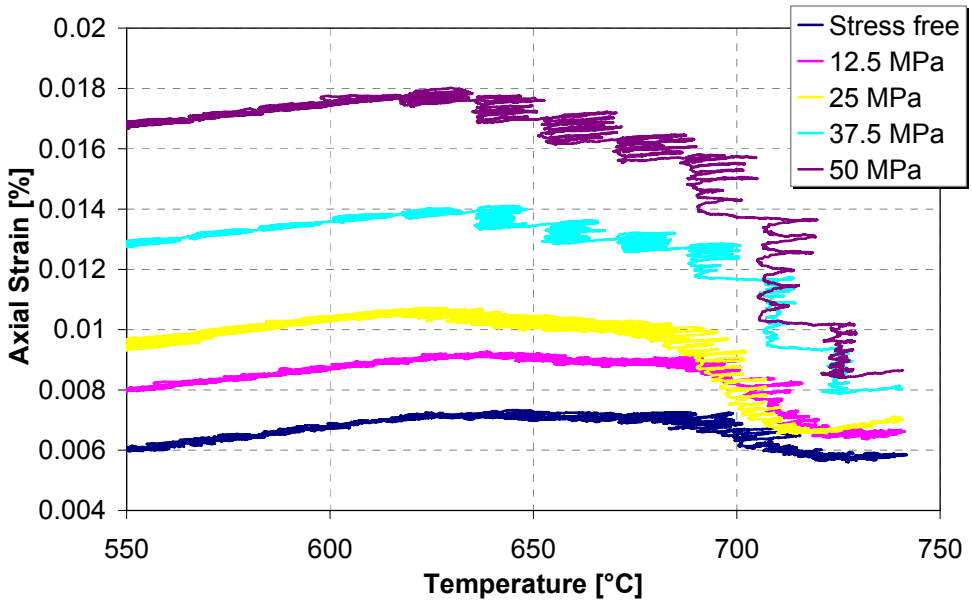

Figure 4.3 Total strain for the five tests

However it was estimated that strain due to creep was negligible with the considered loads, therefore the shift of the curves was ascribed to the elastic deformation and the curves were reasonably set to zero at 740°C. All data were filtered in order to eliminate noise and the calculations were made on them. Then transformation plasticity strain was calculated as the difference from the strain measured in stress-free tests and the one measured in the stressed ones, Figure 4.4.

The application of different level of stress was responsible of changes in the transformation kinetics which justified the differences in the temperatures at which the phase transformation started. However the effect of these differences was estimated to be negligible on calculations. The total amount of transformation plasticity strain corresponds to the maximum value of strain obtained from test at the end of transformation, as suggested by literature. The average value of ε^{tp} was therefore calculated for the different

loads in the plateau zone, as summarized in Table 4.4, and the influence of the applied true stress on ε^{tp} is displayed in Figure 4.5.

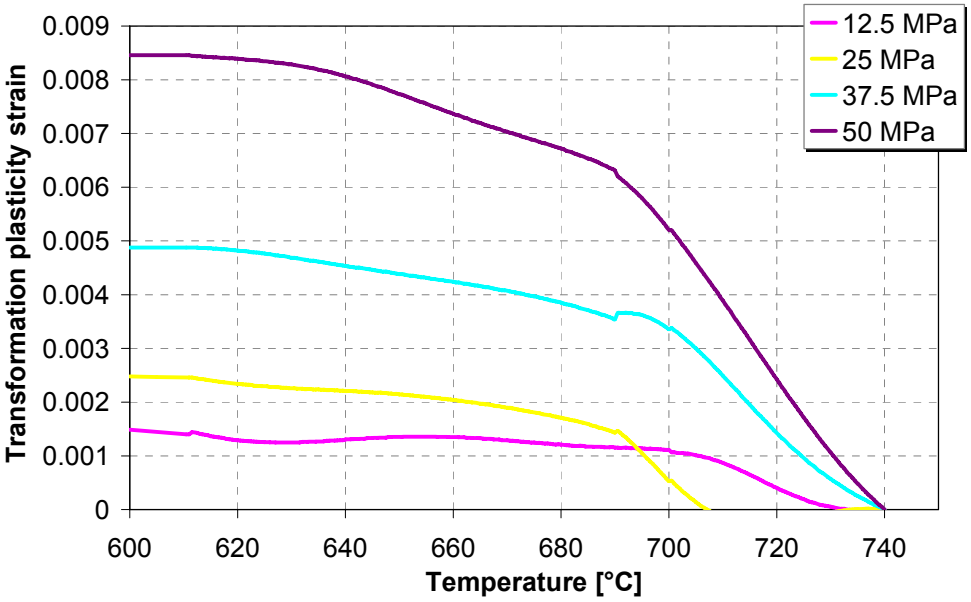

Figure 4.4 Transformation plasticity strain

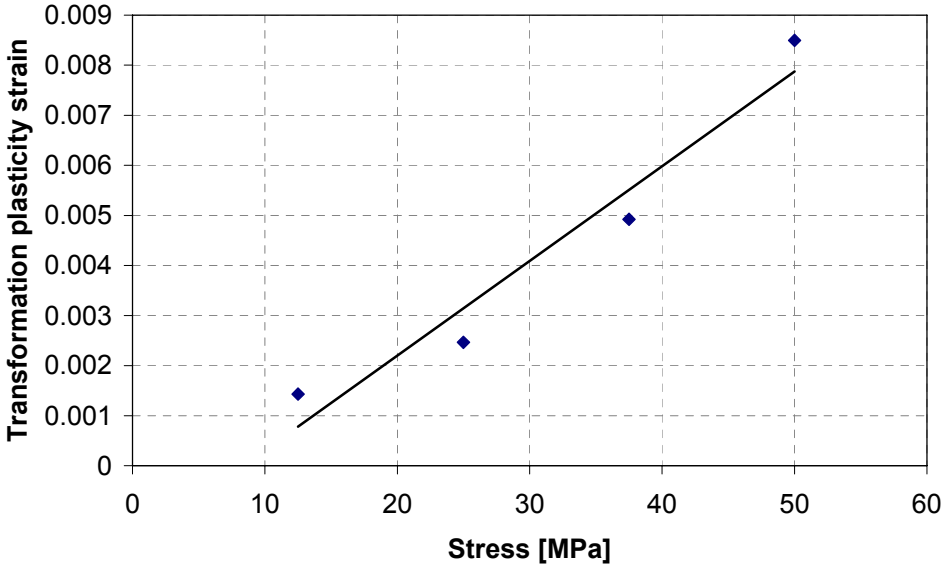

Figure 4.5 Transformation plasticity strain as function of the applied load

Table 4.4 Average values of transformation plasticity strain

Stress [MPa]	*12.5*	*25*	*37.5*	*50*
ε^{tp} $[10^{-3}]$	*1.43*	*2.47*	*4.92*	*8.50*

The transformation plasticity strain increases with the applied load and it confirms the few results found in the literature [85], and an almost linear trend of transformation plasticity strain is exhibited with respect to applied stress.

Finally the transformation plasticity coefficients were calculated according to (4.4). It seems important to underline that, in order to carry out such calculations, the percentage of the new formed phase should be at least 70%, as suggested by literature, in fact a saturation in transformation plasticity can be observed next to this percentage as it can be deduced from the previous diagram showing ε^{tp} trend.

Table 4.5 Values of transformation plasticity coefficient

Stress [MPa]	*12.5*	*25*	*37.5*	*50*
k $[10^{-4}]$	*1.15*	*0.99*	*1.31*	*1.70*

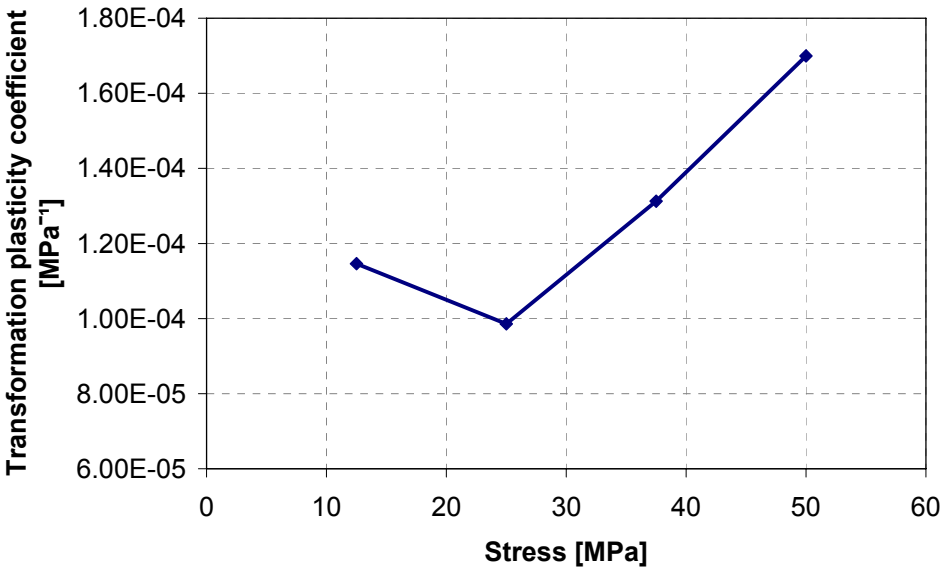

Figure 4.6 Transformation plasticity coefficient trend

4.1.3 Bainite

The procedure used to determine transformation plasticity of bainite was similar to the one used for the mix of ferrite and pearlite. As it was said in the previous paragraphs, applied loads have to be inferior to the yield stress of the weaker phase present at the loading temperature. The tests were carried out on new specimens of the reference material 22MnB5. The setting up of the most suitable thermal cycle required trials in order to maximize the percentage of the transformed phase. The reference thermal cycle is summarized in the following table:

Table 4.6 Thermal cycle parameters

Heating rate [K/s]	*Austenitization temp. [°C]*	*Soaking time [s]*	*Cooling rate [K/s]*
10	*900*	*180*	*10*

The resulting thermal cycle and the stress-free dilatometric measurement are represented in the following figures.

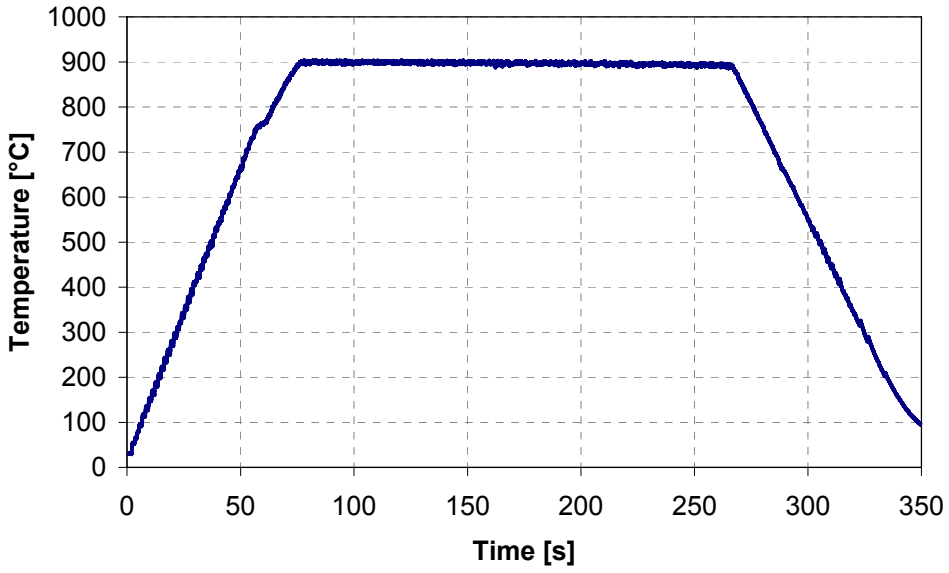

Figure 4.7 Reference thermal cycle

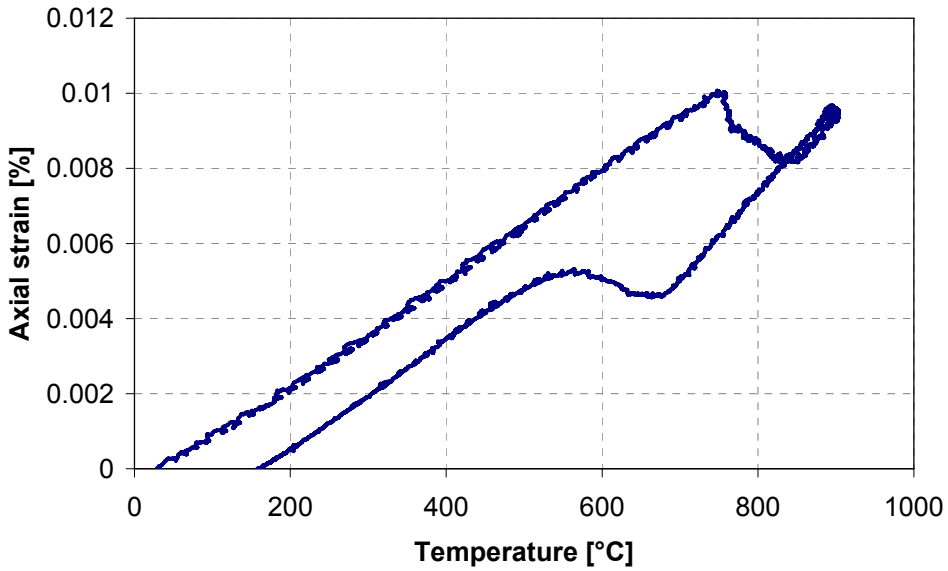

Figure 4.8 Stress-free dilatometric curve

The most significant thermal parameters can be obtained from the previous diagram and they are summarized in Table 4.7. The bainitic transformation starts about 680°C and it seems to finish about 530°C, while the ferritic and martensitic transformation don't appear in the curve. It can be remarked that the initial and the final parts of the curve are not coincident due to the different specific volume of the microstructures at the two conditions.

Table 4.7 Relevant thermal parameters

Ac_1 [°C]	Ac_2 [°C]	B_S [°C]	B_F [°C]	α_α [°C^{-1}]	α_γ [°C^{-1}]	$\Delta\varepsilon_{12}$
758	842	675	530	$1.51 \cdot 10^{-5}$	$2.37 \cdot 10^{-5}$	0.0012

where Ac_1 and Ac_3 identify the start and the end of γ transformation, B_S and B_F represent the limit of the bainitic transformation and $\Delta\varepsilon_{12}$ is the thermal strain due to the different microstructure.

4.1.3.1 Determination of transformation plasticity

The thermal cycle previously described was used in the tests with the applied stress and it was estimated that the most appropriate temperature for the load application was about 700°C; the procedure followed in the experiments was:

- Heating from room temperature up to 900°C with heating rate of 10K/s
- Soaking at 900°C for 3min

- Cooling from 900°C with a cooling rate of 10K/s
- Constant load application during cooling starting from 700°C

The applied elastic stresses are summarized in Table 4.8

Table 4.8 Levels of applied stress during tests

Test	*1*	*2*	*3*	*4*	*5*
Stress [MPa]	*12.5*	*25*	*37.5*	*50*	*62.5*

The corresponding loads to be applied were easily calculated as the section dimensions of the specimen were known. Also in this case the stress was applied before the onset of phase transformation in order to avoid any influence on the kinetics of phase transformation during loading. The curves representing the axial strain as function of temperature obtained from the tests with applied stress are presented in Appendix A.

The calculation of the transformation plasticity strain was performed starting from the results obtained from dilatometric measurements as suggested by the procedure indicated in [38]. For all test conditions the strain vs. temperature were cut and aligned at 685°C, differences arising in the strain were mainly due to the elastic component of the strain and the creep deformation, see Figure 4.9.

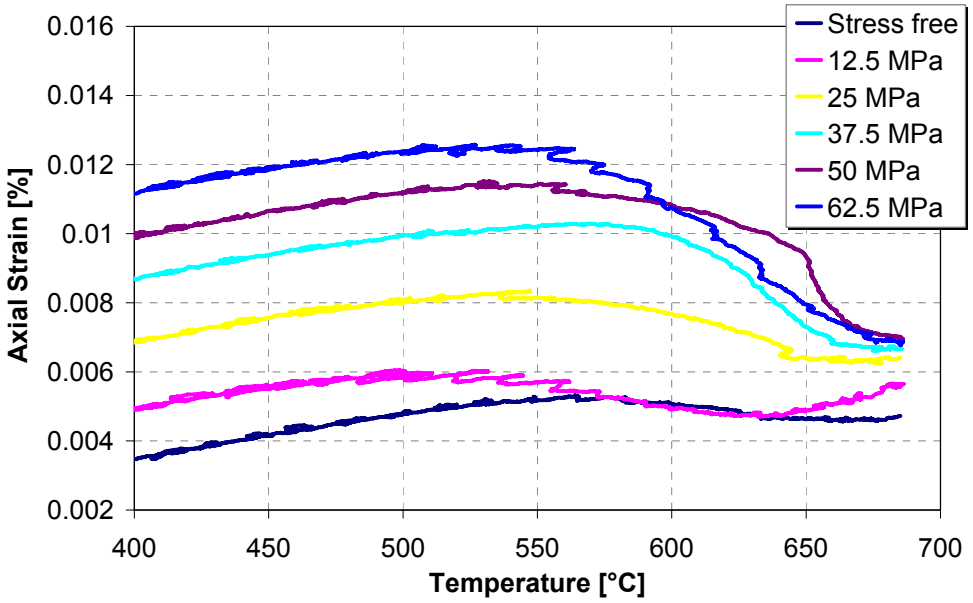

Figure 4.9 Total strain for the six tests

All data were filtered in order to eliminate noise and the calculations were made on them. Also in this transformation the strain due to creep was negligible with the considered loads, therefore the shift of the curves could be ascribed to the elastic deformation and the curves were reasonably set to zero at 685°C. Transformation plasticity strain was thus calculated following the procedure previously illustrated, see Figure 4.10.

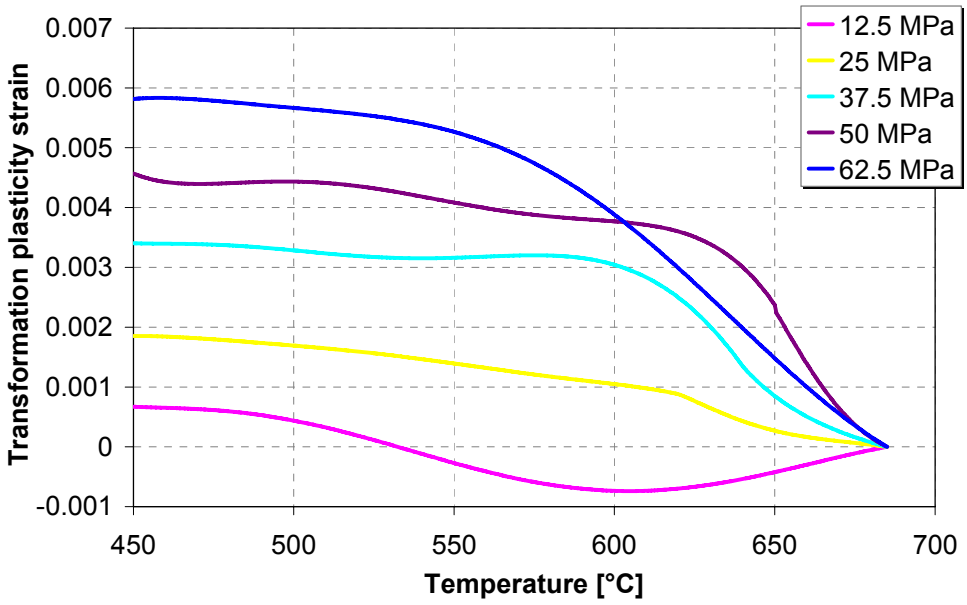

Figure 4.10 Transformation plasticity strain

The evolution of transformation plasticity strain ε^{tp} and coefficient k with applied load was calculated and it is represented as follows.

Table 4.8 Average values of transformation plasticity strain

Stress [MPa]	*12.5*	*25*	*37.5*	*50*	*62.5*
ε^{tp} $[10^{-3}]$	*0.31*	*1.64*	*3.24*	*4.39*	*5.61*

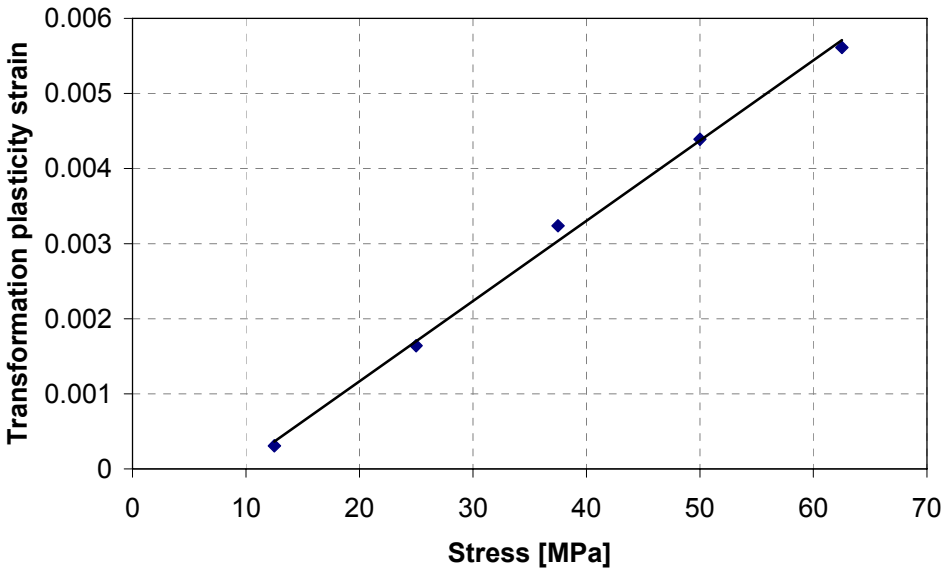

Figure 4.11 Transformation plasticity strain as function of the applied load

Also for the bainitic transformation the transformation plasticity strain increases with the applied load and exhibits an almost linear trend with respect to the applied stress.

Table 4.9 Values of transformation plasticity coefficient

Stress [MPa]	*12.5*	*25*	*37.5*	*50*	*62.5*
k [10^{-5}]	*2.46*	*6.57*	*8.64*	*8.78*	*8.98*

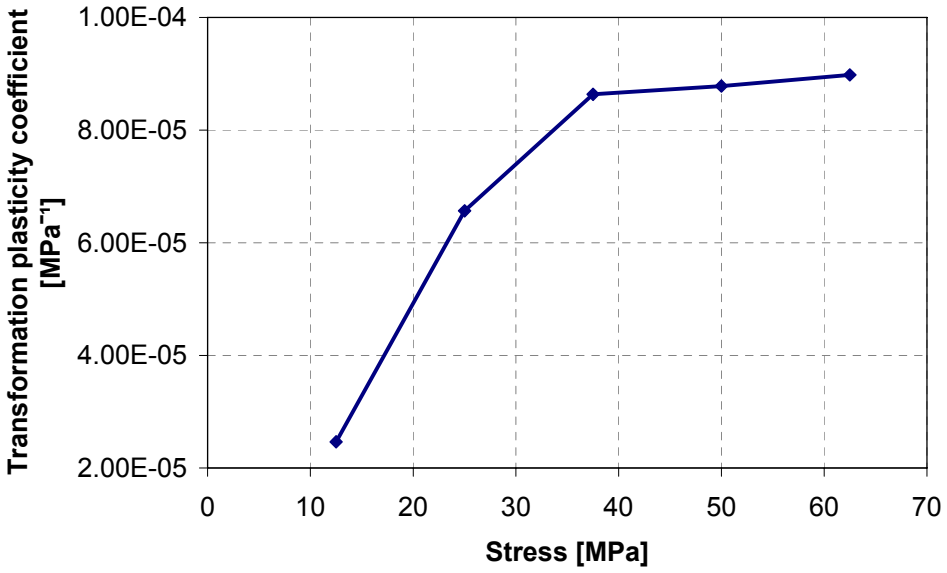

Figure 4.12 Transformation plasticity coefficient trend

4.1.4 Martensite

The transformation plasticity of martensite for the 22MnB5 was determined by means of the same procedure used for the other phases. A cooling rate of 35K/s was applied in order to obtain a fully martensitic microstructure at the end of the tests and avoid any bainitic transformation. The imposed thermal cycle is presented in Table 4.10.

Table 4.10 Thermal cycle parameters

Heating rate [K/s]	*Austenitization temp. [°C]*	*Soaking time [s]*	*Cooling rate [K/s]*
10	*900*	*180*	*35*

The thermal cycle and the stress-free dilatometric measurement are represented in the following figures.

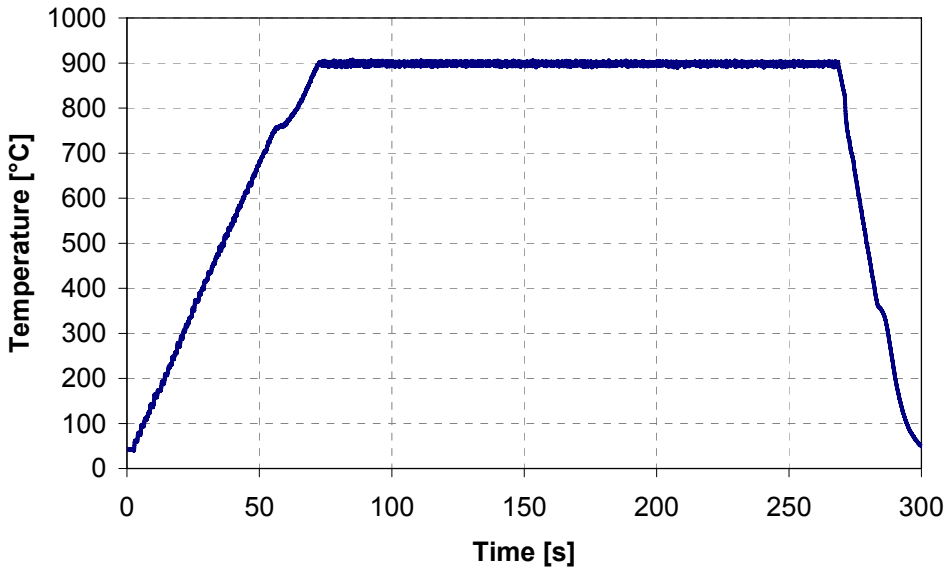

Figure 4.13 Reference thermal cycle

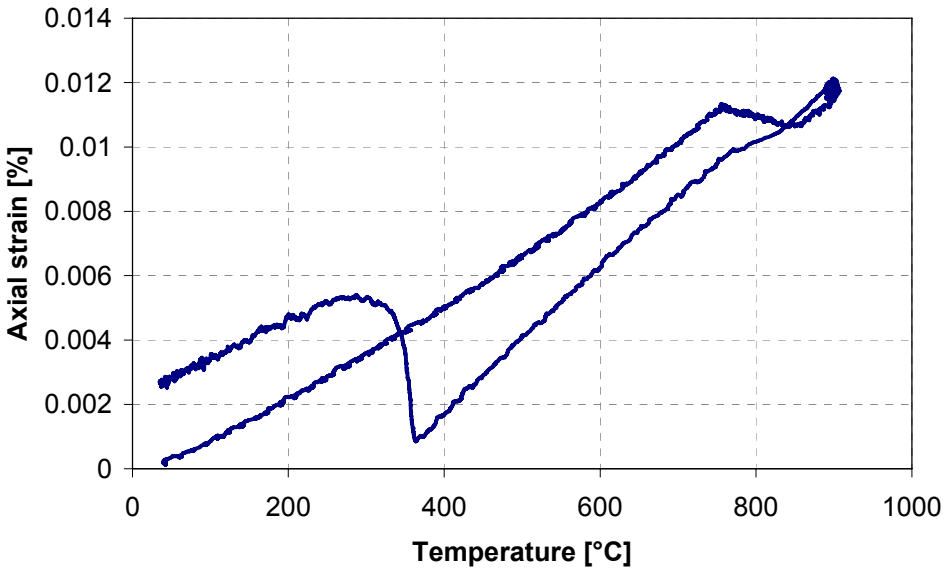

Figure 4.14 Stress-free dilatometric curve

The martensitic transformation starts at about 380°C and finishes at almost 290°C, no other phase transformations appear in the dilatometric curve. The initial and the final parts of the curve are not coincident due to the different specific volume of the two microstructures. The obtained thermal parameters are summarized in Table 4.11.

Table 4.11 Relevant thermal parameters

Ac_1 [°C]	Ac_2 [°C]	M_S [°C]	M_F [°C]	α_α [°C^{-1}]	α_γ [°C^{-1}]	$\Delta\varepsilon_{12}$
754	837	376	284	$1.76 \cdot 10^{-5}$	$2.23 \cdot 10^{-5}$	0.0083

where Ac_1 and Ac_3 identify the start and the end of γ transformation, M_S and M_F represent the onset and the end of the martensitic transformation and $\Delta\varepsilon_{12}$ is the thermal strain due to the different microstructure.

4.1.4.1 Determination of transformation plasticity

The lower temperature at which the loads were applied to evaluate the transformation plasticity of martensite, 450°C, allowed to increased the applied elastic stresses as shown in Table 4.12. The resulting thermo-mechanical cycle used in the tests was:

- Heating from room temperature up to 900°C with heating rate of 10K/s
- Soaking at 900°C for 3min
- Cooling from 900°C with a cooling rate of 35K/s

- Constant load application during cooling starting from 450°C

Table 4.12 Levels of applied stress during tests

Test	*1*	*2*	*3*	*4*	*5*	*6*
Stress [MPa]	*12.5*	*25*	*50*	*75*	*100*	*125*

Also in this analysis the stress was applied before the onset of phase transformation in order to avoid any influence on the phase transformation kinetics during loading. The dilatometric curves obtained from the transformation plasticity tests with applied stress are displayed in Appendix A.

The calculation of the transformation plasticity strain was performed starting from the results obtained from the dilatometric measurements. For all test conditions the strain vs. temperature were cut and aligned at 400°C as shown in Figure 4.15, where the initial differences are mainly due to the elastic component of the strain and the creep deformation.

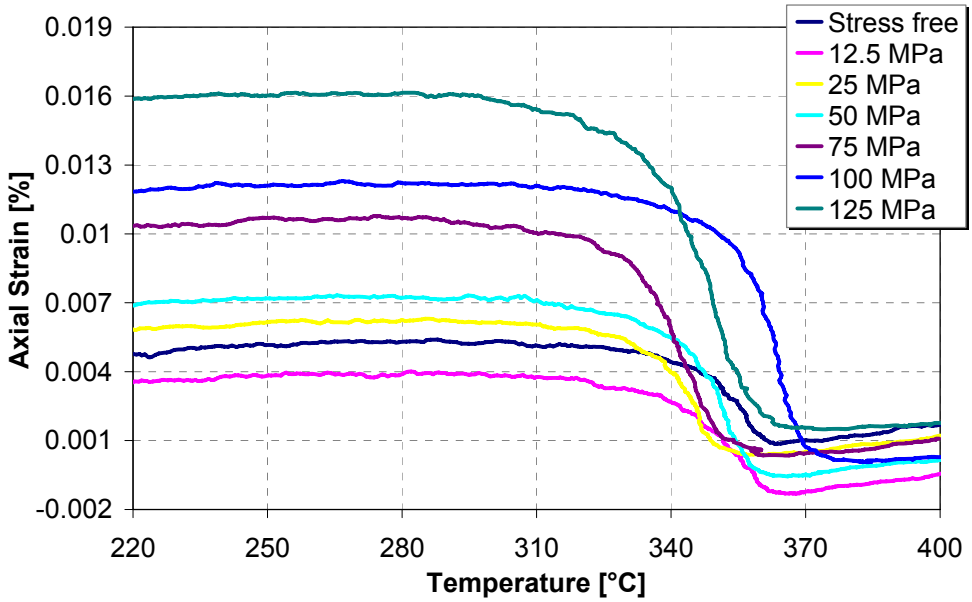

Figure 4.15 Total strain for the six tests

Data were filtered in order to eliminate noise and also for this transformation the strain due to creep was neglected, therefore the shift of the curves was due to the elastic deformation and the curves were set to zero at 400°C. In Figure 4.16 it is possible to notice the transformation plasticity strain evolution with different applied loads.

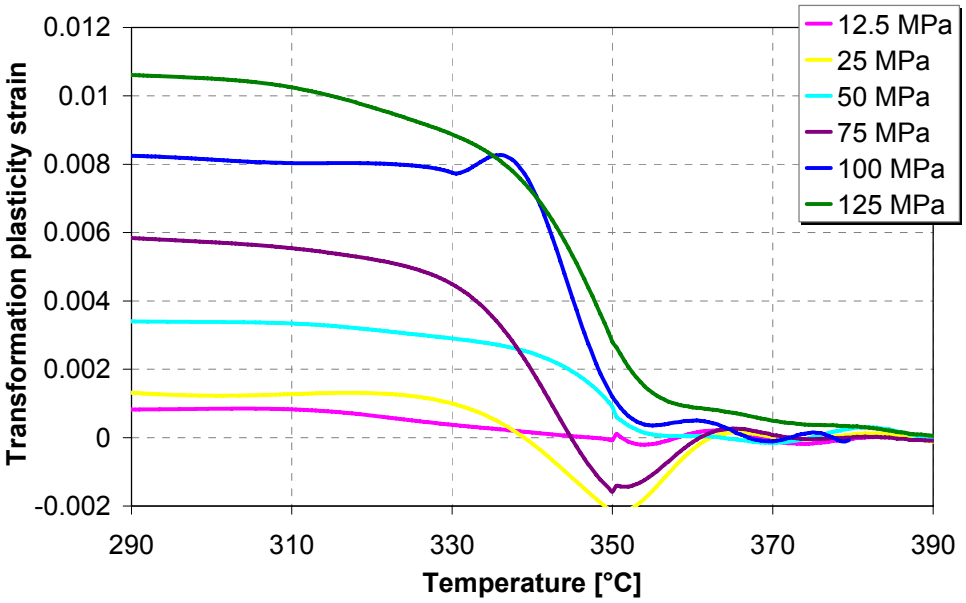

Figure 4.16 Transformation plasticity strain

The transformation plasticity strain ε^{tp} was calculated for the different applied loads and the results are displayed in Table 4.13.

Table 4.13 Average values of transformation plasticity strain

Stress [MPa]	*12.5*	*25*	*50*	*75*	*100*	*125*
ε^{tp} $[10^{-3}]$	*0.83*	*1.32*	*3.4*	*5.84*	*8.28*	*10.6*

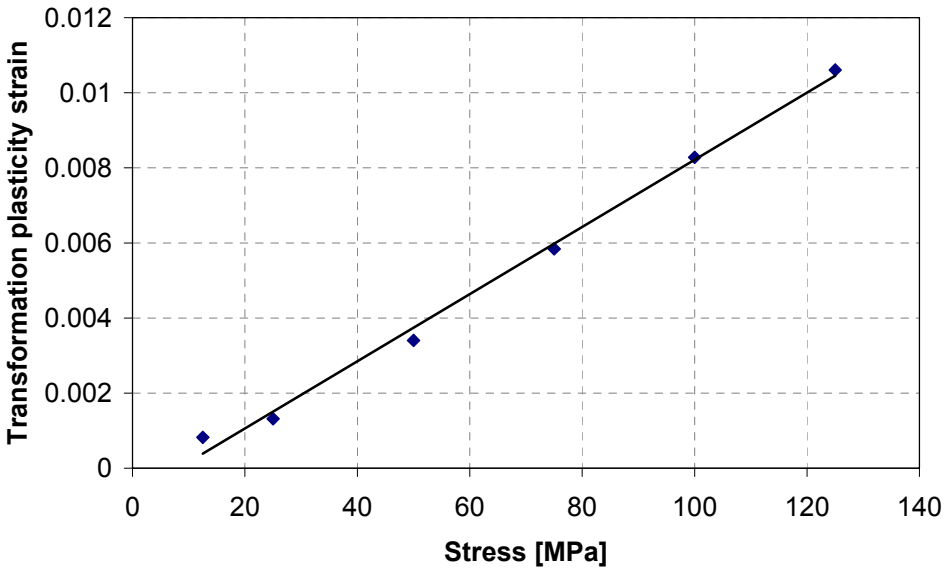

Figure 4.17 Transformation plasticity strain as function of the applied load

The transformation plasticity strain increases with the applied load for martensite as well as for the other investigated phases and exhibits an almost linear trend with respect to the applied stress. The transformation plasticity coefficients were finally calculated.

Table 4.14 Values of transformation plasticity coefficient

Stress [MPa]	*12.5*	*25*	*50*	*75*	*100*	*125*
k [10^{-3} MPa]	*6.60*	*5.28*	*6.80*	*7.80*	*8.28*	*8.49*

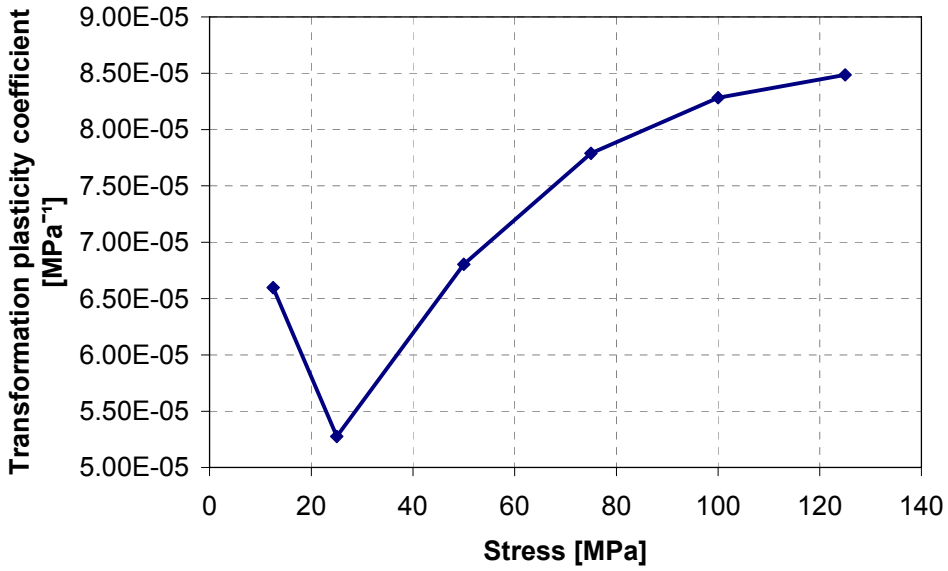

Figure 4.18 Transformation plasticity coefficient trend

4.2 Shift of TTT curves due to applied stress

The hot stamping of quenchenable high strength steels is a non-isothermal sheet metal forming process, in which the final part is produced by combining both the forming and the hardening stages in a single step through continuous-cooled dies. Thus information given by CCT and TTT diagrams found in the literature isn't useful, as they are obtained through stress-free experiments, because the stress state during deformation may modify the phase transformation kinetics. The new experimental apparatus described in § 3.4.1 was therefore used to perform phase transformation tests in order to identify the shift of 22MnB5 TTT curves due to applied stress. After some preliminary tests to evaluate the most influencing parameters, the influence of applied stresses on the ferritic and bainitic

phase transformation kinetics has been studied in the same range of temperatures typical of the industrial hot stamping process, as described in the following paragraphs.

4.2.1 Preliminary results

The experimental setup used to evaluate the material transformation plasticity was also utilized to impose coupled thermo-mechanical cycles in order to study the influence of applied stress and strain on phase transformation kinetics of the 22MnB5. Some preliminary experiments were carried out in order to evaluate the influence of load application temperature on the shift of the microstructural transformation onset, and its sensitivity to both elastic and plastic stresses applied during cooling. To detect the phase transformation onset the high temperature axial extensometer was used and appropriately adapted to work as a dilatometer. Specimens were austenitized at 900°C for 3min, then they were applied a cooling rate of approximately 100K/s down to the testing temperature to avoid any phase transformation and to assure the holding phase starting with a still fully metastable austenite. The holding temperature was set equal to 700°C for all the tests (ferritic transformation) and the reference thermal cycle is summarized in Table 4.15.

Table 4.15 Reference thermal cycle parameters

Heating rate [K/s]	*Austenitization temp. [°C]*	*Soaking time [s]*	*Cooling rate [K/s]*	*Holding temp. [°C]*	*Holding time [s]*
15	*900*	*180*	*100*	*700*	*60*

In the following figures the thermal cycle and the stress-free dilatometric measurement are presented, where the change in the slope of the dilatometric curve indicates the onset of the microstructural transformation (the austenite-to-ferrite one in the this case).

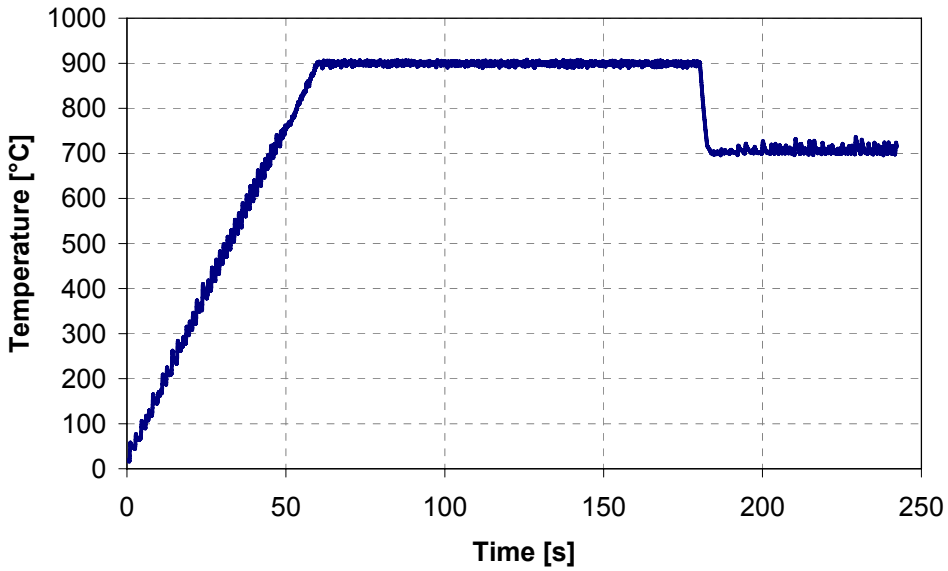

Figure 4.19 Reference thermal cycle (T_h = 700 °C)

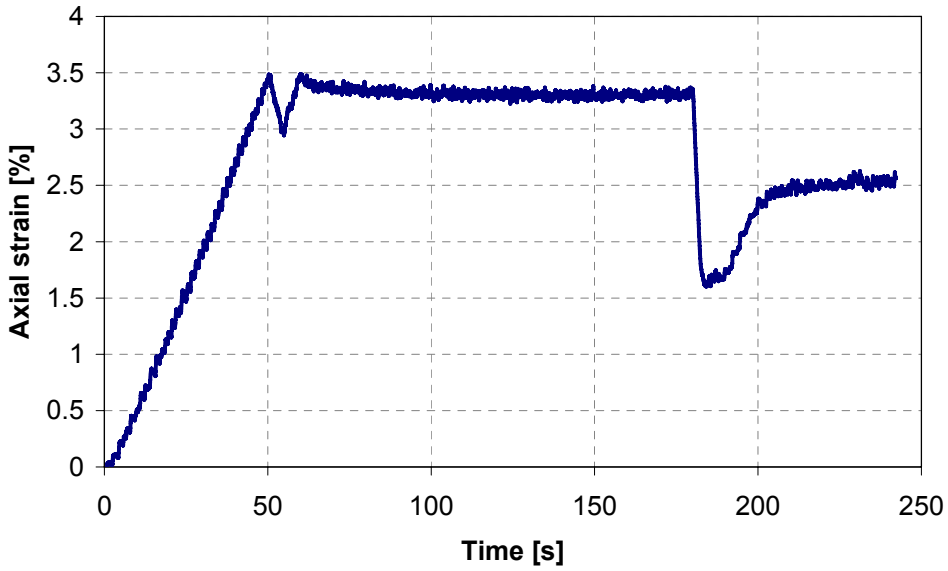

Figure 4.20 Stress-free dilatometric acquisition at T = 700 °C

In the following analyses the dilatometric curves will be represented starting from two seconds after the beginning of the cooling phase in order to emphasize the differences on the phase transformation onset.

Different levels of stress (in both elastic and plastic range of metastable austenite) were applied during cooling and removed during the holding phase, by superimposing some

mechanical cycles to the reference thermal profile, and the resulting testing procedure is summarized in the following figure.

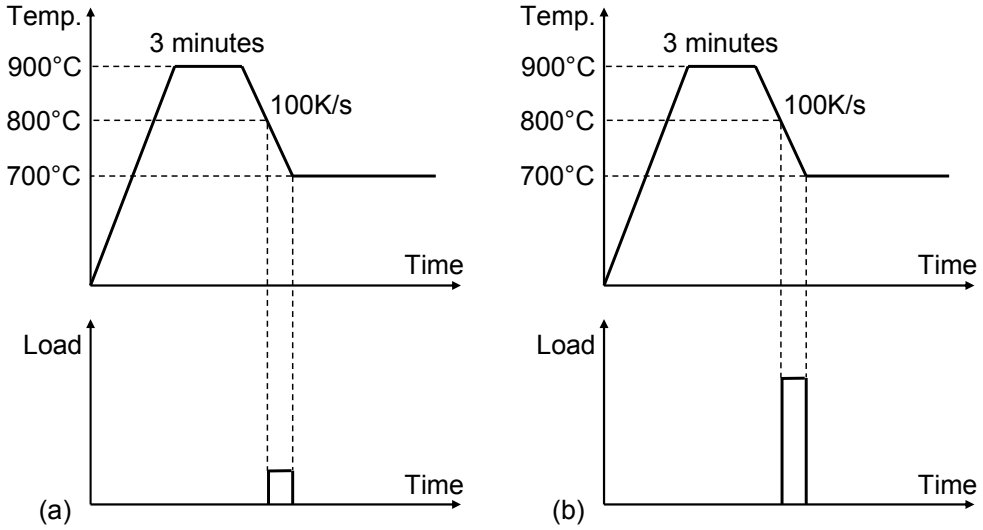

Figure 4.21 Elastic (a) and plastic (b) load application tests

In Figure 4.22 it is possible to notice that both elastic and plastic loads applied during cooling do not influence the phase transformation kinetics if they are removed before the transformation onset.

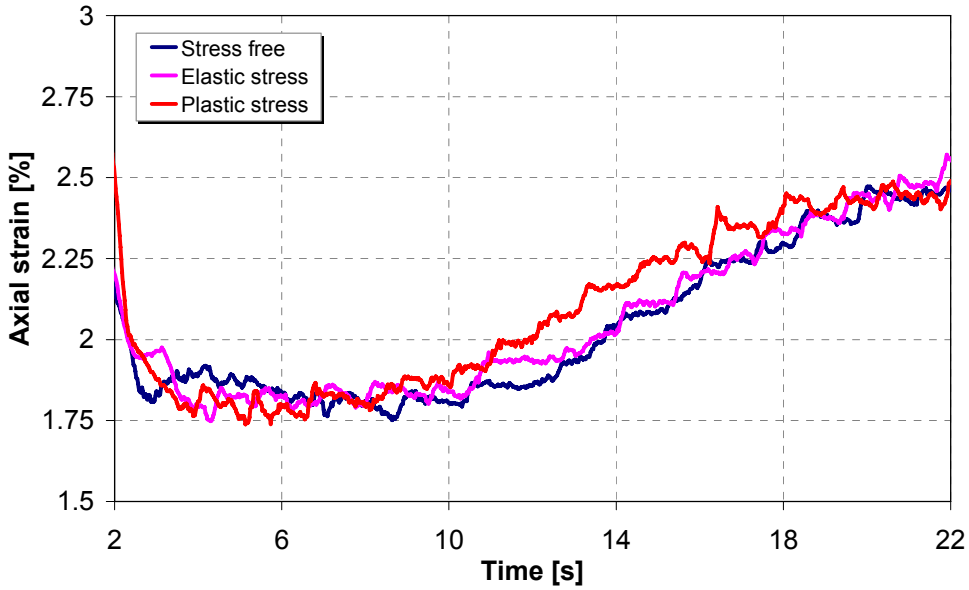

Figure 4.22Influence of elastic and plastic stresses removed before the transformation onset

Further investigations, displayed in Figure 4.24, show that also the load application temperature does not seem to influence the onset of phase transformation but only the entity of the load which is applied and maintained at constant temperature modifies the shift of the TTT curves of the material.

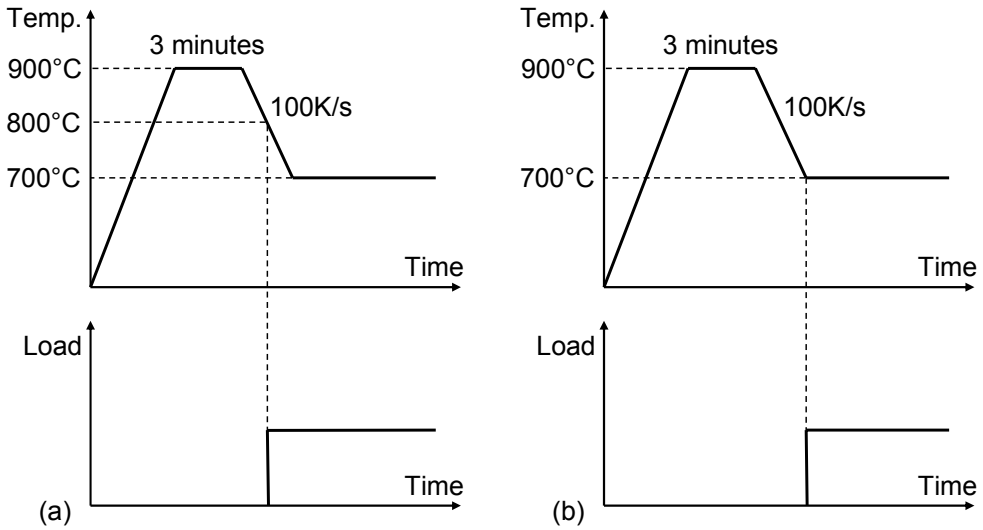

Figure 4.23 Different load application temperature tests

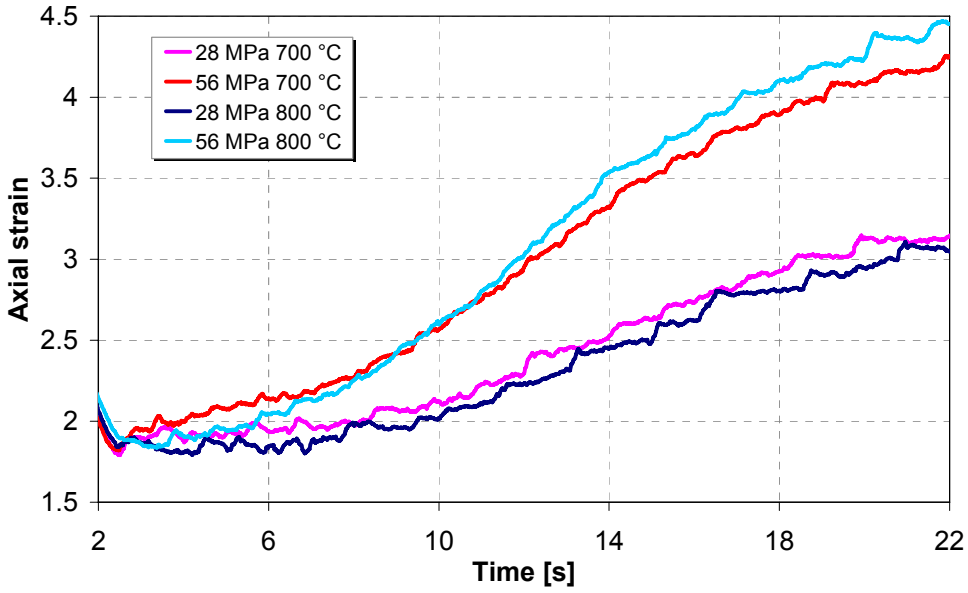

Figure 4.24 Influence of load application temperature on phase transformation onset

4.2.2 Ferritic transformation

The influence of applied stresses on the 22MnB5 ferritic phase transformation kinetics has been studied. Specimens were austenitized at 900°C for 3min and cooled down to 700°C by applying a cooling rate of 100K/s in order to assure the test starting in fully austenitic conditions. Different σ_a loads, both elastic and plastic, were applied at 800°C and maintained during the entire tests and the shift of the onset of the ferritic transformation were measured by means of the modified axial extensometer. The thermo-mechanical reference cycle is shown in the next table. The thermal cycle and the stress-free dilatometric curve are displayed in Figures 4.19-20.

Table 4.16 Thermo-mechanical reference cycle parameters

Heating rate [K/s]	*Austenitization temp. [°C]*	*Soaking time [s]*	*Cooling rate [K/s]*	*Holding temp. [°C]*	*Holding time [s]*	*Load application temperature [°C]*
15	*900*	*180*	*100*	*700*	*60*	*800*

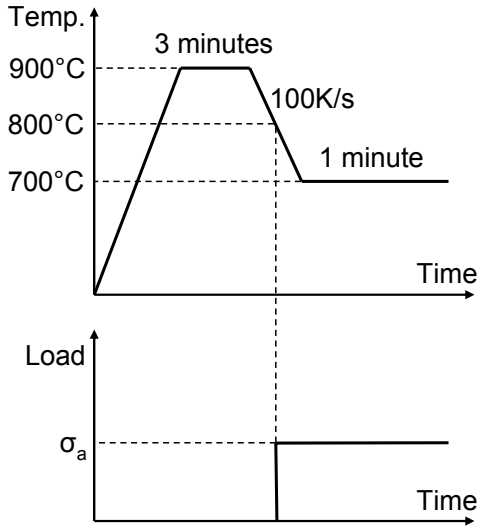

Figure 4.25 Thermo-mechanical reference cycle

The values of stresses chosen for the experimental campaign are shown in Table 4.17, where the last value (84MPa) corresponds to a plastic deformation induced in the specimen.

Table 4.17 Experimental plan for the ferritic phase transformation tests

Test	*1*	*2*	*3*	*4*
σ_a [MPa]	*0*	*28*	*56*	*84*

The axial strain vs. time curves obtained from the dilatometric analyses are displayed in Figure 4.26.

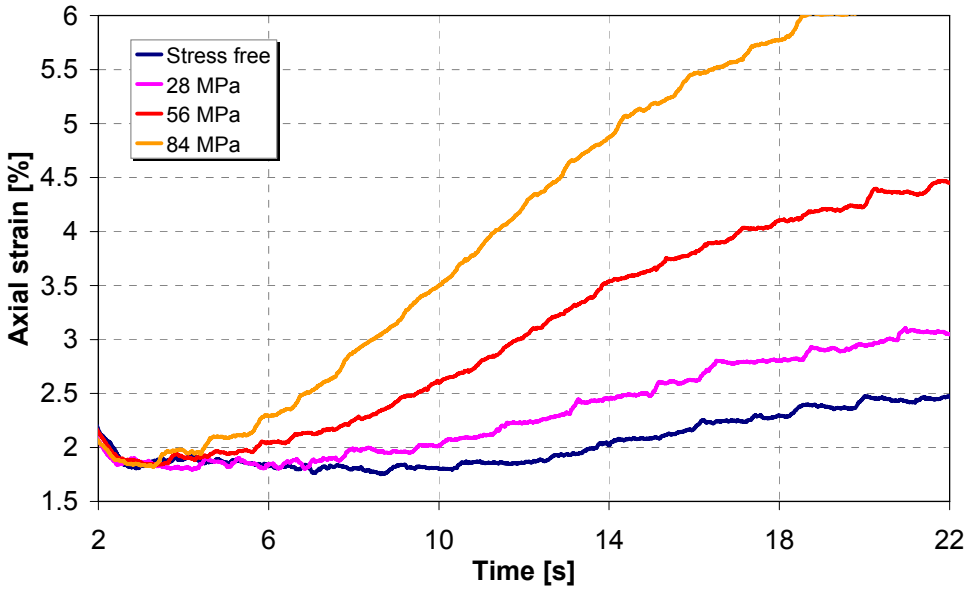

Figure 4.26 Axial strain measured by the extensometer as function of applied stress at T = 700 °C

As the level of applied stress increases, the time needed to obtain the ferritic transformation reduces in an almost proportional way, thus proving that the application of a load anticipate the transformation phase and the higher is the applied stress the bigger is the magnitude of the shift of the TTT curve.

4.2.3 Bainitic transformation

The same kind of analysis previously described was performed regarding the 22MnB5 bainitic transformation but two different testing temperatures were used to better describe the shift of the TTT curves. In fact at 600°C, which corresponds to the nose of the bainitic curve, the time interval before the transformation onset was too limited to evaluate this phenomenon with an acceptable accuracy, therefore the experimentation was performed also at 500°C.

Table 4.18 Thermo-mechanical reference cycles parameters

Heating rate [K/s]	*Austenitization temp. [°C]*	*Soaking time [s]*	*Cooling rate [K/s]*	*Holding temp. [°C]*	*Holding time [s]*	*Load application temperature [°C]*
15	*900*	*180*	*100*	*600*	*60*	*700*
15	*900*	*180*	*100*	*500*	*60*	*600*

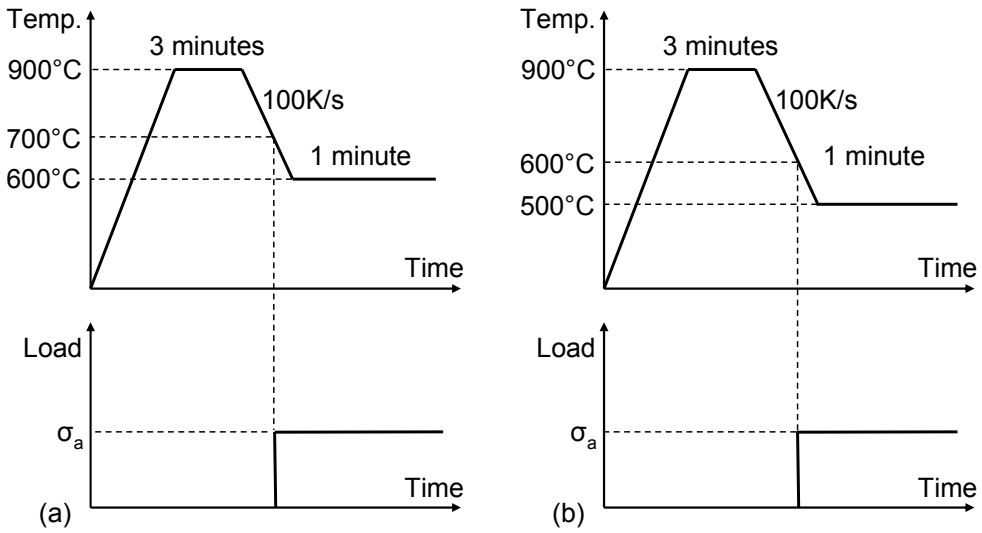

Figure 4.27 Thermo-mechanical reference cycles for the bainitic transformation kinetics investigation

The values of stresses chosen for the experimental campaign are shown in Table 4.19, where for each testing temperature the last stress value correspond to a plastic induced deformation.

Table 4.19 Experimental plan for the bainitic phase transformation tests

T [°C]	*600*	*500*
σ_a [MPa]	*28-56-84-112*	*28-56-84-140*

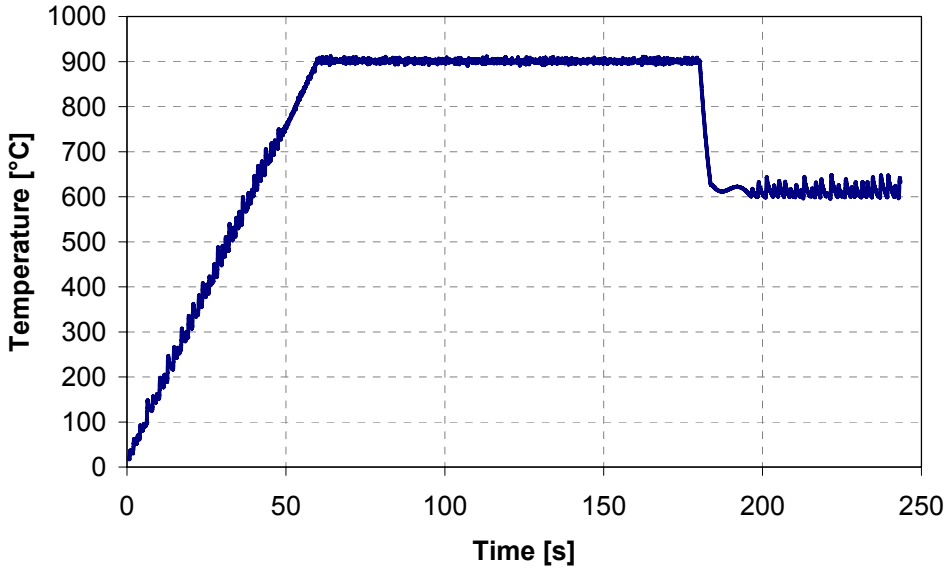

Figure 4.28 Reference thermal cycle at T = 600 °C

Figure 4.28 shown the thermal reference cycle and the dilatometric acquisition in stress-free conditions for the testing temperature of 600°C is displayed in the following figure.

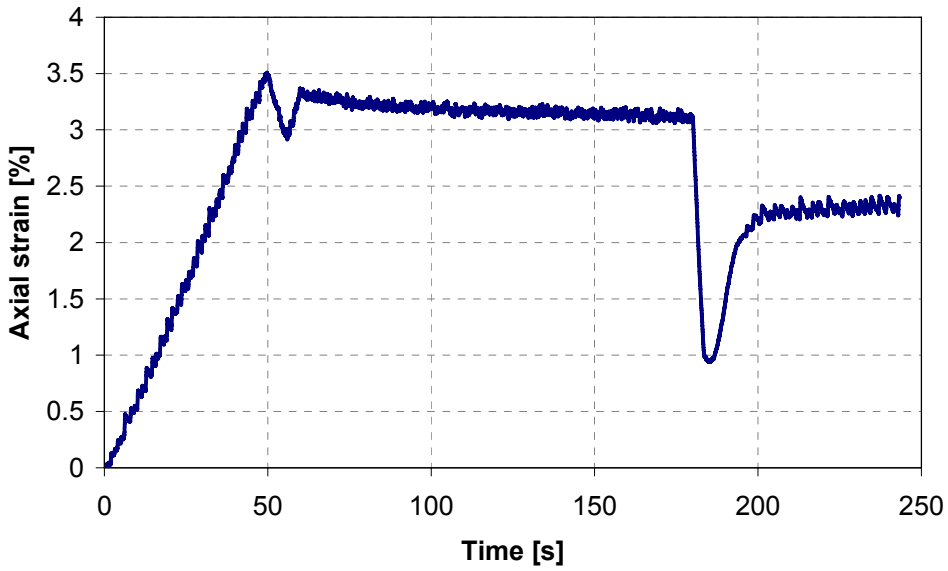

Figure 4.29 Stress-free dilatometric acquisition at T = 600 °C

Figure 4.30 shows the influence of applied stresses on the bainitic transformation kinetics at 600°C.

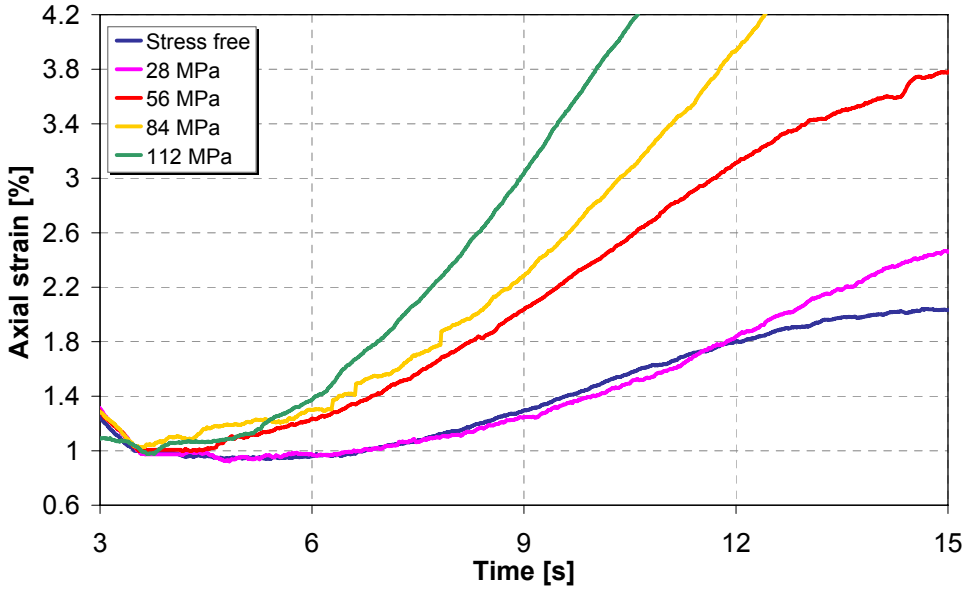

Figure 4.30 Axial strain measured by the extensometer as function of applied stress at T = 600 °C

In the following figures the thermal reference cycle and the stress-free dilatometric curve with respect to the bainitic phase transformation at 500°C are presented.

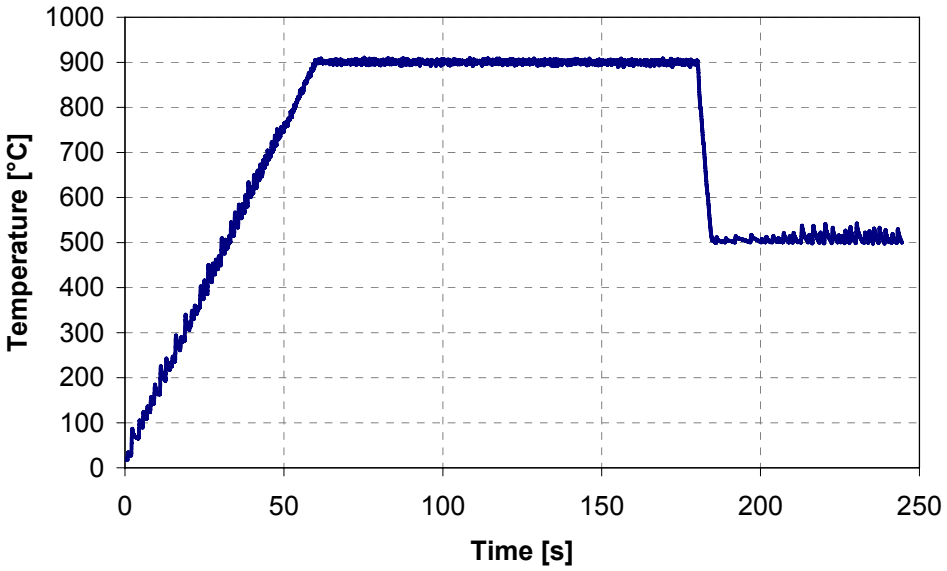

Figure 4.31 Reference thermal cycle at T = 500 °C

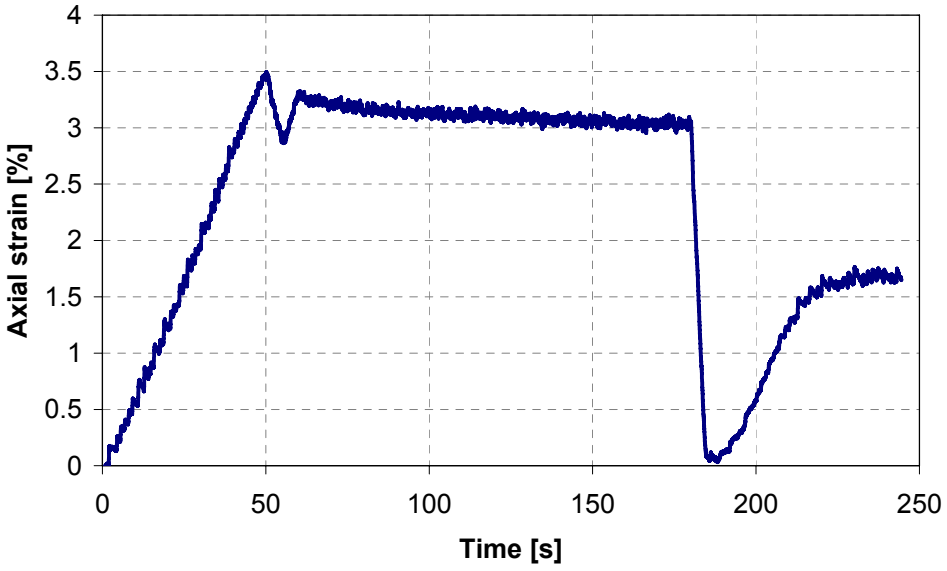

Figure 4.32 Stress-free dilatometric acquisition at T = 500 °C

The following figure shows the influence of applied stresses on the bainitic phase transformation kinetics at 500°C.

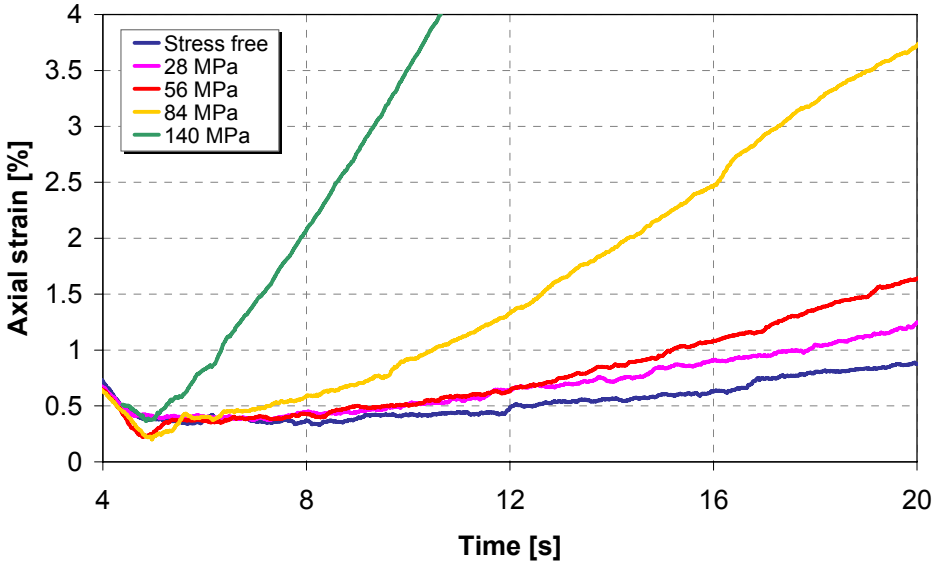

Figure 4.33 Axial strain measured by the extensometer as function of applied stress at T = 500 °C

Also the bainitic transformation kinetics is strongly influenced by the applied load, as shown in Figure 4.33. The shift of the TTT curves has been evaluated with a better accuracy at 500°C, at which temperature the material exhibits a behaviour similar to the ferritic transformation, in fact the higher is the applied load the more anticipated is the microstructural transformation onset.

4.3 Conclusions

Phase transformation kinetics of the high strength steels 22MnB5 was studied by means of a new experimental setup in order to provide an accurate calibration of FE models of the hot stamping process and perform reliable numerical simulations.

An extensometric analysis was performed to investigate the phase transformation plasticity evolution for all phases transformations occurring to the material from austenitization to room temperature (ferrite/pearlite, bainite and martensite).

The influence of applied stress on the phase transformation kinetics was also investigated by reproducing the conditions governing the microstructural evolution during hot stamping. It was found that as the level of applied stress increases, the time needed to have both the ferritic and the bainitic transformation reduces, proving that the application of a load

anticipates the transformation onset and this phenomenon is more pronounced the higher is the applied stress. When the load, even if plastic, is instead applied before reaching the testing temperature, but not keep at constant temperature, no shift in the transformation onset is observed. It must be remarked that stresses were applied at constant temperature, then the analysed shift regards the TTT curves of the material.

CHAPTER 5
MATERIAL FORMABILITY

Among data needed to settle a reliable numerical model of the hot stamping process, information about material formability may help in better designing and optimizing hot forming operations. A new experimental apparatus based on the Nakazima concept and developed to perform formability tests at elevated temperature is presented in § 5.2 and its testing parameters, optimized in order to act as a physical simulation of the industrial process by replicating the typical thermo-mechanical conditions, are displayed in § 5.3. A suitable procedure to determine FLC taking into account their correlation with material microstructure evolution due to phase transformation is presented in § 5.4, together with the results in terms of FLCs obtained at constant temperature and defined microstructure.

5.1 Experimental apparatus

A new experimental apparatus for sheet metal formability testing at elevated temperature has been developed at the Chair of Manufacturing Technology at the University of Padova. The test is based on the Nakazima procedure, which allows to obtain different strain path on the material by using rectangular specimens of different width (from 200mm to 20mm) in order to determine the whole forming limit curve (FLC). The sheet metal blanks are heated up to the austenitization temperature as in the industrial process, then cooled down to the testing temperature and deformed until fracture.

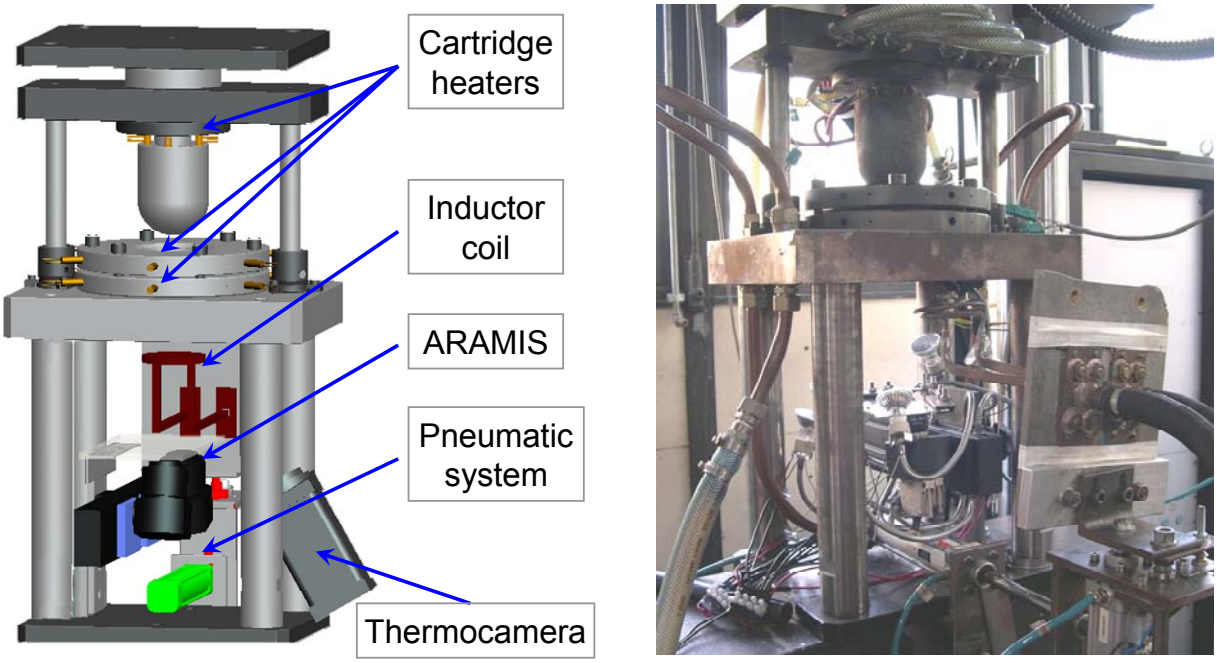

Figure 5.1 CAD drawing of the Nakazima device (a) and physical prototype (b)

The experimental device is made of a hemispherical punch, whose diameter is 100mm, a die, a blank-holder and a draw-bead which prevents a possible uncontrolled drawing-in of sheet material during deformation. The dedicated machine is a 1000kN INSTRON™ hydraulic press that permits a punch velocity in the range between 10mm/min and 1500mm/min.

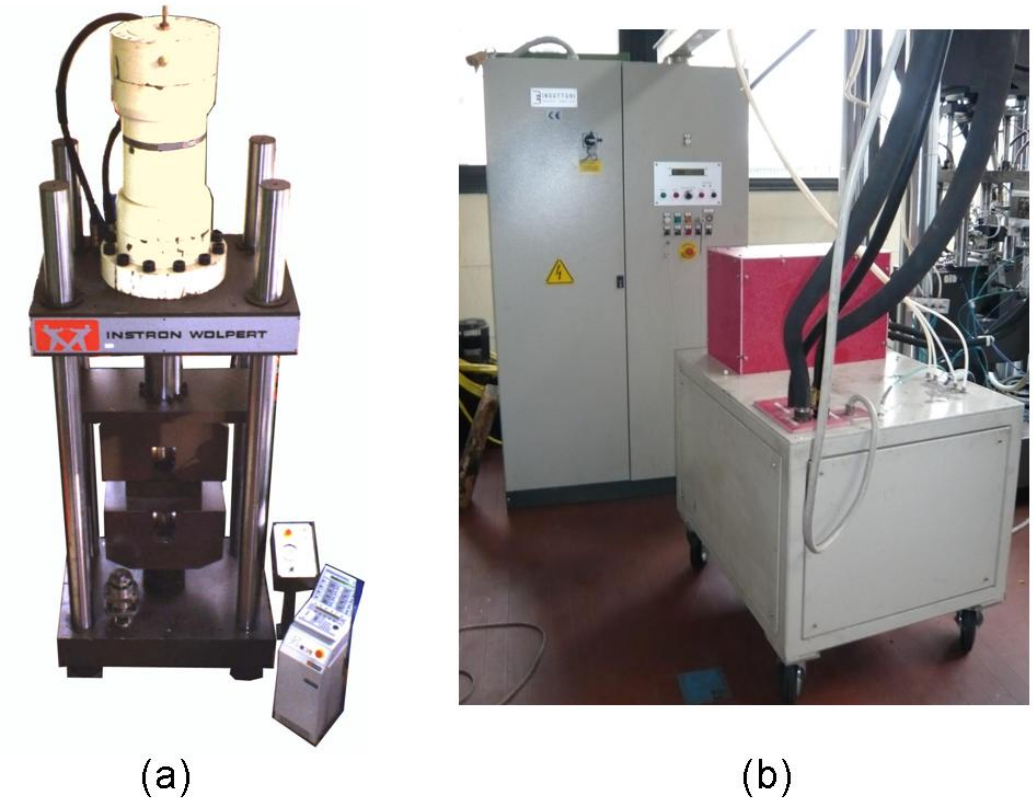

Figure 5.2 INSTRON hydraulic press (a) and induction power supply (b)

The punch, the die and the blank-holder are equipped with cartridge heaters to control and vary the thermal field of the sheet metal blank during the tests. The specimens are heated up to the austenitization temperature through inductor heads, whose shapes and dimensions are carefully designed and optimized: pancake for blanks larger than 100mm and rectangular frontal inductors for smaller specimens in order to obtain a controlled homogeneous thermal field. A pneumatic system maintains the copper coil and the specimen at the set distance during the heating phase and removes the inductor to allow the deformation performed by the punch. During the heating and the deformation phases, the temperature of the specimen and of the dies equipment can be monitored using both an infrared thermo-camera and K-type thermocouples spot-welded in different points of

the sheet surface interested by deformation. The specimen can be cooled down after austenitization by means of four compressed-air nozzles in order to obtain cooling rates up to 100K/s.

The strain field in the sheet is measured by the GOM-ARAMIS™ optical system, made of two cameras and equipped with a proper lighting equipment, providing the possibility to display 3D-coordinates of the surface by means of a stochastic pattern previously applied to the sheet metal that can resists during deformation at elevated temperature. Figure 5.3 shows an example of a deformation state acquired through the camera and the corresponding strain field calculated by the ARAMIS™ software.

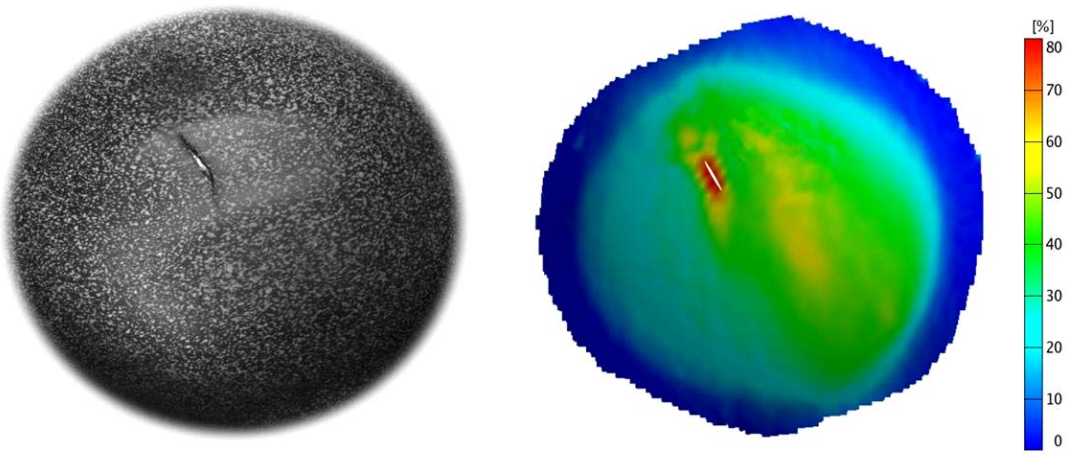

Figure 5.3 Deformed specimen and its corresponding major stain field

A dedicated LabView™ program acquires the force and stroke signals to control the press movements, elaborates all the thermocouples measurements, activates the cartridge heaters and adjusts the inductor power in order to impose the desired thermal cycle to the specimen during the test. It also activates the compressed-air jets until the desired testing temperature is reached during the cooling phase and synchronizes the optical system acquisition with the deformation phase. Thus all the relevant parameters of the thermo-mechanical cycle (e.g. austenitization time and temperature, cooling rate, ram speed, equipment and specimen temperature at the beginning of deformation) can be arbitrary set according to the testing requirements.

5.1.1 Lighting system optimization

The optical system is not able to self adjust the shutter time and take into account the variation of emissivity of sheet metal with temperature, therefore small differences in the temperature evolution during deformation can change the lighting conditions, thus compromising the correct acquisition of the surface pattern, see Figure 5.4.

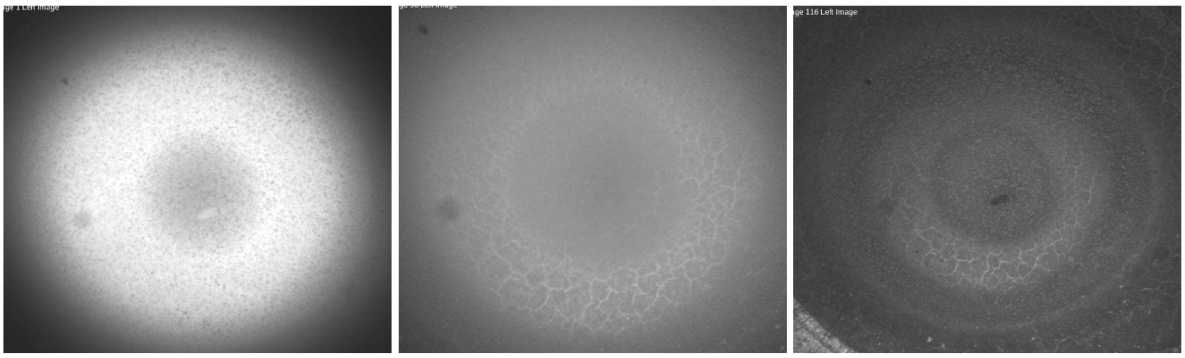

Figure 5.4 Changes in the lighting conditions due to temperature variations

The lightning system has been optimized by using eight 50W halogen lights, carefully placed around the cameras, to obtain a uniform sheet lighting and avoid any reflection. This device has been calibrated and thus the light intensity is adjusted by a dimmer control system in order to compensate the variations of the material emission and obtain a constant lighting condition during the entire deformation phase.

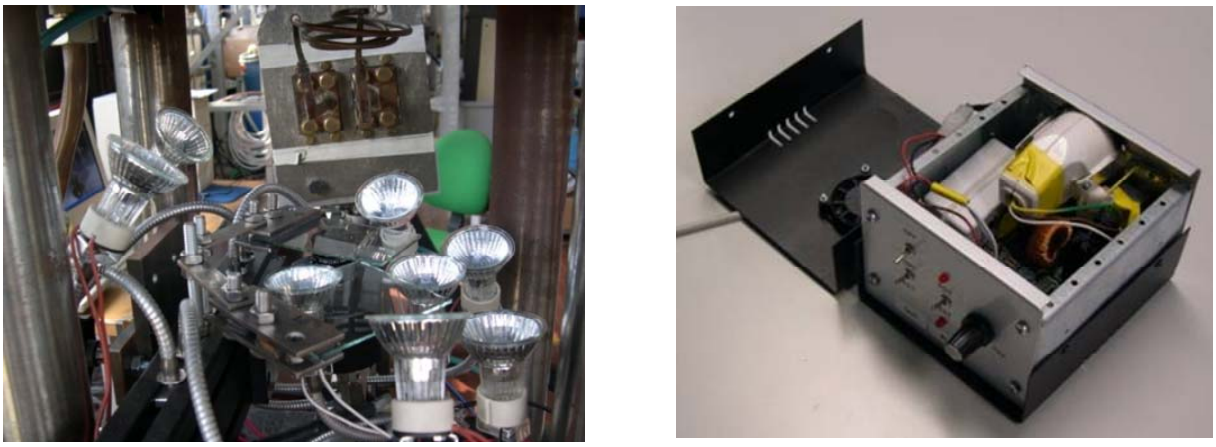

(a) (b)

Figure 5.5 Optimized lighting device (a) and its dimmer control system (b)

5.1.2 Punch and die equipment heating system

The punch is equipped with four 800W cartridge heaters and can be heated up to 600°C. Its temperature evolution is measured and controlled by means of an embedded thermocouple and the surface thermal field is measured through an infrared thermo-camera in order to assure an homogeneous thermal field in the area of interest that comes in contact with the sheet during the tests. In Figure 5.6 it is possible to notice the punch with the holes that contain cartridge heaters and the thermocouple, together with an infrared acquisition of the heated punch.

(a) (b) (c)

Figure 5.6 Cartridge heaters (a), punch (b) and infrared image of the heated punch (c)

Both the die and the blank-holder are thermically controlled by means of six 800W cartridge heaters inserted in radial direction. They can reach a maximum temperature of 650°C in order to reduce the heat loss of the sheet during cooling and maintain the specimen at almost constant temperature during the experiments. In Figure 5.7 the die equipment can be seen together with its infrared analysis.

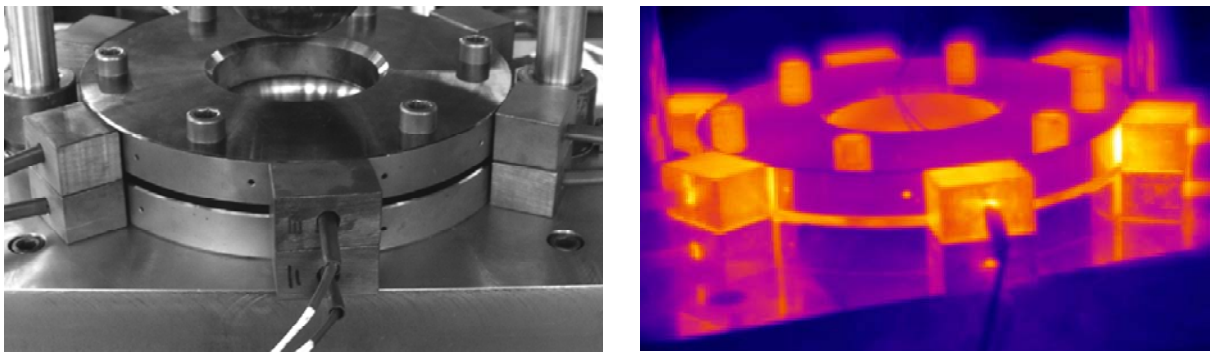

(a) (b)

Figure 5.7 Die equipment (a) and its infrared image during heating (b)

The steel plates that support the die and the punch are equipped with a water cooling system to dissipate the heat that is generated by the heating devices and to maintain the support equipment at room temperature.

5.1.3 Induction heating optimization

Specimens of different geometry have to be used in order to perform all the strain paths on the sheet and thus obtain a complete FLC. In Figure 5.8 it is shown a typical set of specimens of different width, from 200mm to 25mm, with the stochastic pattern sprayed in the zone interested by deformation during the tests.

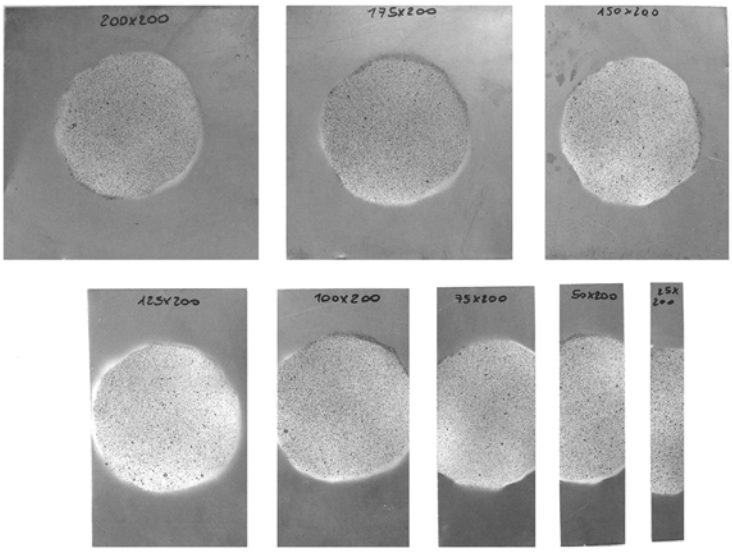

Figure 5.8 Set of specimens for Nakazima tests

The use of samples of different dimensions requires inductor coils of several shapes in order to guarantee a complete austenitization in every location of the sheet interested by deformation, as well as a uniform thermal field. Four different inductor coils are therefore necessary to assure an homogeneous heating of all the specimens and they are displayed in Figure 5.9.

The efficiency of the designed inductor heads was evaluated through heating trials, coils of different shapes were tested until a homogeneous temperature distribution was obtained for every specimen geometry. In particular the distance between the inductor and the blank as well as the PID coefficients of the control system were properly chosen to assure that. Some heating tests were therefore performed in order to evaluate the efficiency of the shape of the different coils, the austenitization temperature was set equal to 900°C with a soaking time in temperature of 5min.

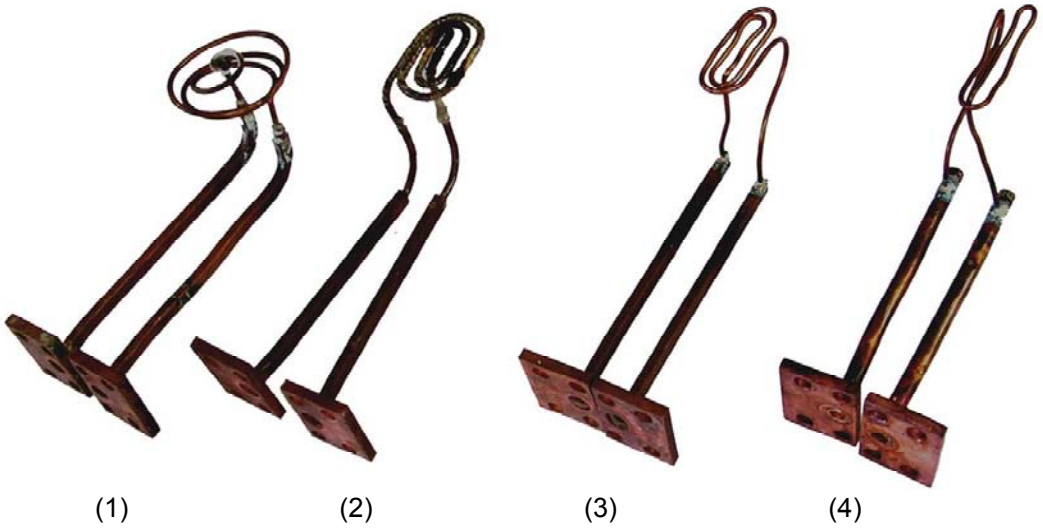

Figure 5.9 Inductor coils with optimized shape

Three thermocouples were spot-welded in the centre of the specimens, 15mm far from each others in radial direction, to identify the thermal gradients during the heating and the holding phases. In the following figures the thermal evolution during tests with two optimized inductors is displayed; it is possible to notice that the temperature differences in all the area of interest are lower than 50°C, and this was chosen as the maximum gap to accept the coil shape.

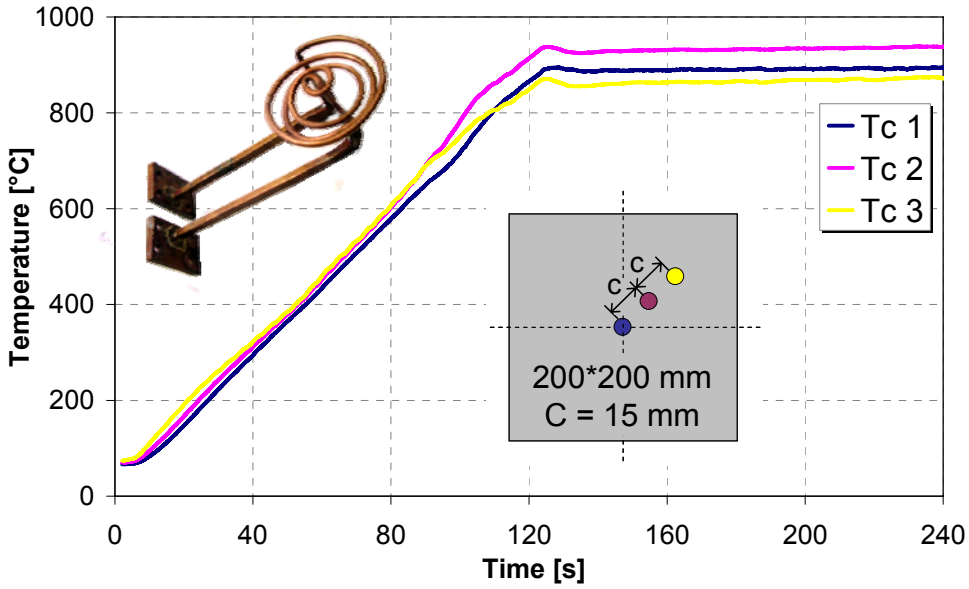

*Figure 5.10 Heating test with the 200*200mm specimen*

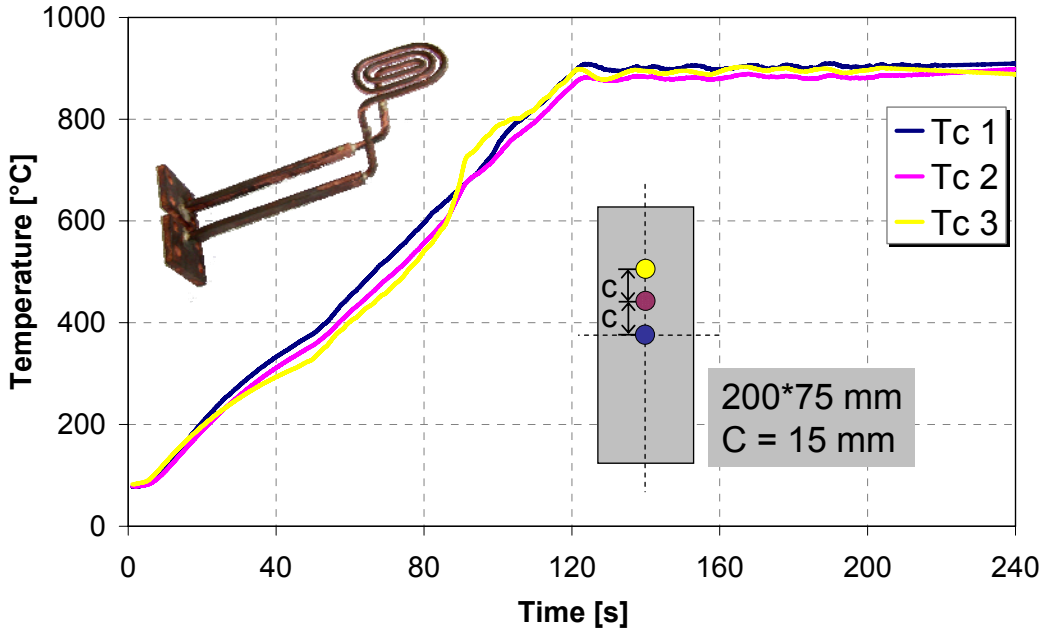

*Figure 5.11 Heating test with the 200*75mm specimen*

This kind of test was performed for all the samples of different width and Table 5.1 shows the specimen geometries that can be heated with each inductor coil in order to obtain a homogeneous temperature distribution.

Table 5.1Inductor types and corresponding specimen widths

Inductor type	*1*	*2*	*3*	*4*
Specimen width [86]	*200, 175 150, 125*	*100, 75*	*50*	*25*

5.2 Physical simulation experiments

In hot stamping operations an accurate evaluation of the influence of process parameters on the properties of stamped components is fundamental in the design and optimization of the forming process. The modified Nakazima device, designed and setup with the above described features, enabled to carry out physical simulation experiments whose aim was to reproduce in a controlled environment those variations of the process parameters that are likely to affect both the material formability and the resulting microstructure of the component at room temperature. In particular, the influence of punch temperature and

ram speed was investigated with regard of the microstructure the sheet presents at room temperature after forming; the investigated material was the boron steel 22MnB5 with a thickness of 1.5mm. Square specimens of 200mm width were austenitized at 900°C for 3min by means of the inductive heating system, then the sheet was cooled in air for 5s, in order to reproduce the heat loss due to the blank moving from the furnace to the press during the industrial practice. Afterward the punch moved down and deformed the sample, while cooling it. The analysis was carried out with two values of the ram speed and two values of the punch temperature. All test were performed until room temperature, Table 5.2 displays the experimental plan.

Table 5.2 Experimental plan for the physical simulation tests

Punch temperature [°C]	*20*	*300*
Punch speed [mm/s]	*5, 20*	*5, 20*

The following figures report the temperature evolution at the three thermocouples location during the forming phase after austenitization for several punch speeds and punch temperatures.

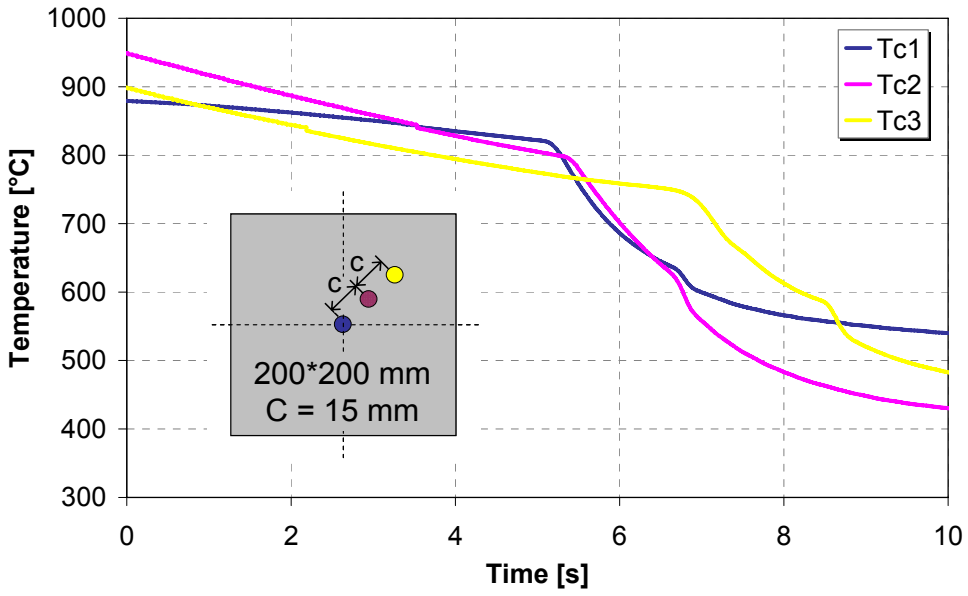

Figure 5.12 Temperature evolution during deformation at 5mm/s with punch temperature of 300°C

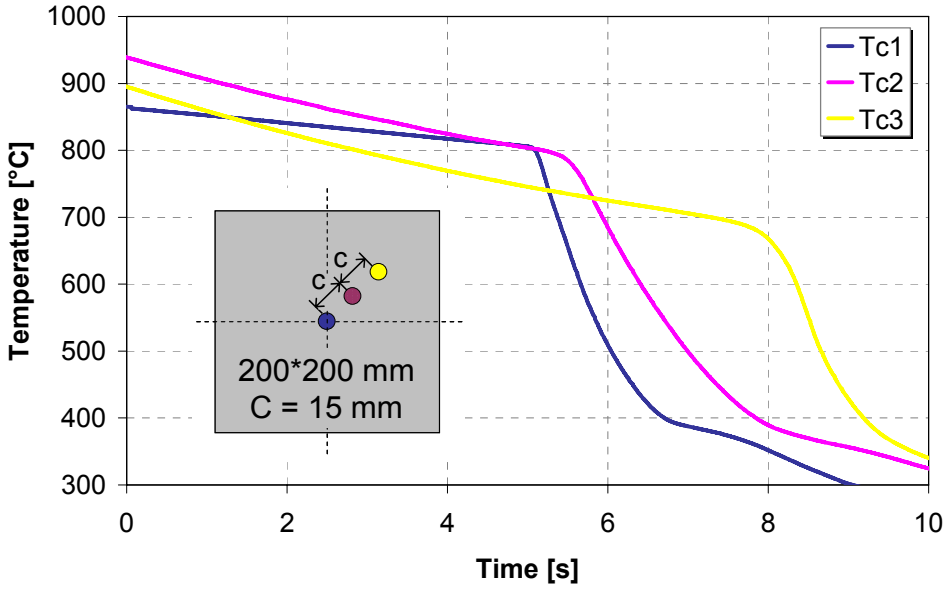

Figure 5.13 Temperature evolution during deformation at 5mm/s with punch temperature of 20°C

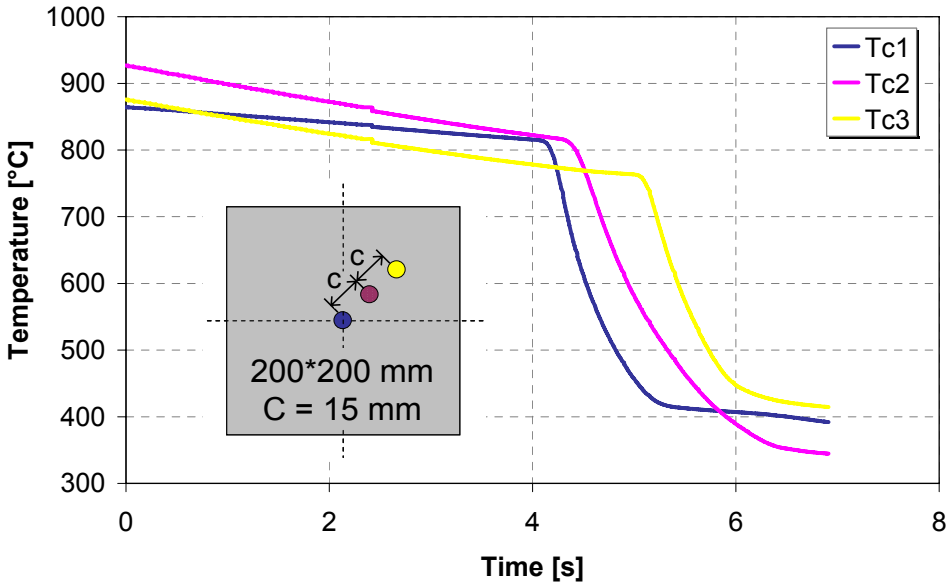

Figure 5.14 Temperature evolution during deformation at 20mm/s with punch temperature of 20°C

Different test conditions produced various cooling rates and thus different microstructure at room temperature. Some micrographs were carried out in the area affected by deformation and Figure 5.15 shows the resulting microstructure in correspondence of the thermocouple positioned 15mm far from the centre (Tc2) .

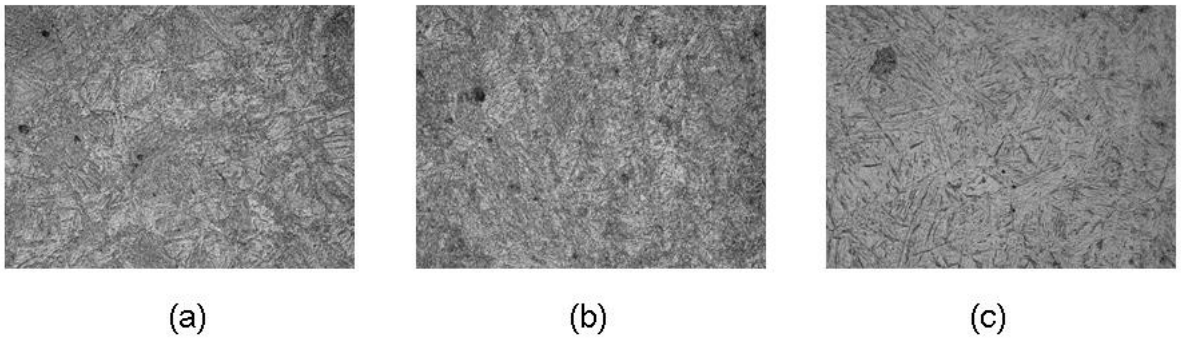

Figure 5.15 Microstructure in Tc2 position after deformation with punch at 300°C and 5mm/s (a), 20°C and 5mm/s (b) and 20°C and 20mm/s (c)

The microstructural analysis displays a ferritic/pearlitic microstructure when deformation is carried out at 5mm/s with punch temperature of 300°C, a mixture of ferritic and bainitic phase with punch speed of 5mm/s and temperature of 20°C, mostly bainite is present after deformation performed at 20mm/s with heated punch. Only deforming at a speed of 20mm/s and keeping the punch at room temperature can assure a fully martensitic microstructure at the end of the tests, as summarized in Table 5.3.

Table 5.3 Resulting microstructure at different test conditions

22MnB5		*Punch speed [mm/s]*	
		5	*20*
Punch temperature [°C]	*20*	*bainite/ferrite*	*martensite*
	300	*ferrite/pearlite*	*mostly bainite*

These results demonstrate that such test can act as physical simulation of the industrial hot stamping process, being capable to reproduce the same thermo-mechanical events and giving an insight of the effect of variations of process parameters on the thermal and microstructural evolution during deformation.

5.3 Forming limit curves determination

The investigations described in the previous chapters were performed to evaluate the material behaviour during press hardening in terms of elastoplastic properties (e.g. flow curves, anisotropy evolution, Young's modulus), as function of temperature and strain rate, and phase transformation kinetics, such as transformation plasticity and shift of the TTT curves due to applied stress, but their correlation with the process parameters and the formability characteristics have not been investigated yet. As reliable FE models of the hot stamping process should require the implementation of Forming Limit Curves at constant temperature, a new approach is proposed to evaluate material formability and determine FLC in isothermal conditions taking into account the effects of microstructural transformation kinetics.

5.3.1 Forming limit curves at elevated temperature

in hot stamping operations the material formability is strongly influenced not only by the stress and strain states, but also by temperature, strain rate and microstructural evolution during deformation, therefore the well-established approach to determine FLC at room temperature can be followed only partially. In conventional sheet metal forming at room temperature material formability is generally described through FLCs obtained by changing the stress state from balanced biaxial to pure shear. Different kinds of test have been developed and applied [77] and the Nakazima and the Marciniak are the more widespread among them. The ISO 12004 [76] standard has been recently improved to guarantee repeatability in tests conduction and results analysis, but the procedures to apply this standard to sheet forming at elevated temperature are far from being established. In particular the FLCs have to be determined at constant temperature and to be relevant only to one microstructural constituent, when applied to press hardening. The use of heated tools at testing temperature can assure the uniform thermal profile on the sheet metal during the test, while the possibility to have only one steel phase during deformation can be fulfilled only if the material phase transformation kinetics is completely understood. Particular attention must therefore be paid to properly identify the cooling rate assuring the whole deformation taking place before phase transformation, in order to obtain FLCs in fully metastable austenite, which is the most critical condition to be reproduced. This cannot prescind from an accurate evaluation of the phase transformation onset as function of both cooling rates and stress conditions characterizing the hot stamping process.

5.3.2 Design of the thermal cycle

Being the metastable austenite the most difficult condition to maintain during the tests with the new Nakazima setup and being the industrial forming operations performed in fully austenitic phase, the formability testing was focused on such microstructure. A preliminary investigation was therefore carried out to identify the most appropriate cooling rate after austenitization for reaching the testing temperature that could assure the whole Nakazima test took place when the material was still in the metastable austenite phase. The experimentation was performed by using the 22MnB5 steel, pre-coated with an aluminium-silicon based layer, with a thickness of 1.5mm. Only 200*200mm squared specimens were used in the preliminary Nakazima tests, in fact their higher thermal inertia represented the most critical condition by producing the lowest cooling rate with respect to the geometries of the other samples. Deformation was performed at 600°C, that corresponds to the nose of the material bainitic curve and thus represents the most crucial testing temperature with the lowest time interval before transformation phase onset. Different cooling rates, obtainable in the Nakazima apparatus, were finally reproduced on the MTS setup described in §3.4.1 to correlate the relevant parameters to the microstructure evolution.

5.3.2.1 Natural air cooling

According to the industrial practice, specimens were austenitized in the Nakazima apparatus at 900°C for 3 minutes, then a natural air cooling was applied, corresponding to an average cooling rate of almost 20K/s, until the testing temperature of 600°C was reached. Afterward deformation was performed in isothermal condition by means of the punch heated at 600°C with a speed of 10mm/s, as summarized in Table 5.4.

Table 5.4 Thermal and mechanical parameters of the Nakazima test

Austenitization temp. [°C]	*Soaking time [s]*	*Cooling rate [K/s]*	*Deformation temp. [°C]*	*Punch temp. [°C]*	*Punch speed [mm/s]*
900	*180*	*20*	*600*	*600*	*10*

Temperature evolution was monitored during the test through a thermocouple spot-welded in the centre of the specimen, in Figure 5.16 the temperature after austenitization vs. time during natural air cooling after austenitization is displayed.

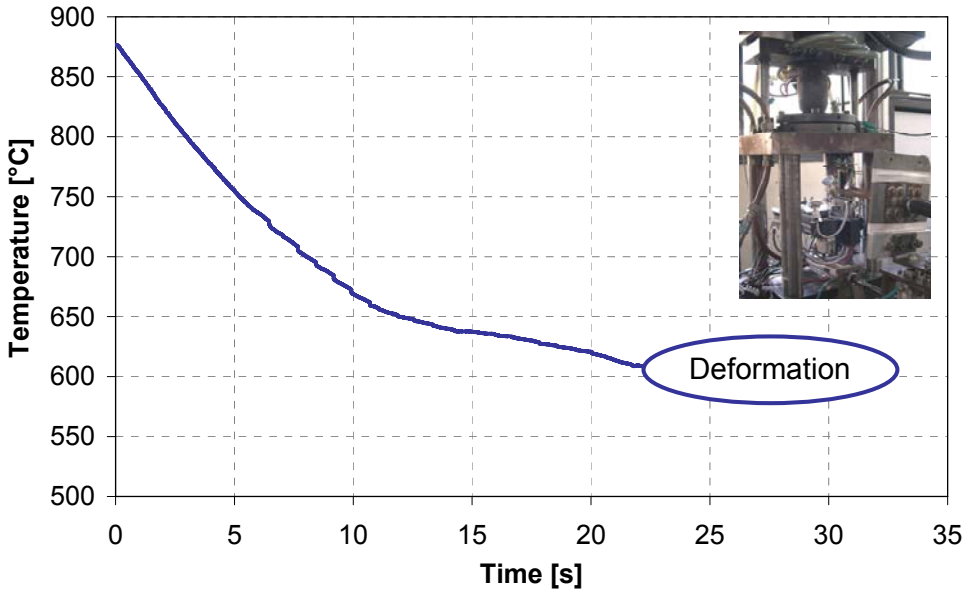

Figure 5.16 Temperature evolution during natural air cooling after austenitization

The MTS experimental setup equipped with the modified axial extensometer described in § 3.4.1 was used in order to perform the corresponding dilatometric measurement and thus verify if deformation took place in austenitic condition during the Nakazima test. After austenitization the same cooling profile was therefore imposed to the tensile specimen, then the holding temperature of 600°C was maintained to identify the onset of phase transformation; the test was carried out in stress-free conditions. The parameters of the test are summarized in Table 5.5.

Table 5.5 Thermal and mechanical parameters of the dilatometric test

Austenitization temp. [°C]	*Soaking time [s]*	*Cooling rate [K/s]*	*Holding temp. [°C]*	*Holding time [s]*	*Applied stress [MPa]*
900	*180*	*20*	*600*	*30*	*0*

Figure 5.17 shows that, in case of stress-free natural cooling rate, the deformation of the sheet metal blank takes place during the austenite-to-bainite phase transformation, therefore the Nakazima tests and the FLC determination cannot be performed in these conditions, and an higher cooling rate should be applied in order to obtain deformation in still metastable austenitic phase.

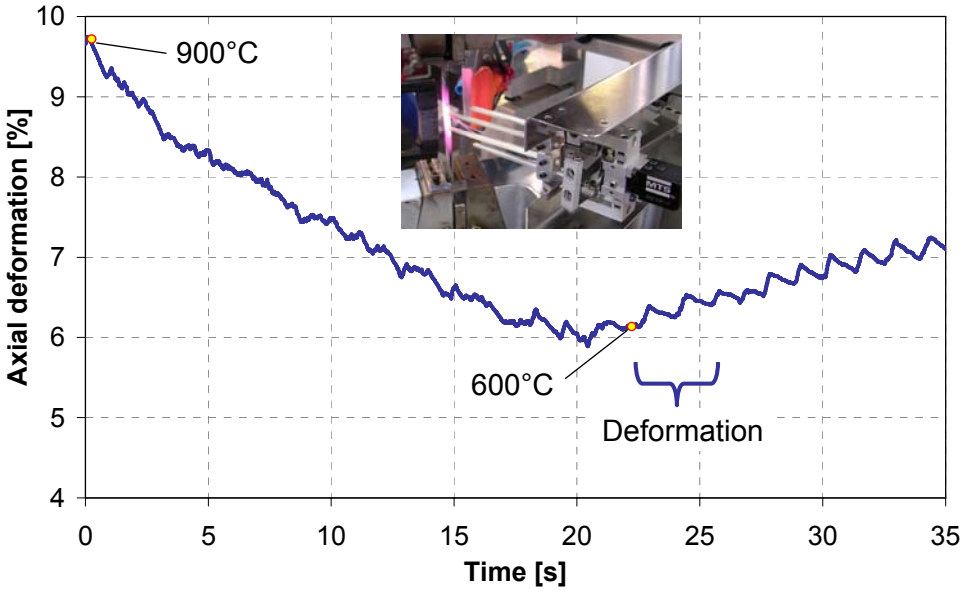

Figure 5.17 Axial strain evolution with natural air cooling in stress-free condition at 600°C

5.3.2.2 Forced air cooling

The Nakazima setup was therefore equipped with an air-compressed cooling system in order to obtain higher cooling rates after austenitization. The sheet metal can thus be subjected to cooling rates up to 100K/s by means of four air nozzles, placed in correspondence of the specimen, whose intensity can be adjusted in order to control the sheet heat loss. After austenitization at 900°C a cooling rate of 100K/s was applied, then deformation was performed at 600°C with a punch speed of 10mm/s, as reported in the following.

Table 5.6 Thermal and mechanical parameters of the Nakazima test

Austenitization temp. [°C]	*Soaking time [s]*	*Cooling rate [K/s]*	*Deformation temp. [°C]*	*Punch temp. [°C]*	*Punch speed [mm/s]*
900	*180*	*100*	*600*	*600*	*10*

The resulting temperature evolution during forced air cooling after austenitization is displayed in Figure 5.18.

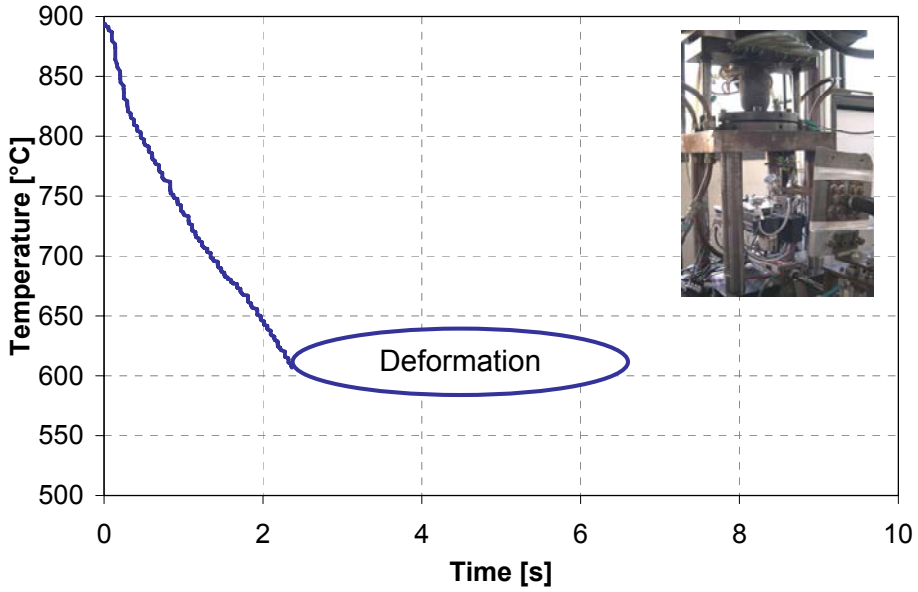

Figure 5.18 Temperature evolution during forced air cooling after austenitization

The same thermal profile was reproduced in the MTS setup, maintaining the specimen at 600°C after cooling, and the thermo-mechanical parameters of the test are summarized in Table 5.7.

Table 5.7 Thermal and mechanical parameters of the dilatometric tests

Austenitization temp. [°C]	*Soaking time [s]*	*Cooling rate [K/s]*	*Holding temp. [°C]*	*Holding time [s]*	*Applied stress [MPa]*
900	*180*	*100*	*600*	*30*	*0, 112*

If a punch speed of 10mm/s is set, then the deformation to failure takes about 2.5s, therefore the phase transformation at the testing temperature must start after this time interval. According to the stress-free dilatometric curve displayed in Figure 5.19, the deformation to failure took place in the constant condition of metastable austenite, before the bainitic phase transformation onset that corresponds to the increase of the axial strain.

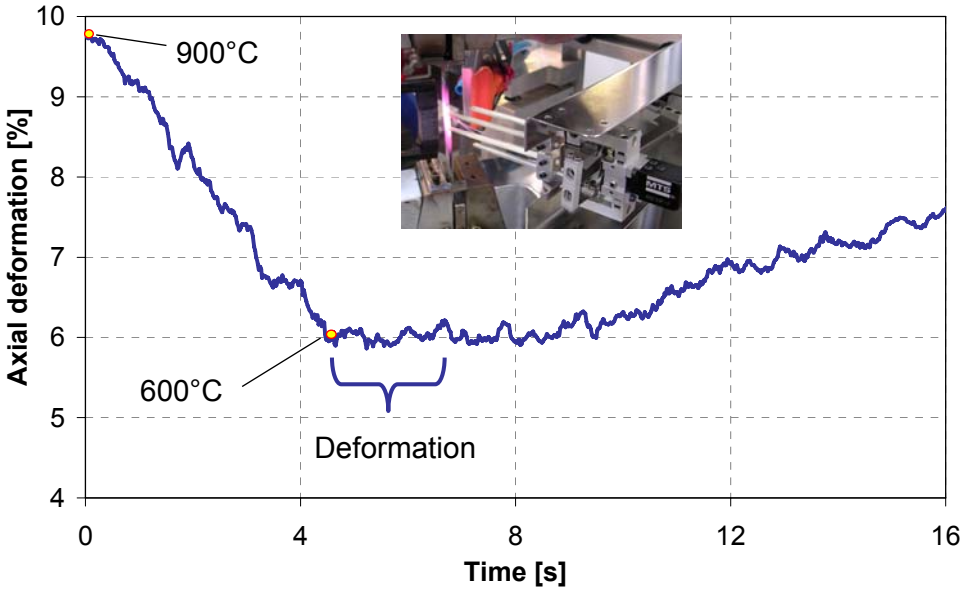

Figure 5.19 Axial strain evolution with forced air cooling in stress-free condition at 600°C

During deformation, Nakazima tests induce in the sheet stress-strain states that can modify the material phase transformation kinetics, as demonstrated in § 4.2, therefore the shift of the TTT curve due to applied stress has to be taken into account in this investigation. To this aim, the same dilatometric analysis was performed with the superimposition of a plastic stress during the holding phase at 600°C after the forced air cooling, and the resulting curve is shown in Figure 5.20.

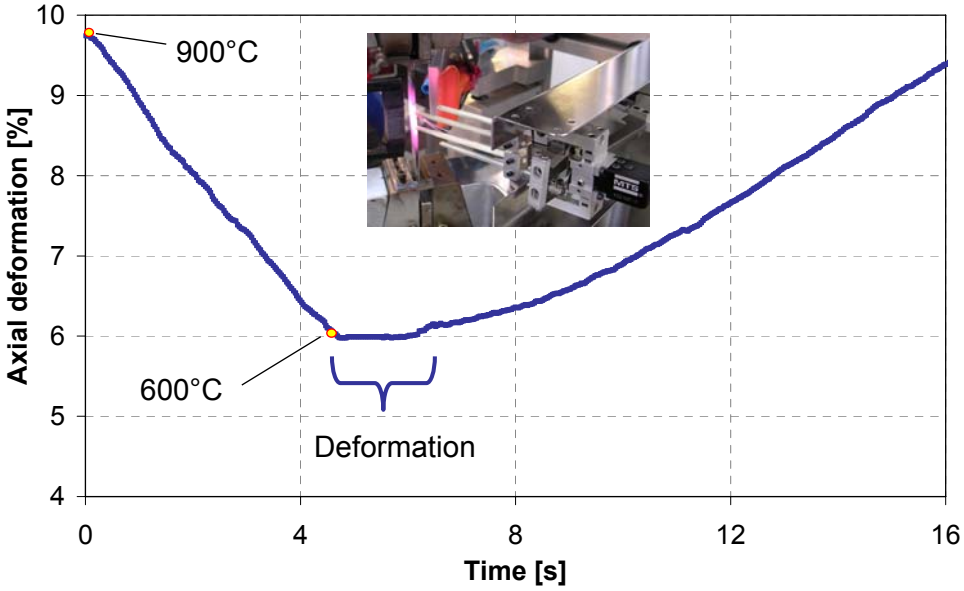

Figure 5.20 Axial strain evolution with forced air cooling and plastic stress superimposition at 600°C

Also in this case the dilatometric analysis confirmed that the deformation was performed in the Nakazima test before the bainitic phase transformation onset, in condition of metastable austenite. It was then recognized that a cooling rate of 100K/s is suitable to perform the tests in fully austenite state at the testing temperature of 600°C, and thus also at lower and higher temperatures where, according to the TTT curves, the transformation onset is delayed.

5.3.3 Results and discussions

The above described Nakazima setup was used to perform tests at high temperature and obtain FLD in isothermal conditions with the material in a fully metastable austenite state. The investigated material was the quenchenable high strength steel 22MnB5, 1.5mm thick. Specimens of different width (from 200mm to 25mm) were austenitized at 900°C for 3min by using inductor coils of different shape, then a rapid cooling rate of 100K/s was applied, by means of compressed-air jets, until the testing temperature of 600°C was reach; deformation was therefore carried out with a punch speed of 10mm/s. The surface punch temperature was set equal to 600°C and it was controlled through a infrared thermo-camera in order to assure a homogeneous thermal profile in the area of interest; graphite foils were used to reduce friction at the punch-sheet interface during deformation and to obtain fracture in correspondence of the apex of the dome. The acquisition rate of the optical strain measurement system was set equal to 12Hz and the lighting system candlepower was adjusted to guarantee a good acquisition at the testing temperature. At least two test runs were performed for each test condition in order to verify the repeatability. The parameters of the experimental campaign are summarized in Table 5.8.

Table 5.8 Testing parameters of the Nakazima tests

Austenitization temp. [°C]	*Soaking time [s]*	*Cooling rate [K/s]*	*Testing temp. [°C]*	*Punch temp. [°C]*	*Punch speed [mm/s]*	*Lubricant*	*Frame rate [Hz]*
900	*180*	*100*	*600*	*600*	*10*	*graphite*	*12*

Figure 5.219 shows the uniformity of temperature profile in the area interested by deformation of a 200*200mm sheet metal sample acquired through the infrared thermo-camera just before the beginning of deformation.

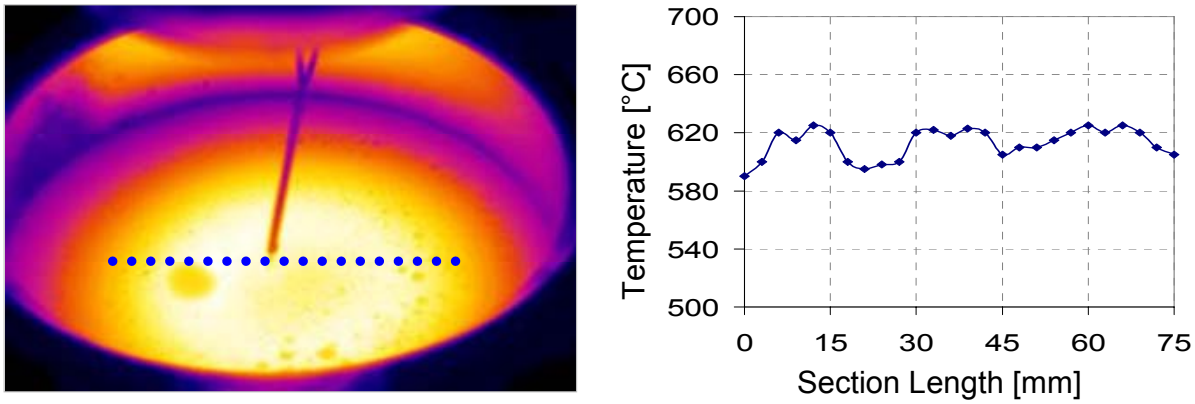

Figure 5.21 Temperature profile monitored at the end of the cooling phase

Figure 5.22 presents the major and minor logarithmic strains in correspondence of a cross section of the failure zone, just before fracture occurs. The very pronounced peak in the major strain represents the post-necking deformation due to the high material sensitivity to strain rate at elevated temperature and this phenomenon was observed in all tests conditions.

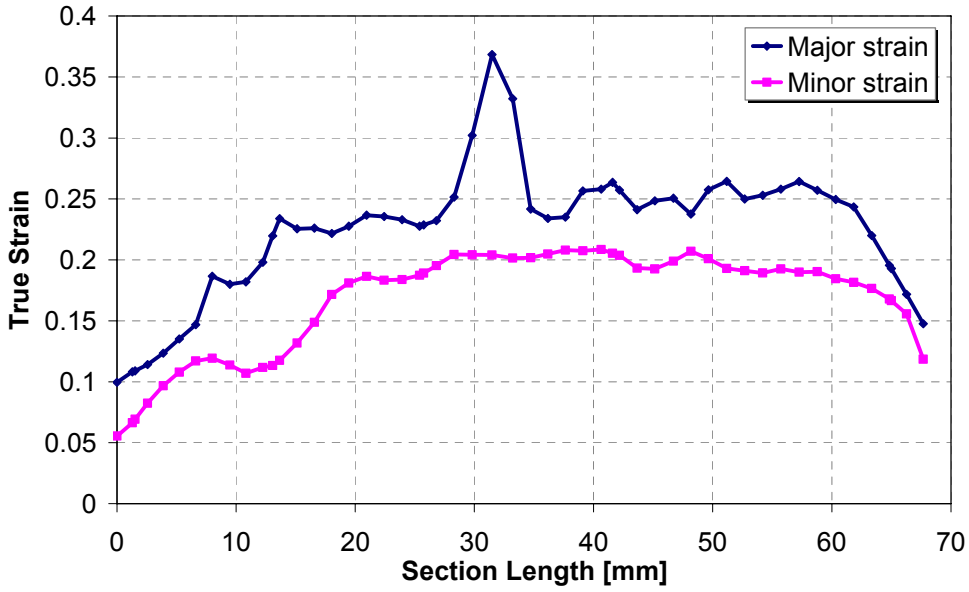

*Figure 5.20 Major and minor true strains across the failure zone (200*200mm specimen)*

Formability data were determined for different strain paths, whose range goes from uniaxial to biaxial tension. One possible representation of these values is represented by the traditional Forming Limit Curve, elaborated with the indications of the standard ISO

12004. The standard analysis procedure is implemented in the ARMAIS™ software and it can be summarized as follows:

- only the last load stage before the crack is computed;
- 3 parallel section, each 2mm apart;
- sections as long as possible, but not up to the edge of the specimen;
- position of the sections for minor strain >0: perpendicular to subsequent crack;
- position of the sections for minor strain <0: as parallel as possible to the edge of the specimen.

The strain across the deformed test piece is determined and the measured strains are processed in such way that the necked or failed area is eliminated from the results. The maximum strain that can be imposed on the material without failing is therefore determined through interpolation. This maximum of the interpolated curve is thus defined as the forming limit. Figure 5.23 displays the FLCs determined in isothermal conditions at 600°C, with a punch speed of 10mm/s, and when the material is in a fully metastable austenite state, together with a set of deformed specimens.

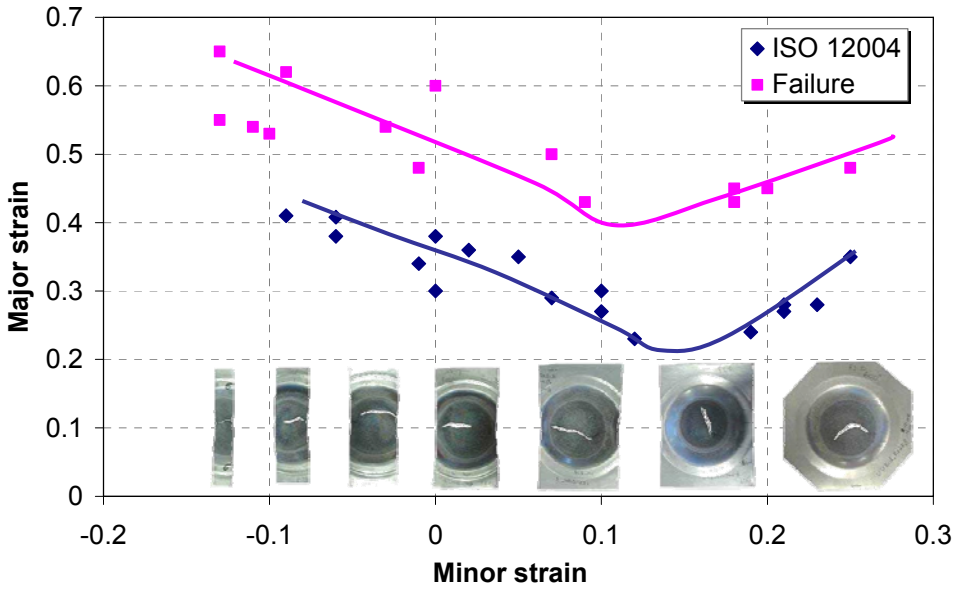

Figure 5.21 Forming Limit Curves of 22MnB5 at 600°C in metastable austenite condition

The blue dots represent the FLC obtained through the ISO 12004 procedure, while the purple ones represent the strains computed at failure. The significant enhancement of formability in the post-necking is demonstrated by the comparison between the two

curves. Therefore the increased material formability allowed by deforming at elevated temperatures during the industrial process can be utilized only in the post-necking deformation.

A new standard to determine FLC at elevated temperatures should de therefore taken into account in order to consider the increased post-necking deformation that sheet metal can undergo during hot forming operations.

5.4 Conclusions

The formability of high strength steels, formed and quenched at the same time during press hardening, has to be investigated under the same process conditions the sheet experiences during the forming phases. On the other hand, the evaluation of the blank thinning and eventually fracture through numerical simulation based on FE models requires the implementation of Forming Limit Curves as function of the various process parameters. To this aim, a innovative apparatus was developed and the new formability testing procedure for the investigation of material formability and microstructure phenomena has been presented. The developed experimental setup can act as a physical simulation of the industrial hot stamping process, being capable to reproduce the same thermal and mechanical events and to offer the possibility to evaluate the influence of testing parameters on thermal and microstructural evolution during deformation. An accurate methodology for the calibration of the phase transformation parameters and the temperature control was implemented and the approach was successfully applied to the determination of the 22MnB5 FLC in metastable austenite state.

CHAPTER 6
NUMERICAL MODEL CALIBRATION

Numerical simulations are even more important in the optimization of the hot stamping operations to obtain the desired mechanical and microstructural properties on final product. In order to compute reliable FE simulations, a coupled thermo-mechanical-metallurgical model has to be used.

In § 6.1 the numerical code and the implemented model utilized to take into account the coupling mechanisms are presented. Particular attention has to be paid to the input data related to material behaviour and interface phenomena necessary to accurately calibrate such a model, thus in § 6.2 these data have been determined by combining experimental techniques and FE inverse analysis. Finally, in § 6.3 the FE model has been validated through an accurate comparison between the results of physical and numerical simulations of a formability test.

6.1 Numerical model

A fully coupled thermo-mechanical-metallurgical FE model was defined to investigate and accurately describe phenomena due to the events that occur during industrial hot forming operations and that significantly influence material behaviour, process performances an final product features. Details on the code, material rheological and microstructural behaviour and inter-object interface conditions are given in the following paragraphs.

6.1.1 The FEM code

The numerical model developed in this work is a thermo-mechanical-metallurgical model implemented in the implicit FE code FORGE®. This software enables coupled modelling of deformation, heat transfer and microstructural evolution for simulation of hot forming operations, and its main features are briefly described.

All material exhibit a characteristic stress-strain curve that determines how the material behaves structurally in FE codes. As a material is deformed plastically, the amount of stress required to incur an incremental amount of deformation is given by the flow stress curve, which corresponds to the plastic region of the true stress-true-strain curve. Flow stress is strongly dependent on several parameters, such as temperature, strain rate and accumulated strain.

The minimum work rate principle is used for accurate calculation of metal flow, thus the velocity distribution which predicts the lowest work rate is the best approximation of the actual velocity distribution, and can be expressed mathematically as follows:

$$\pi = \int_V \bar{\sigma} \cdot \dot{\bar{\varepsilon}}\, dV - \int_S F_i u_i dS \tag{6.1}$$

$$\delta\pi = \int_V \bar{\sigma} \cdot \dot{\bar{\varepsilon}}\, dV - \int_S F_i \delta u_i dS + K \int_V \dot{\varepsilon}_V\, \delta\, \dot{\varepsilon}_V\, dV = 0 \tag{6.2}$$

(6.1) is a balance of the body forces versus the surface tractions and it is solved according to (6.2). The velocities are solved when the variation in the functional is stationary, by integrating the volumetric strain rate and multiplying by a large constant.

The manner in which the problem is divided into little subproblems that are easier to formulate is a process called meshing and represents the principle of FEM theory. Bodies are divided in several elements representing a portion of material and the solutions for (6.1) and (6.2) are the velocities at each node; FORGE® uses a four nodes tetrahedron discretization with automatic remeshing procedure. Finally in order to provide a unique solution to the problem the boundary conditions have to be specified.

6.1.2 Rheology

The material rheological behaviour in FORGE® is described by the Norton-Hoff law:

$$s = 2k\left(T, \bar{\varepsilon}, \ldots\right)\left(\sqrt{3}\,\dot{\bar{\varepsilon}}\right)^{m-1} \dot{\varepsilon} \tag{6.3}$$

The deviatoric stress tensor *s* is linked to the strain rate tensor $\dot{\bar{\varepsilon}}$ through the consistency *K* and the strain rate sensitivity *m*. The consistency forms a function that depends on the particular thermo-mechanical conditions and various standard functions that are integrated in the code. When the consistency is established through a function of the thermo-mechanical conditions, the strain-hardening power law combined with Arrhenius law for the temperature *T*, gives the following equation:

$$K\left(T, \bar{\varepsilon}\right) = K_0 \left(\bar{\varepsilon} + \varepsilon_0\right)^n e^{\frac{\beta}{T}} \tag{6.4}$$

The constant term K_0, the term of strain-hardening regulation ε_0, the coefficient of sensitivity to strain-hardening *n* and the temperature term β have to be defined.

Another type of evolution available in FORGE® is the Hansel-Spittel rheology defined as follows:

$$\sigma_f = A \cdot e^{m_1 T} \cdot \varepsilon^{m_2} \cdot \dot{\varepsilon}^{m_3} \cdot e^{m_4/\varepsilon} \cdot (1+\varepsilon)^{m_5 T} \cdot e^{m_7 \varepsilon} \cdot \dot{\varepsilon}^{m_8 T} \cdot T^{m_9} \tag{6.5}$$

where ε is the equivalent deformation (total strain), $\dot{\varepsilon}$ the equivalent deformation rate, T the temperature *and A, m_1, m_2, m_3, m_4, m_5, m_7, m_8, m_9* are the regression coefficients.

6.1.3 Microstructural behaviour

The microstructural evolution during cooling is represented through the material TTT diagrams. The FORGE® module uses information of specific material TTT curves along with thermal and elastic parameters, information about volume change for phase transformations and phases expansion parameters. Scheil (2.7) and Jhonson-Mehl-Avrami (2.6) models describe the germination and growing respectively.

Each phase expands and contracts depending on the temperature. A global thermal expansion coefficient for the material is obtained through a mix law and the global phase transformation enthalpy is calculated locally from a mix of each phase transformation enthalpy as function of temperature.

The model takes into account the plastic deformation (transformation plasticity) generated by the phase change and the influence of applied stresses on the shift of the transformation times by using the equation:

$$D = \frac{t_i - t_i^{'}}{t_i} \tag{6.6}$$

where the characteristic times t_i are changed in $t_i^{'}$ and the parameter D is defined as a function of the equivalent stress using a point to point or a polynomial law.

6.1.4 Thermal computation

Inside a physical system the temperature evolution is the result of the interaction between the internal heat conduction and the internal heat dissipation, under the constraints defined on the boundary zone in terms of imposed temperature or in terms of heat exchange (radiation, conduction, convection). This temperature evolution can be described by the following equation together with several boundary conditions:

$$\rho c \frac{\delta T}{\delta t} = div\left(k \cdot grad\left(T\right)\right) + \dot{W} \tag{6.7}$$

The internal dissipation for the system is typically generated by the plastic deformation, which dissipates the heat power $\dot{W}$, and can be represented using the Norton-Hoff law:

$$\dot{W} = \eta \cdot \sigma_{ij} \cdot \varepsilon_{ij} = \eta \cdot K \sqrt{3}\, \dot{\bar{\varepsilon}}^{\,m+1} \tag{6.8}$$

where η represents the efficiency of deformation.

The radiation affects the area boundary with a flux exchange term Φ_r, described by the equation:

$$\Phi_r = \sigma \cdot \varepsilon \left(T^4 - T_0^4 \right) \tag{6.9}$$

where σ is the Stefan constant and ε is the material emissivity, T represent the area boundary local temperature and T_0 the exterior area temperature.

The area boundary is affected by the conduction and the convection through the flux exchange Φ_c which is defined as follows:

$$\Phi_c = h\left(T - T_0 \right) \tag{6.10}$$

where h represents the global heat transfer coefficient (HTC) taking into account conduction and convection.

Also the friction type dissipation process Φ_{fr} can generate heat exchanges at the boundary and the two concerned bodies share the dissipated power at the interface with flux relative to their respective effusivity, see (6.11).

$$\Phi_{fr} = \frac{b_1}{b_1 + b_2} \alpha \cdot K \cdot \Delta v^{p+1} \tag{6.11}$$

where α id the friction coefficient, K the consistency of the material, Δv is the relative velocity between bodies, p the sensitivity to the sliding speed and b_i is the effusivity of the body when a thermal balanced-sheet is processed, calculated as:

$$b = \sqrt{k \cdot \rho \cdot c} \tag{6.12}$$

where k is the conductivity, ρ the density and c the heat capacity.

The thermal phenomena for an area with a part of its boundary thermically regulated and a part with heat flux exchanges are summarized in Figure 6.1. A plastic deformation is additionally submitted to this body.

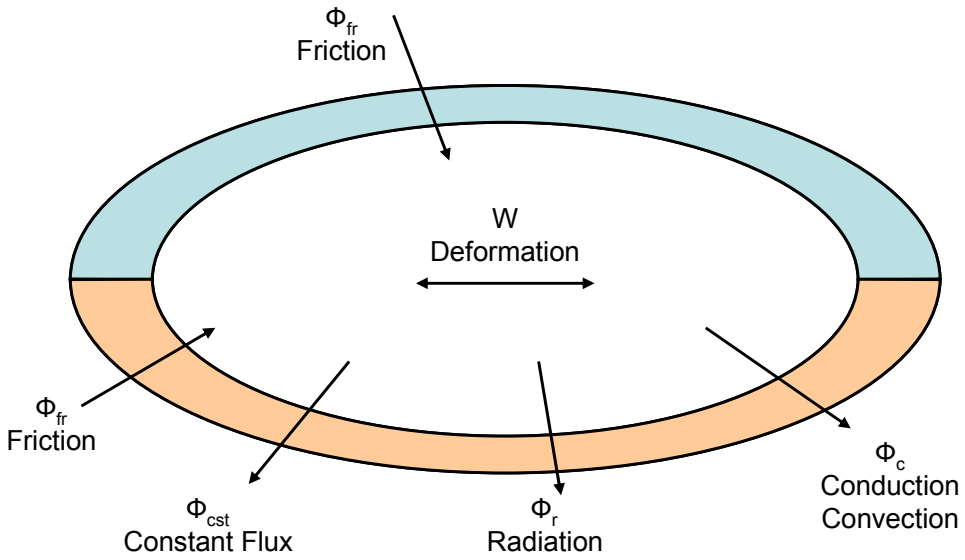

Figure 6.1 Thermal phenomena schematization

6.1.5 Modelling of friction

Friction between the part and the tool can be modelled in FORGE® by means of three available laws.

The viscoplastic friction law is described by the following equation:

$$\tau = -\alpha \cdot K(T,\varepsilon) \cdot \Delta v^{p-1} \cdot \Delta v \qquad (6.13)$$

This relation defines the shearing created by the difference in velocity *Δv* between the two bodies trough the sensitivity to the sliding speed *p* and the friction coefficient *α*. The consistency of the material *K* represents the characteristic of the mechanical substrate, while the friction coefficient *α* characterizes the complete interface, this being the workpiece surface state as well as the lubricant (if present), or the surface state of the tooling.

The Tresca friction law is described by (6.14), where $\overline{m}$ is the Tresca friction factor.

$$\tau = -\overline{m}\frac{\sigma_0}{\sqrt{3}} \qquad (6.14)$$

The Coulomb friction law is written in the following general form:

$$\tau = \sigma_n \cdot \mu \qquad (6.15)$$

where the friction shear stress is equal to the normal stress multiplied by the friction coefficient μ or to a fraction of the maximum shear stress sustainable by the material.

6.1.6 Thermo-mechanical-metallurgical coupling

Most of the mechanical and thermal parameters exhibit a noticeable evolution when the temperature range is significant. The mechanical equations are generally expressed as the virtual work principle. A time derivative of the temperature is introduced by a dilatation term, while the temperature itself is present as result of thermal variation of constitutive parameters and of boundary conditions. The set of mechanical equations can be therefore be expressed as:

$$R\left(V, X, \dot{T}, T\right) = 0 \tag{6.16}$$

where the array $V, X, \dot{T}, T$ denote the set of nodal values of velocity, nodal coordinates, time derivative of temperature and temperature respectively, being:

$$V = \frac{dX}{dt} \tag{6.17}$$

and

$$\dot{T} = \frac{dT}{dT} \tag{6.18}$$

The heat equation (6.7) written in integral form can be discretized in finite elements and the term that contains the velocity is introduced by the heat dissipation of plastic or viscoplastic work; the heat equation is therefore:

$$S\left(V, X, \dot{T}, T\right) = 0 \tag{6.19}$$

The thermal and mechanical coupling is expressed by the ordinary differential equations, given in implicit form by the nonlinear equations (6.16) and (6.19), and the derivatives in (6.17) and (6.18).

A Newton-Rapson method is used to resolve simultaneously (6.16) and (6.19). New values are computed from the increments ΔV and $\Delta \dot{T}$ starting from the initial value of V and $\dot{T}$ by solving the system:

$$\begin{bmatrix} \frac{\delta R}{\delta V} & \frac{\delta R}{\delta \dot{T}} \\ \frac{\delta S}{\delta V} & \frac{\delta S}{\delta \dot{T}} \end{bmatrix} \begin{bmatrix} \Delta V \\ \Delta \dot{T} \end{bmatrix} = \begin{bmatrix} -R\left(V, X, T, \dot{T}\right) \\ -S\left(V, X, T, \dot{T}\right) \end{bmatrix} \tag{6.20}$$

where

$$H = \frac{\delta R}{\delta V} \tag{6.21}$$

is the usual matrix derivative for the purely mechanical problem,

$$C = \frac{\delta S}{\delta \dot{T}} \tag{6.22}$$

represents the heat capacity matrix fro the thermal problem, $\frac{\delta R}{\delta T}$ is the thermal coupling in the mechanical equation and $\frac{\delta S}{\delta V}$ describes the coupling of mechanics on temperature distribution.

The use of the Newton-Rapson method on all the nodal unknowns significantly increases the CPU time, therefore an alternative method is utilized by FORGE®, which solves the mechanical problem alone, then it uses the new velocity field in the heat equation and solves the time derivative of temperature, afterward the velocity field is updated tacking into account the new value of $\dot{T}$. If the coupling terms are smaller than the main matrices the methods converges rapidly and the time time-integration scheme can be chosen independently.

The integration of microstructural-mechanical coupling introduces equations taking into account the elastic and elastoplastic component arising during phases transformations and a Gauss-Seidel algorithm is used to achieve this coupling.

Figure 6.2 shows the thermo-mechanical-microstructural coupling algorithm where ΔT_{max} is set by the user and 0 < q < 1. The thermo-microstructural coupled problem is formerly solved and the calculated time step is utilized to solve the mechanical problem and the coupling is achieved by iterating the procedure.

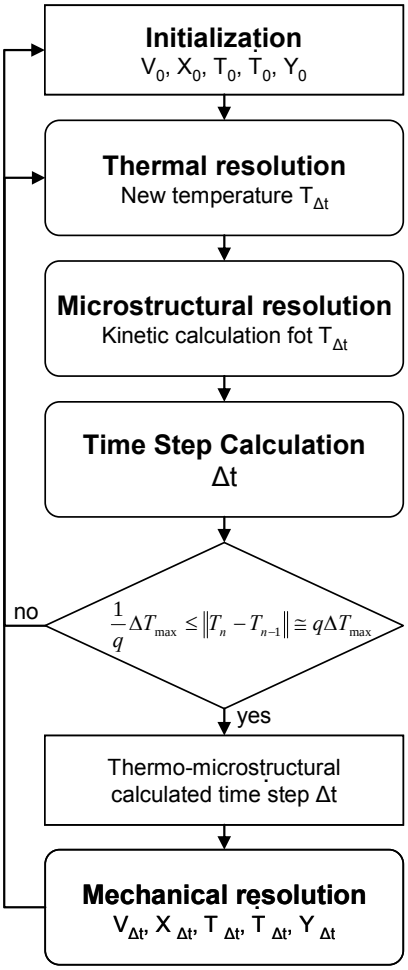

Figure 6.2 Thermo-mechanical-microstructural coupling algorithm

6.2 Calibration of the numerical model

The accurate calibration of the numerical model previously described is a strong requirement to improve the quality and reliability of numerical simulations of the hot stamping process. Such a model was therefore calibrated through both material testing experiments, to determine the rheological and microstructural parameters, and inverse analysis method to get a feasible heat transfer description. The investigated material was the boron steel 22MnB5, pre-coated with an aluminium-silicon protective layer, produced by ARCELOR with the commercial name of USIBOR 1500 P®.

6.2.1 Rheological behaviour characterisation

The material rheological characterization is essential for a proper FE model calibration, therefore the experimental device described in § 3.2 was used to carry out tensile tests at elevated temperature and thus generate reliable data as function of temperature and strain rate. The rheological behaviour of the material was described by means of the Hansel-Spittel model given by (6.5)

$$\sigma_f = A \cdot e^{m_1 T} \cdot \varepsilon^{m_2} \cdot \dot{\varepsilon}^{m_3} \cdot e^{m_4/\varepsilon} \cdot (1+\varepsilon)^{m_5 T} \cdot e^{m_7 \varepsilon} \cdot \dot{\varepsilon}^{m_8 T} \cdot T^{m_9}$$

where σ is the stress tensor, ε the strain tensor, $\dot{\varepsilon}$ the strain rate tensor and T the temperature of the test. The Hansel-Spittel coefficients for the 22MnB5 were determined by means of a non-linear regression analysis of the flow curves of the material, previously presented in § 3.2.2. The results are given in Tables 6.1.

Table 6.1 Hansel-Spittel coefficients for 22MnB5 at elevated temperature

A	m_1	m_2	m_3	m_4	m_5	m_7	m_8	m_9
0.18151	-0.00465	0.35149	-0.02881	0.00281	-0.00179	0.13348	0.000020	1.7299

In Figure 6.3 it is possible to notice the comparison between the experimental flow curves and the numerical description of the 22MnB5 rheological behaviour through the Hansel-Spittel model.

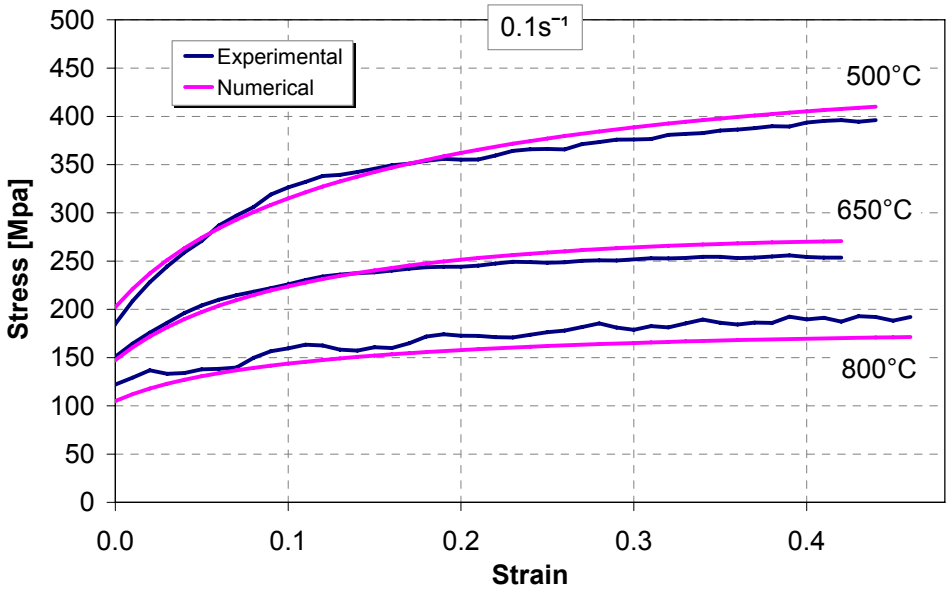

Figure 6.3 Comparison between 22MnB5 experimental data and Hansel-Spittel numerical model

6.2.2 Microstructural behaviour characterization

Microstructural data obtained from the experiment presented in § 3.1 were used to generate the 22MnB5 metallurgical database necessary to calibrate the FE model; in particular, an average grain size of 27μm was introduced into the code. To accurately represent the cooling phase and the 22MnB5 phase transformation kinetics, the material TTT curves (Figure 2.3) were implemented into the FORGE® TTT modulus, tacking into account the shift of the TTT curves evaluated in § 4.2 according to (6.6). The martensite start temperature was set equal to 380°C and a value of 300°C was chosen for the martensite finish temperature. The transformation plasticity strains as function of applied stress, determined in § 4.1, were also implemented in the model for all the phase transformations occurring to austenite during cooling (ferritic, bainitic and martensitic).

6.2.3 Heat transfer coefficient determination

Hot stamping is a non-isothermal process where deformation takes place simultaneously with quenching, thus the time-temperature sequence is essential to determine the final properties of the formed component. The proper determination of the heat transfer coefficient is therefore a strong requirement to obtain an accurate calibration of the FE model and perform reliable simulations of hot forming operations. In press hardening the thermal exchange depends both on the characteristics of materials in contact and on interface conditions (e.g. temperature, contact pressure, lubricant, surface quality, sliding length and velocity, etc.). Phenomena occurring at the sheet-die interface are usually studied by coupling experimental modelling with inverse analysis techniques or analytical approaches [46]. The experimental apparatus developed and setup at the Chair of Manufacturing Technology at the University of Erlangen-Nuremberg [10] was used to perform some quenching tests and evaluate the influence of contact pressure on the USIBOR 1500 P® heat transfer coefficient through inverse analysis.

6.2.3.1 Experimental apparatus

The experimental device developed at the Chair of Manufacturing Technology at the University of Erlangen-Nuremberg consists of a universal Schenk-Treble testing machine with a maximum force of 400kN [10, 46]. The lower and the upper tools are symmetrical and they are equipped with an exchangeable contact plate fixed on a base plate, which is water cooled in order to guarantee comparable temperature conditions at each test run, see Figure 6.4.

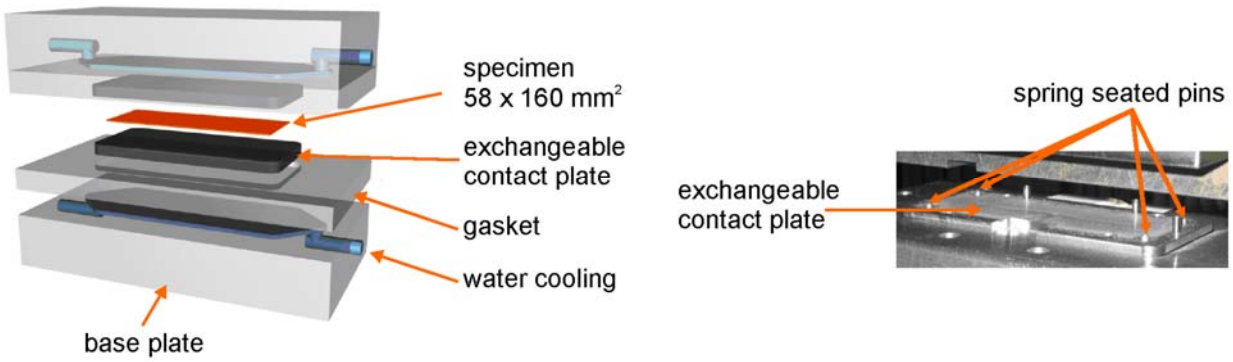

Figure 6.4 Details of the experimental setup [10] used to determine the heat transfer coefficients

The specimen is heated into a furnace and then placed upon three spring seated pins embedded in the lower contact plate which disappear when the tool is closed; they reduce heat loss due to the contact with the lower plate before the contact pressure is applied. After the specimen positioning into the die set, the upper tool moves downwards at 5mm/s until contact pressure starts to increase, then the speed is reduced until the defined load is reached. It takes about 10s to 12s from taking the specimen out of the furnace to the tool closing.

The temperature evolution is measured by means of four Ni/Cr-Ni thermocouples place at 1mm and 8mm beneath the surface of the contact plates and one inserted into a 1mm diameter hole which has been previously drilled in the middle of the specimen. A typical graph of the thermal evolution during the test is shown in Figure 6.5.

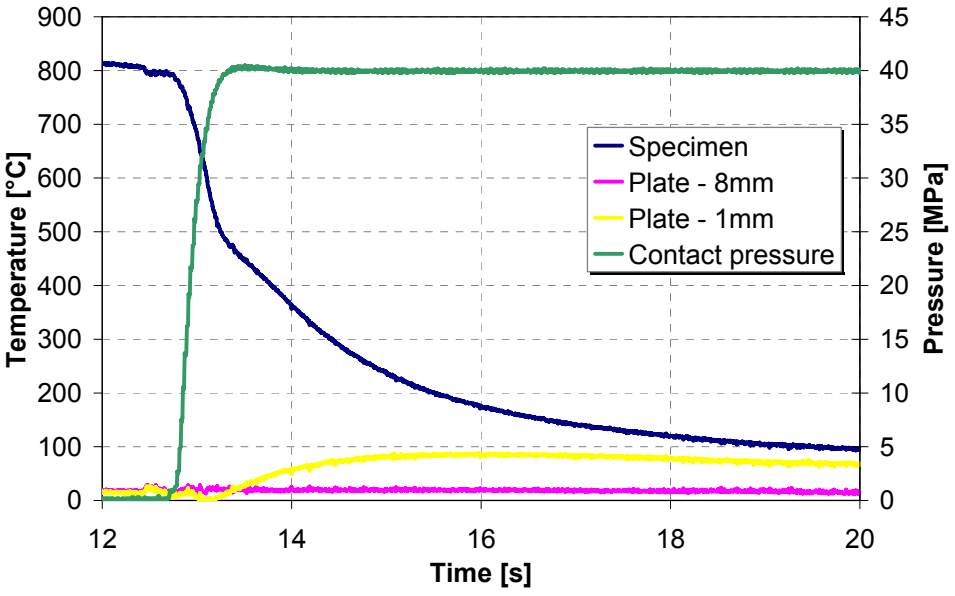

Figure 6.5 Typical temperatures and contact pressure evolution during the tests

6.2.3.2 Experimental results

USIBOR 1500 P® sheets produced by ARCELOR, with a thickness of 1.75mm, were used in this investigation. Specimens were austenitized in the furnace at 950°C for 5min and then rapidly transferred into the dieset; the experiments were carried out with contact pressure in the range 5-40MPa. Table 6.2 summarises the main test parameters:

Table 6.2 Testing parameters of the quenching tests

Austenitization temp. [°C]	*Soaking time [s]*	*Contact pressures [MPa]*
950	*300*	*5, 10, 20, 30, 40*

In Figure 6.6 it is possible to notice the temperature evolutions obtained during cooling by superimposing different contact pressures.

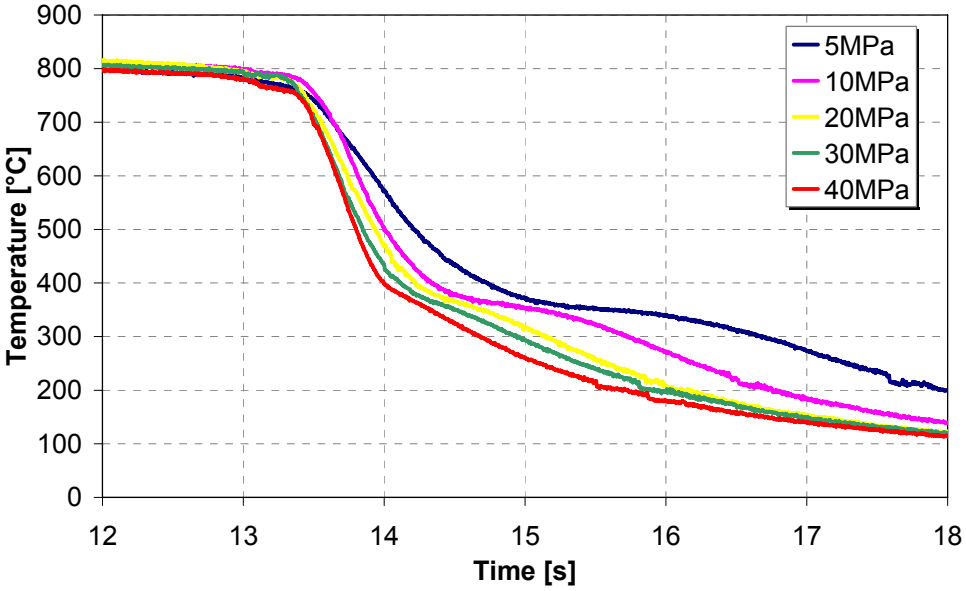

Figure 6.6 Experimental thermal evolution with different contact pressures

6.2.3.3 Inverse analysis application

The theoretical bases of the inverse analysis approach have been introduce in § 2.2. The identifications of the parameters is therefore an optimization problem with a final target of minimizing a cost function *Q* and needs the following points to be stated:

- a suitable experimental observable choice;
- choice of a proper law describing the physical phenomena;

- definition of the objective function Q;
- definition of a direct model of simulation able to the calculated values M^c by means of the chosen law starting from a set of parameters;
- definition of a minimizing algorithm;
- choice of a criteria to stop the research.

The method was therefore applied to evaluate the influence of contact pressure on the heat transfer coefficients at the die-workpiece interface of the experimental results presented in § 6.2.3.2. Temperature in the centre of the specimen was chosen as observable entity and a finite element model was used as direct model of simulation. The least square function (2.20) was chosen as cost function. The minimization algorithm was a Gauss-Newton method with sensitivity matrix evaluated through finite differences, jointed to a linear search algorithm inspired to the golden section linear search method.

6.2.3.4 Numerical model of the case study

In this investigation the numerical simulations were performed by using the commercial FE-code FORGE® by TransValor™. This software enables thermo-mechanical-metallurgical coupled simulations modelling deformation and heat transfer in cold, warm and hot conditions. The contact plates were modelled as both rigid and deformable bodies in order to compare the two different approaches.

The rheological behaviour was implemented in the model by means of the 22MnB5 thermo-mechanical parameters described in §6.2.1. The thermal conductivity and specific heat of the born steel were taken from the literature [87]. The temperature of the dies was 20°C and a specific heat of 461J/kgK was used for the contact plates while modeled as deformable bodies [13], the thermal and mechanical properties of the tool material were provided from database, which are shown in Table 6.4. A bilateral-sticking condition was assumed at the contact plate-specimen interface.

Table 6.3 Mechanical and thermal parameters of the tool material

Young's modulus [GPa]	*Poisson's ratio*	*Density [kg/m^3]*	*Conductivity [W/m K)*	*Specific heat [J/kg K]*
210	*0.28*	*7800*	*23*	*461*

Table 6.4 Thermal parameters for 22MnB5

Temperature [°C]	*Conductivity [W/m K]*	*Specific heat [J/kg K]*
20	*46.1*	*377*
100	*46.1*	*477*
200	*44.8*	*511*
400	*39.8*	*590*
600	*34.3*	*741*
800	*26.4*	*821*
1000	*27.2*	*821*

The simulation was divided into four steps in order to reproduce with a better accuracy the different phases of the experimental test. The four phases and the corresponding numerical conditions can be summarized as follows:

1. Natural air cooling, no dies in contact.
2. Upper tool moves downwards, one die in contact.
3. Increasing contact pressure, two dies in contact.
4. Maximum contact pressure, two dies in contact.

The thermal profiles of the specimen and of the dies at the end of each step were implemented as initial condition in the following step. The initial temperature of the specimen was assumed to be homogenous and equal to 950°C and the heat loss during the sheet transfer was simulated by using an heat transfer coefficient with air of 20W/kgK, reproducing the natural air cooling until the upper die comes in contact with the specimen.
The three-dimensional model of the experimental setup was preliminary compared with the two-dimensional one in order to evaluate their difference in terms of temperature evolution. In the following figures the two different models are shown with the contact plates modelled as deformable dies. In both models a sensor was placed in the middle of the specimen in order to measure the temperature evolution during the tests.

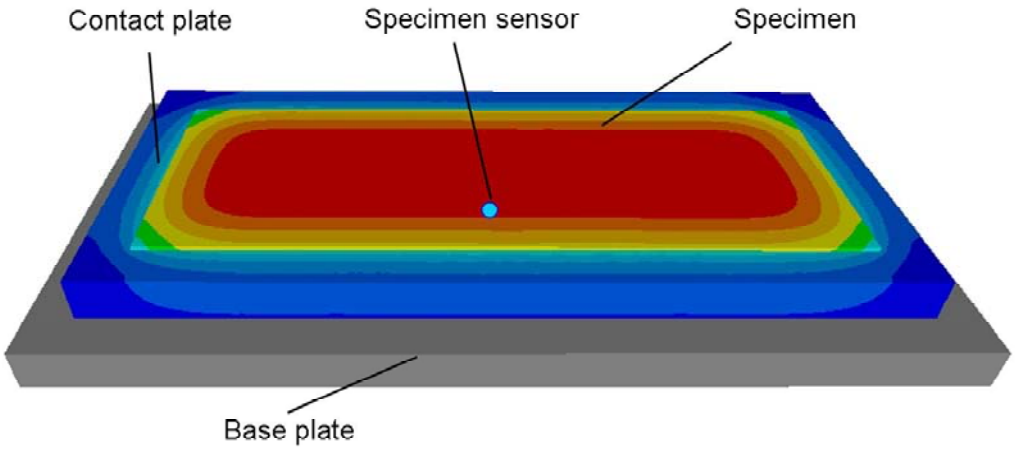

Figure 6.7 3D model of the case study

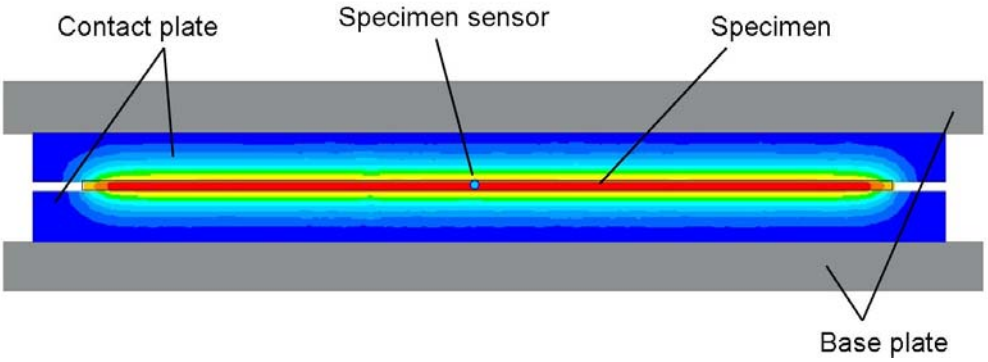

Figure 6.8 2D model of the case study

After the air cooling up to 800°C, the quenching into the dies was simulated assuming three different heat transfer coefficient for the following steps as reported in Table 6.5.

Table 6.5 Heat transfer coefficients used for the 2D and 3D simulations

Step	*1*	*2*	*3*	*4*
Heat transfer [MPa]	*20*	*500*	*2000*	*4000*

The comparison between temperature evolutions with the two models is displayed in Figure 6.9. The comparison shows a similar temperature evolution during cooling between the 2D and 3D models, thus the two-dimensional model was used in the investigation to significantly reduce the simulation time.

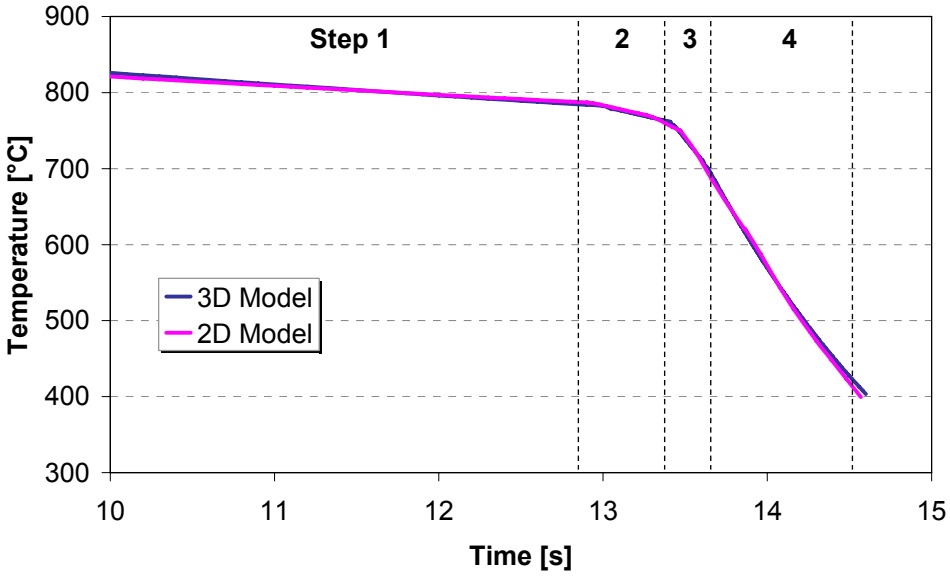

Figure 6.9 Temperature evolution with the 2D and 3D model

The time vs. temperature curves simulated by the numerical model were therefore compared in the cost function with the measured experimental profiles in order to minimize their difference. The influence of contact pressure on heat transfer coefficient during quenching was evaluated through the inverse analysis by modelling the contact plates both as rigid and as deformable dies, see Figure 6.10.

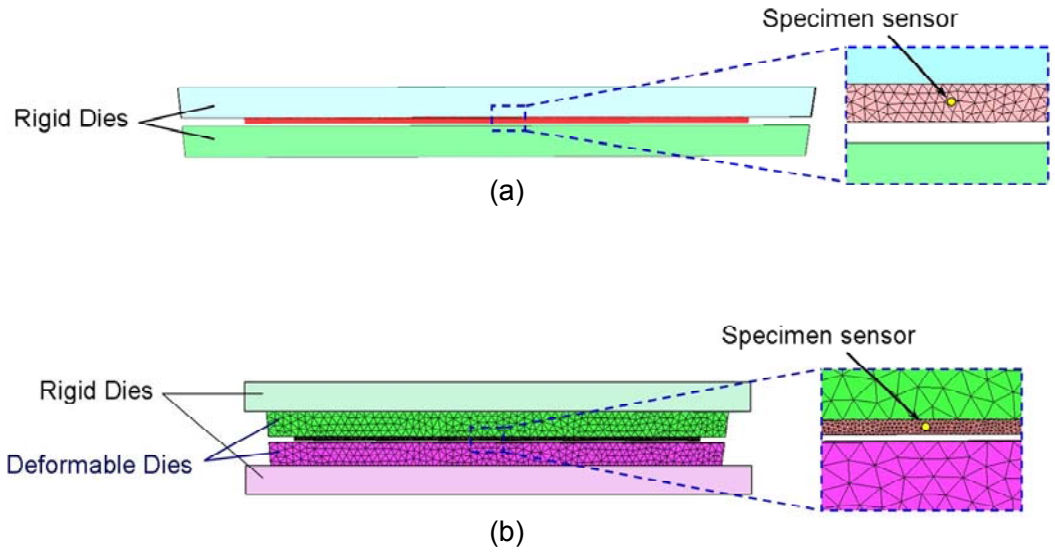

Figure 6.10 2D FE model of the case study modelling the contact plates as rigid (a) and deformable dies (b)

6.2.3.5 Results

The heat loss during the blank transfer from the furnace into the dieset was simulated in order to determine the heat transfer coefficient with air. The thermal and mechanical parameters of the material have been described in the previous paragraph and the initial temperature was assumed to be homogeneous and equal to 950°C. A good match between numerical and experimental result temperature evolution was achieved by using an HTC with air of 20W/kgK for all tests conditions. Afterward the resulting thermal field of the specimen was implemented in the following step.

The tests were carried out with contact pressure of 5, 10, 20, 30 and 40MPa. Latent heat was released due to the formation of martensite at a temperature of about 400°C but this phenomena was not taken into account in this analysis and particular attention was paid to obtain a good match in the range between 750°C and 450°C, which is typical of industrial hot stamping operations, thus the fourth step was stopped before the beginning of the martensitic transformation. For each test condition a good agreement between the numerical and experimental results was achieved with both rigid and deformable dies and the complete comparison between experimental and simulated temperature profile is given in Appendix B.

A heat transfer coefficient of 20W/m^{2}K for the first simulation step (natural air cooling) and a value of 500W/m^{2}K for the second simulation step (one die in contact) allowed to obtain a good match between experimental and numerical results, therefore these values were used for all test conditions. The influence of contact pressure on heat transfer coefficient for USIBOR 1500 P® is summarized in Figure 6.11, for contact plates modelled as rigid dies, and in Figure 6.12, for contact plates modelled as deformable bodies. The most interested results are the ones corresponding to the fourth step, where the contact pressure reaches the maximum value and is maintained constant. These data can therefore provide a guideline for the choice of heat transfer parameters in coupled thermo-mechanical simulations of press hardening process.

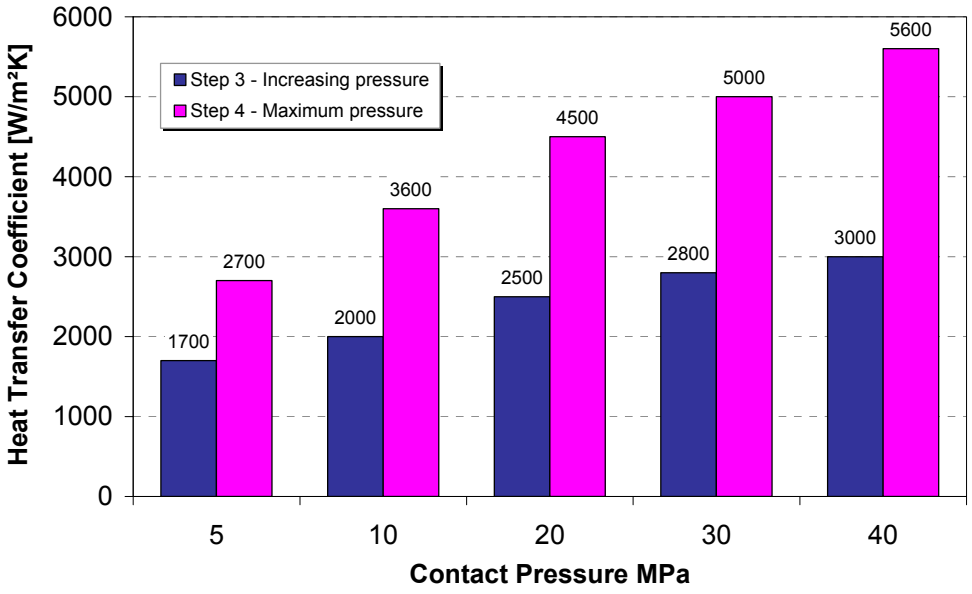

Figure 6.11 Heat transfer coefficients obtained by the inverse analysis on the tests on the Al-Si pre-coated 22MnB5 modelling the contact plates as rigid bodies

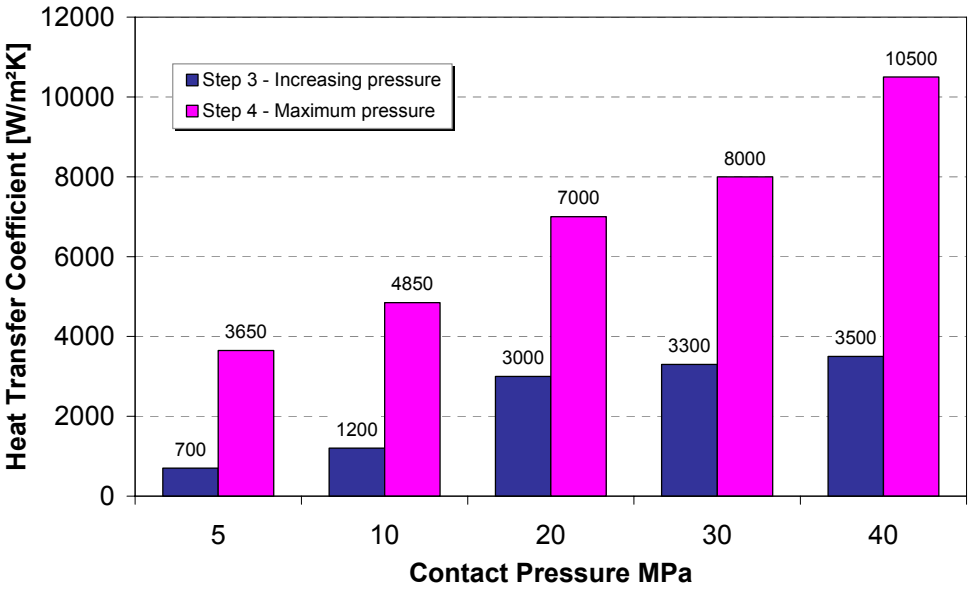

Figure 6.12 Heat transfer coefficients obtained by the inverse analysis on the tests on the Al-Si pre-coated 22MnB5 modelling the contact plates as deformable bodies

6.3 Numerical model validation

The numerical model, previously calibrated, was validated through the comparison between the physical and numerical simulation of a formability test performed on a USIBOR 1500 P® blank. The thermo-mechanical cycle typical of the hot stamping process was reproduced by means of the new Nakazima apparatus and the testing conditions of the deformation phase were implemented in the FE model, in order to compare the results in terms of stroke vs. force curve and temperature evolution.

6.3.1 Physical simulation of the deformation phase

In § 5.2 it has been shown how the new experimental setup, based on the Nakazima concept, can act as a physical simulation of the hot stamping process by reproducing the same thermal and mechanical conditions that sheet metal undergoes during hot forming operations.

Figure 6.13 Physical prototype of the experimental setup

Squared specimens of the Al-Si pre-coated boron steel 22MnB5, with a thickness of 1.5mm, were austenitized at 900°C for 3min and cooled in air for 5s to simulate the heat loos during the blank transfer into the press. Samples were then deformed with the

hemispherical punch, kept at room temperature, with a ram speed of 20mm/s until fracture occurred and no lubricant at the sheet-punch interface was used in the experiments. The thermo-mechanical parameters utilized in the tests are summarized in Table 6.6.

Table 6.6 Thermal and mechanical parameters of the experimental test

Austenitization temp. [°C]	*Holding time [s]*	*Air cooling [s]*	*Punch temp. [°C]*	*Ram speed [mm/s]*
900	*180*	*5*	*25*	*20*

The temperature evolution during forming was measured by means of three thermocouples spot-welded in the area interested by deformation of the specimen and the strain field was monitored through the optical measurement system ARAMIS™.

6.3.2 Numerical simulation of the deformation phase

A 3D thermo-mechanical coupled simulation of the formability test was computed through the commercial FE code FORGE®. The symmetry of the case study model was taken into account in order to significantly reduce the computation time. The numerical model replicates the experimental setup described in § 5.2 and is made up of a punch, modelled as a deformable body, a die and a blank-holder, modelled as rigid bodies, and the workpiece, see Figure 6.14.

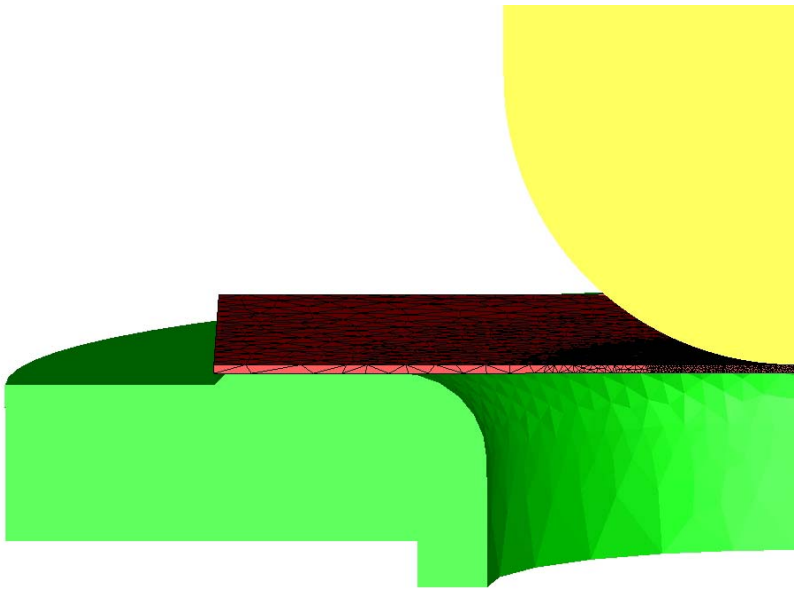

Figure 6.14 FE model of the experimental case study

The thermal and mechanical parameters of the material workpiece have been previously presented in § 6.2, that describes the calibration of the numerical model, and are afterwards summarized.
The workpiece rheological behaviour was described according to the Hansel-Spittel model (6.5), whose coefficients are reported in Table 6.7.

Table 6.7 Hansel-Spittel coefficients for 22MnB5 at elevated temperature

A	m_1	m_2	m_3	m_4	m_5	m_7	m_8	m_9
0.18151	-0.00465	0.35149	-0.02881	0.00281	-0.00179	0.13348	0.000020	1.7299

The interface conditions between workpiece and dies were implemented through a bilateral-sticking condition, in fact no material flow was observed in that zone during the experiments, whereas a Coulomb law (6.15) was used to describe friction between the workpiece and the punch, and the friction coefficient μ was set equal to 0.15.
A coupled thermo-mechanical simulation was carried out and the thermal parameters used for the workpiece and for the punch, made of W300, were chosen according to literature [13] and are summarized in the following tables:

Table 6.8 Thermal parameters for 22MnB5

Temperature [°C]	Conductivity [W/m K]	Specific heat [J/kg K]
20	46.1	377
100	46.1	477
200	44.8	511
400	39.8	590
600	34.3	741
800	26.4	821
1000	27.2	821

Table 6.9 Mechanical and thermal parameters for W300

Young's modulus [GPa]	Poisson's ratio	Density [kg/m^3]	Conductivity [W/m K)	Specific heat [J/kg K]
210	0.28	7800	23	461

The influence of contact pressure on the heat transfer coefficient evolution was taken into account by implementing in the FE model the results obtained from the inverse analysis,

see Figure 6.12. A liner interpolation was used to implement the HTC values between deformable bodies, as shown in Table 6.10.

Table 6.10 Heat transfer coefficient evolution with contact pressure

Contact pressure [MPa]	*5*	*10*	*20*	*30*	*40*
Heat transfer coefficient [W/m^{2}K]	*3650*	*4850*	*7000*	*8000*	*10500*

Dies temperature was assumed to be 25°C whereas the specimen temperature profile at the beginning of the deformation phase was measured during experiments by means of an infrared thermo-camera and implemented in the FE model as the initial thermal condition of the workpiece as shown in Figure 6.15.

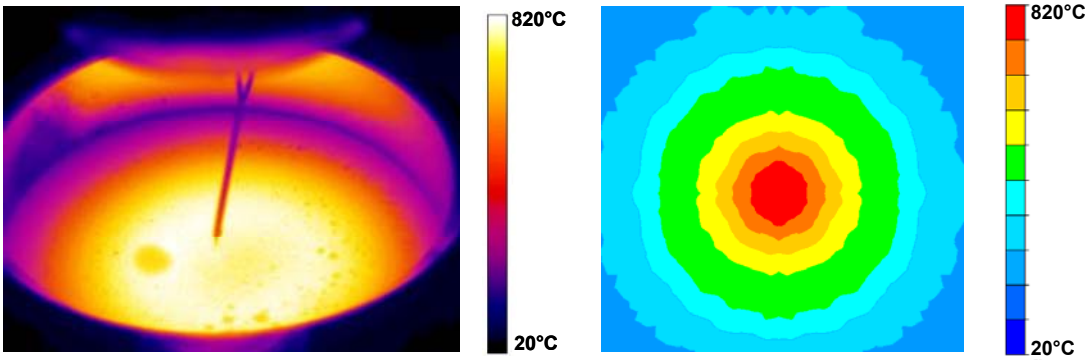

(a) (b)

Figure 6.15 Thermal field before deformation acquired through the thermo-camera (a) and implemented in the FE model (b)

Temperature evolution during simulation was monitored by means of sensors applied on the workpiece surface in correspondence of the thermocouples of the specimen used to perform the test.

6.3.3 Results and discussions

The results of the physical and numerical simulations have been compared in order to evaluate the reliability of the calibrated FE model implemented to simulate hot forming operations. In Figure 6.16 the comparison between the experimental and numerical force vs. stroke curves is displayed and it is possible to notice the good matching between the two curves.

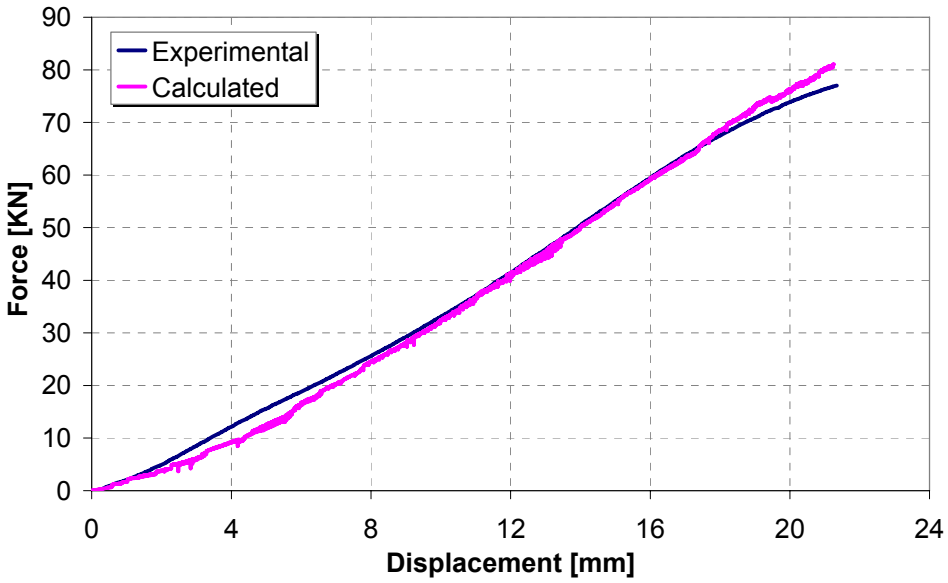

Figure 6.16 Experimental and numerical force vs. stroke curves of the deformation phase

It must be remark that, using this model, the comparison it is sensible only for the first part of the curve, where the force increase in correspondence of deformation before necking, in fact a calibrated fracture criterion should be implemented to correctly simulate also the sheet failure. Nevertheless the specimen strain distribution just before fracture, measured during the test by means of the ARAMIS™ optical system, shows a good agreement with the simulated strain field, as displayed in Figure 6.17, thus confirming the capability of the model to correctly predict the material flow behaviour

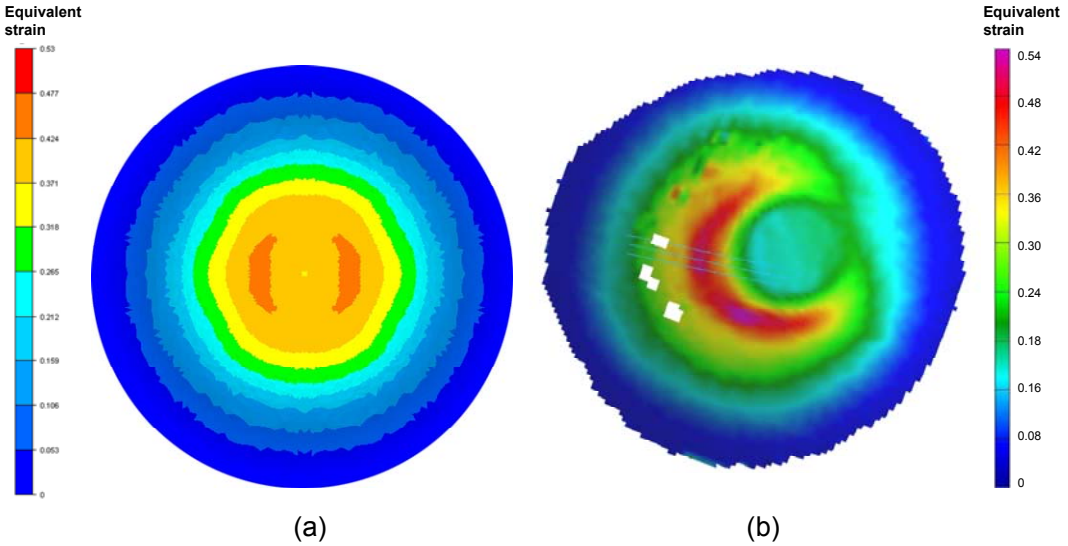

Figure 6.17 Calculated (a) and measured (b) equivalent strain field just before fracture

The experimental temperature evolution measured through the three thermocouples was finally compared with the thermal profiles of the coupled thermo-mechanical simulation, as shown in the following figures.

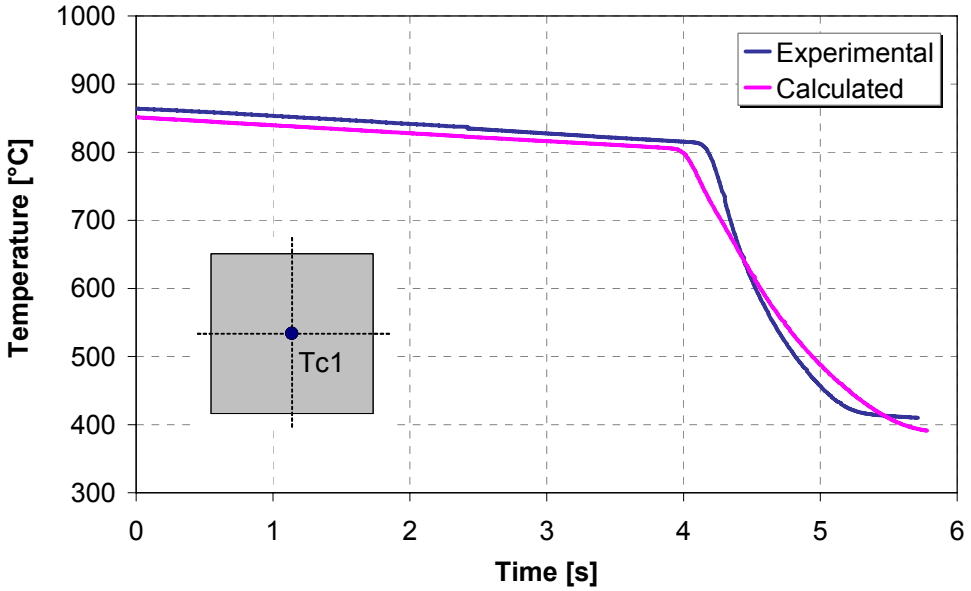

Figure 6.18 Experimental and numerical temperature evolution during deformation in correspondence of Tc1

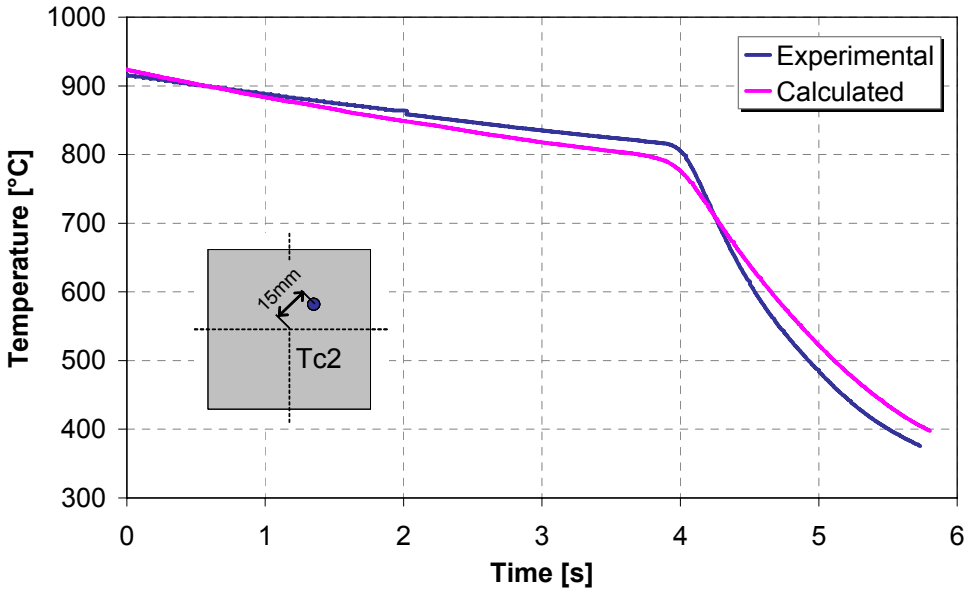

Figure 6.19 Experimental and numerical temperature evolution during deformation in correspondence of Tc2

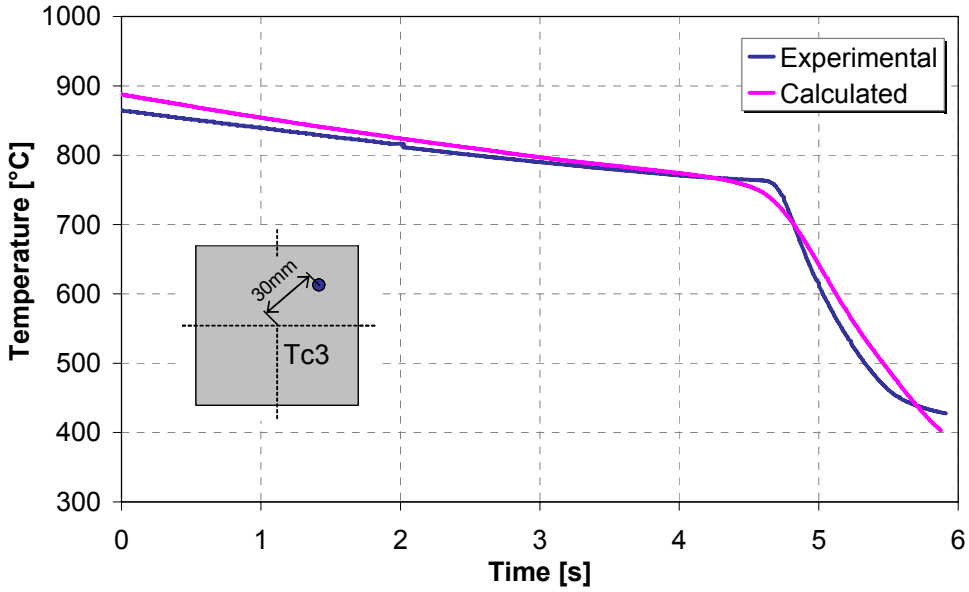

Figure 6.20 Experimental and numerical temperature evolution during deformation in correspondence of Tc3

The implemented and calibrated numerical model proved to be suitable to simulate both the mechanical and thermal events during hot forming operation with a great accuracy, nevertheless further investigation are necessary to validate the predictive capability of the model with regard to the microstructural evolution.

CHAPTER 7
CONCLUSIONS

Nowadays the hot stamping of high strength steels is proving to be a challenging technology gaining the strict requirements of automotive producers. The high formability and the reduced springback exhibited during deformation at elevated temperature, together with the controlled microstructural evolution during quenching are the main issues that make this process suitable to produce complex parts with reduced thickness maintaining crash and safety requirements, due to the enhanced strength-to-mass ratio.
However, compared to conventional sheet metal forming operation at room temperature, the optimization of press hardening process chains require a deep knowledge of both material behaviour and interface phenomena at high temperature. Furthermore, the correct design of the forming and the cooling phases involves the utilization of numerical simulation where a coupled thermo-mechanical-metallurgical model has to be properly implemented and calibrated.
In this PhD thesis, a new approach has been presented, focused on testing and modelling to analyze and correctly describe the different phenomena that affect material, process and product performance during and after the thermal, mechanical and microstructural events in hot stamping operations.
In particular, an experimental setup was designed and developed in order to determine the elasto-plastic properties of sheet metal at elevated temperature (e.g. flow curves, plastic anisotropy and Young's modulus evolution with temperature). This testing equipment was also modified to study the influence of applied stress and strain on the phase transformation kinetics together with the material transformation plasticity by means of an extensometric analysis.
A new testing procedure for the investigation of sheet formability, taking into account the microstructural aspects in hot stamping of high strength steels, was developed. An innovative experimental apparatus was designed according to the Nakazima concept, presenting an accurate methodology for the calibration of the phase transformation parameters and the temperature control during the test. This formability test acted as a physical simulation of the industrial press hardening process and, at the same time, it was used to determine forming limit curves at elevated temperature in isothermal conditions.
A numerical model capable to perform a coupled thermo-mechanical-metallurgical simulation of the hot stamping process was implemented in a commercial FE-code. The mechanical and microstructural properties of the Al-Si pre-coated quenchenable high strength steel 22MnB5 were determined by means of the experimental setups mentioned above and the heat transfer coefficient at the die-workpiece interface was evaluated by an

inverse analysis approach in order to properly calibrate such a model. Finally, the numerical model was validated through a comparison between a physical and a numerical simulation of a hot forming operation.

The developed approach can be considered general enough to characterize the thermal, mechanical and microstructural behaviour of high strength steels and to improve the quality of FE simulations and virtual process prototyping techniques when they are applied to analysis and design of the hot stamping process.

APPENDIX A

Ferritic/pearlitic transformation plasticity test curves

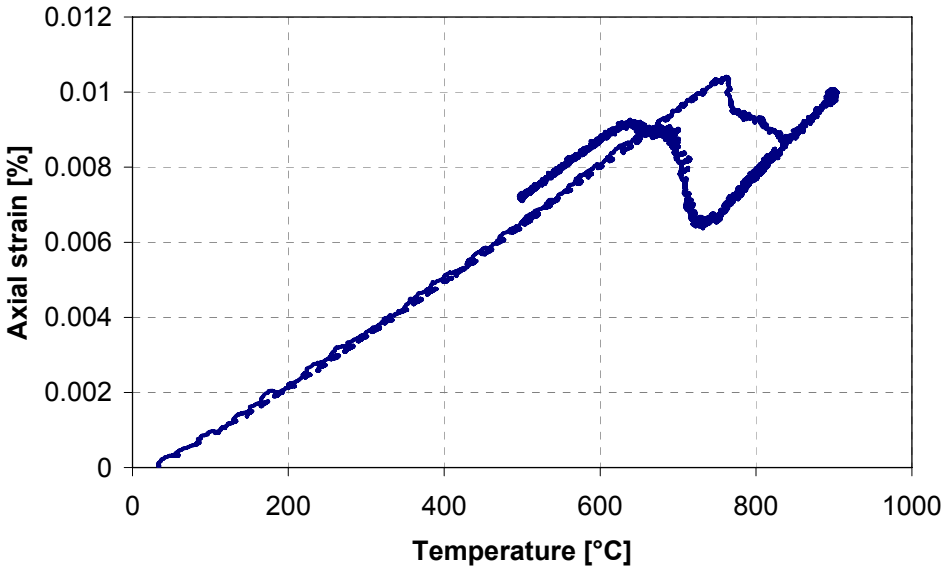

Figure A.1 Ferritic\pearlitic transformation plasticity test curve at 12.5 MPa

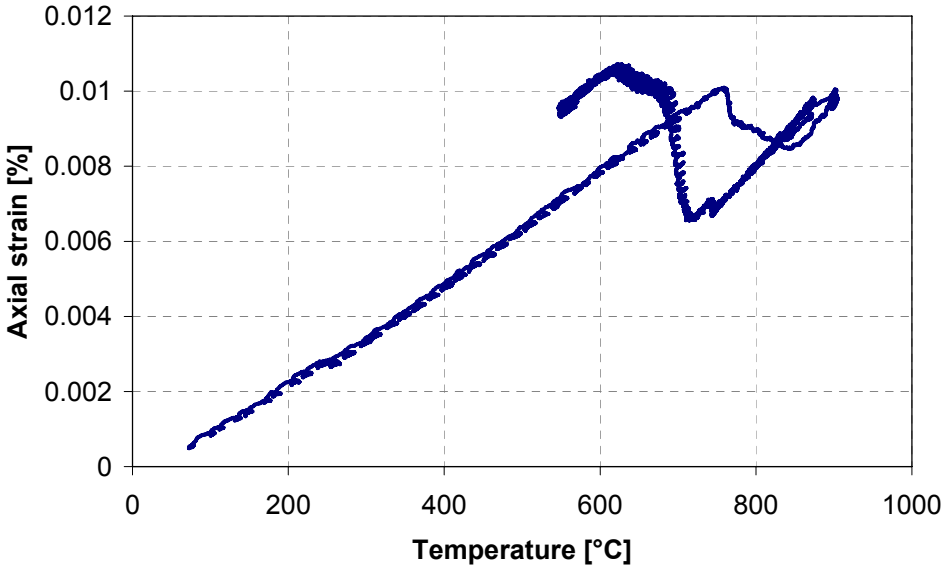

Figure A.2 Ferritic\pearlitic transformation plasticity test curve at 25 MPa

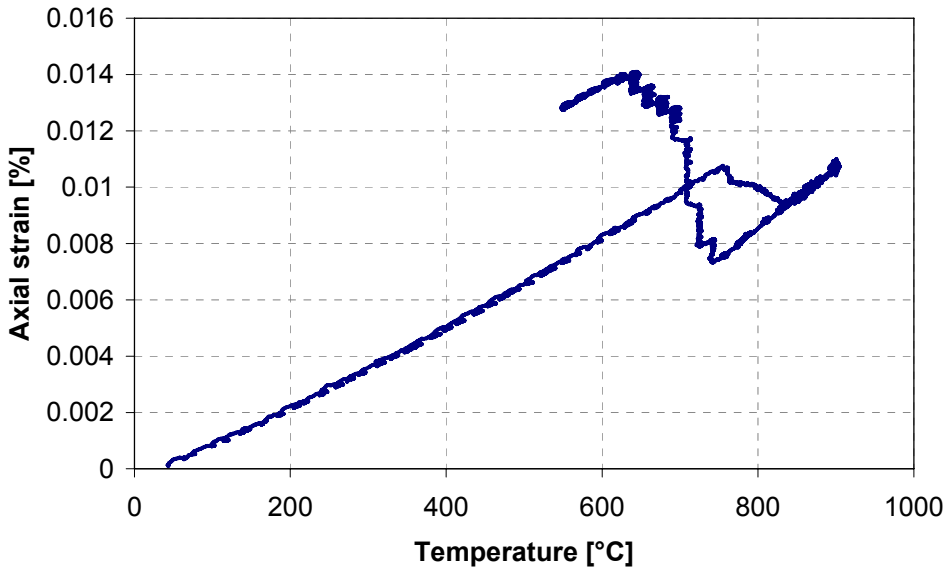

Figure A.3 Ferritic\pearlitic transformation plasticity test curve at 37.5 MPa

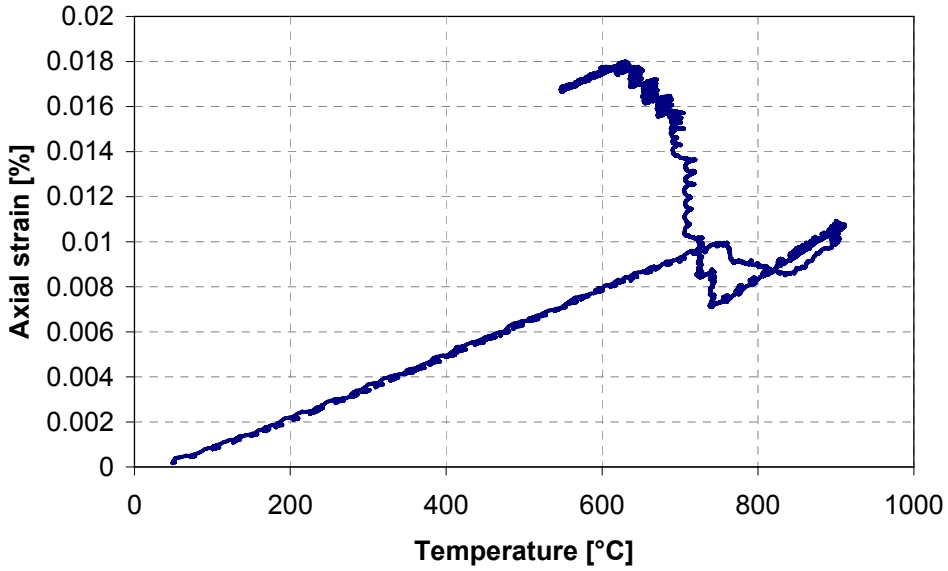

Figure A.4 Ferritic\pearlitic transformation plasticity test curve at 50 MPa

Bainitic transformation plasticity test curves

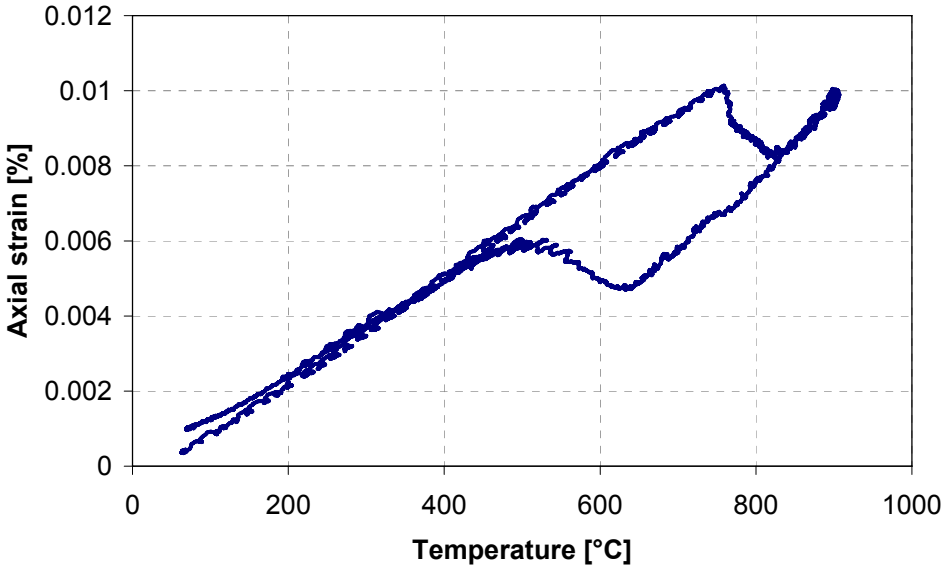

Figure A.5 Bainitic t transformation plasticity test curve at 12.5 MPa

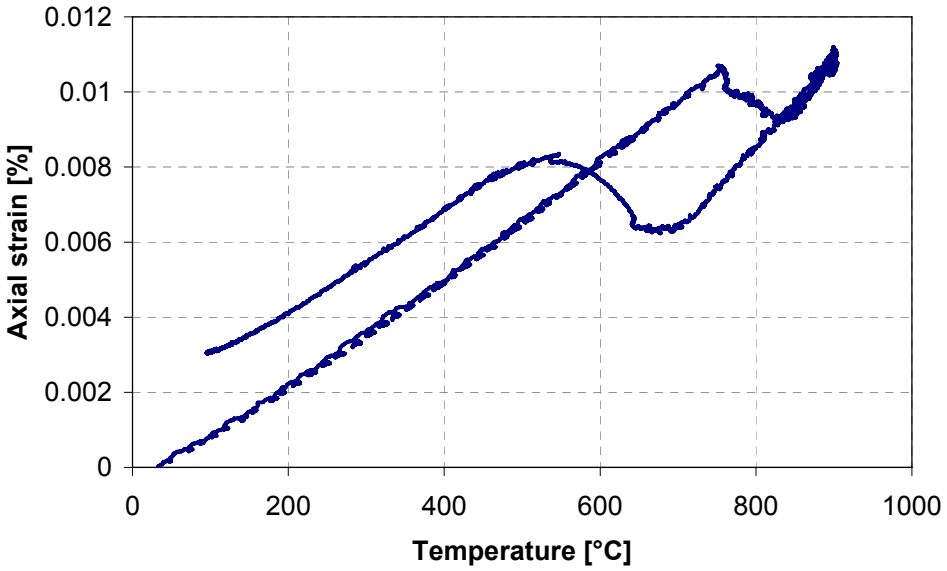

Figure A.6 Bainitic t transformation plasticity test curve at 25 MPa

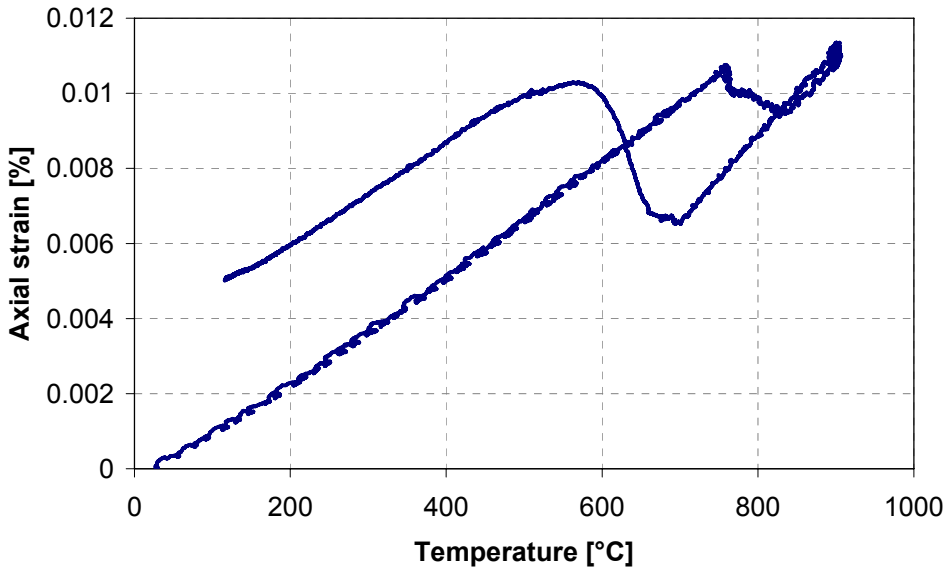

Figure A.7 Bainitic t transformation plasticity test curve at 37.5 MPa

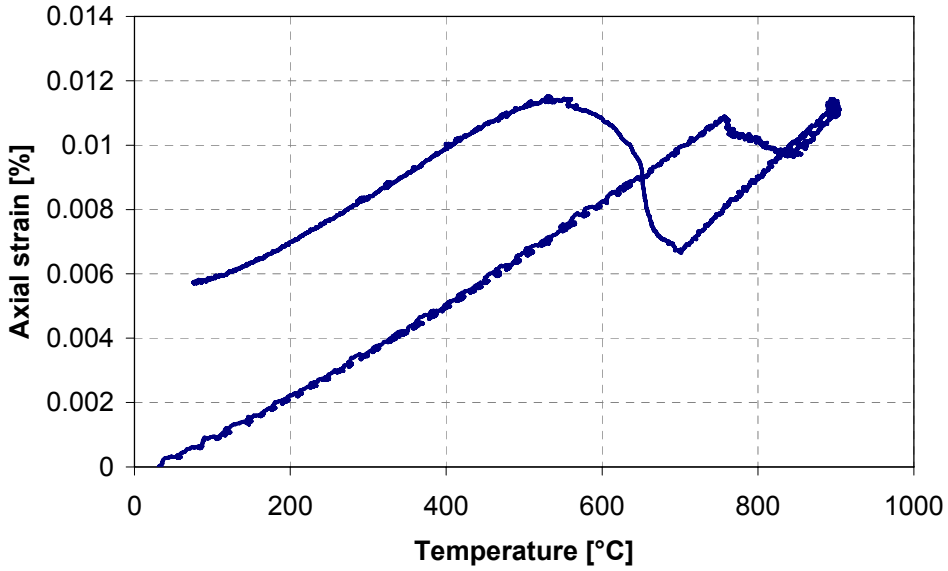

Figure A.8 Bainitic t transformation plasticity test curve at 50 MPa

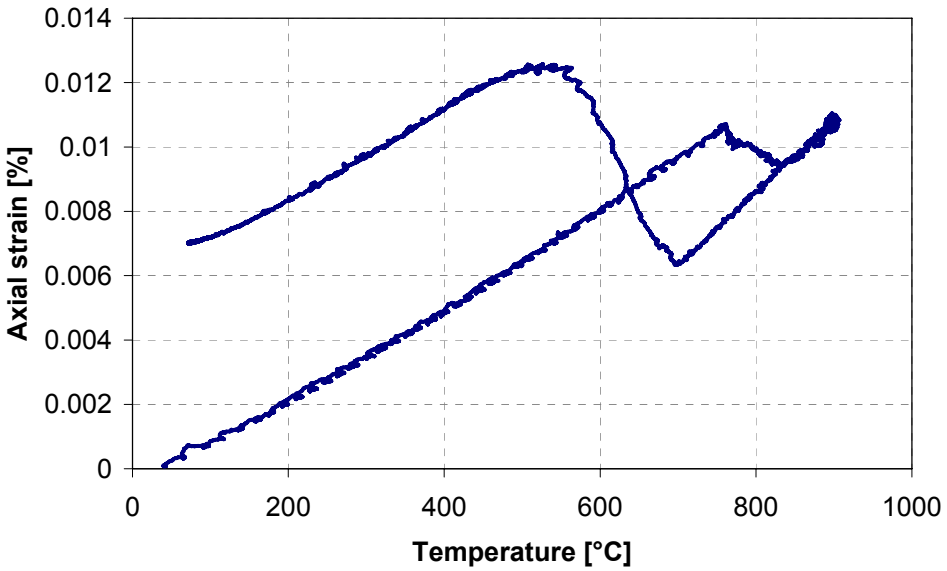

Figure A.9 Bainitic t transformation plasticity test curve at 62.5 MPa

Martensitic transformation plasticity test curves

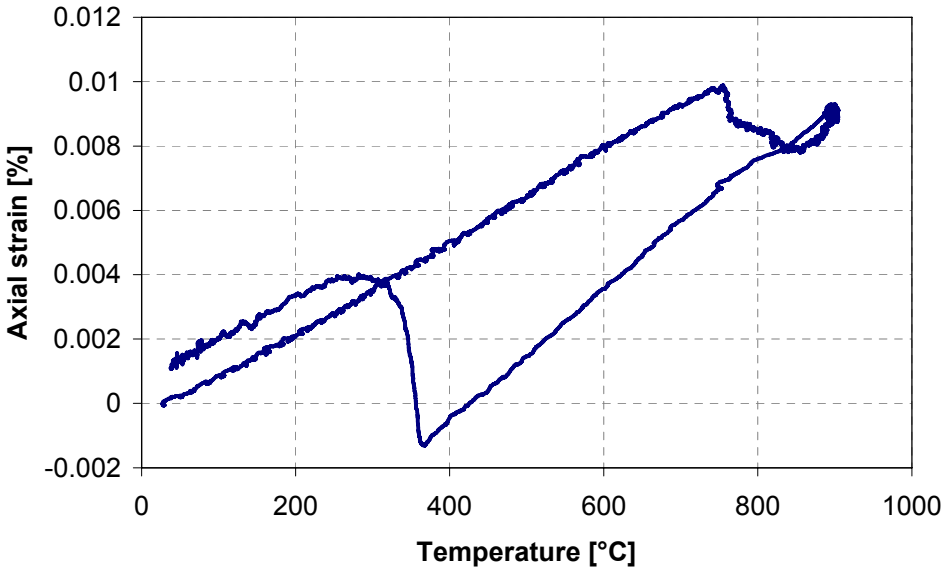

Figure A.10 Martensitic t transformation plasticity test curve at 12.5 MPa

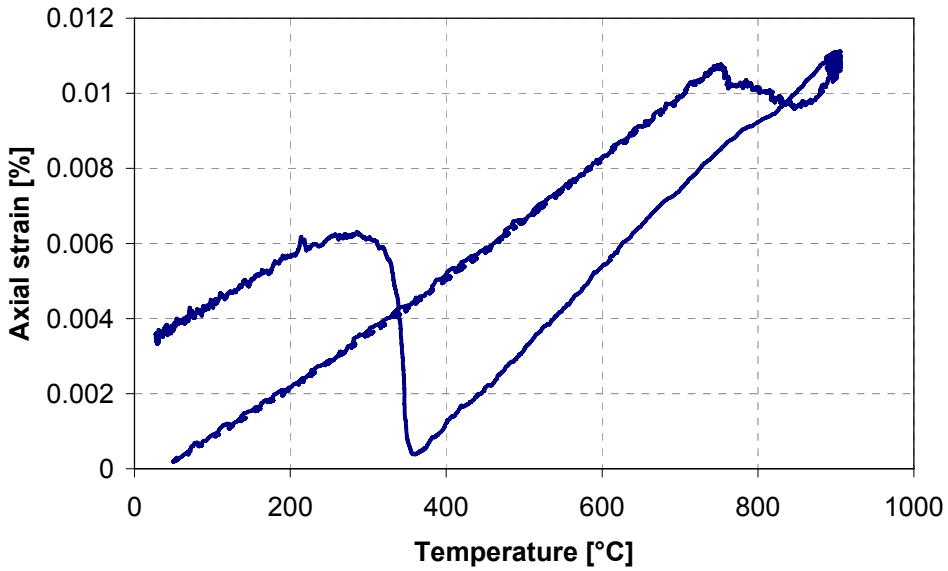

Figure A.11 Martensitic t transformation plasticity test curve at 25 MPa

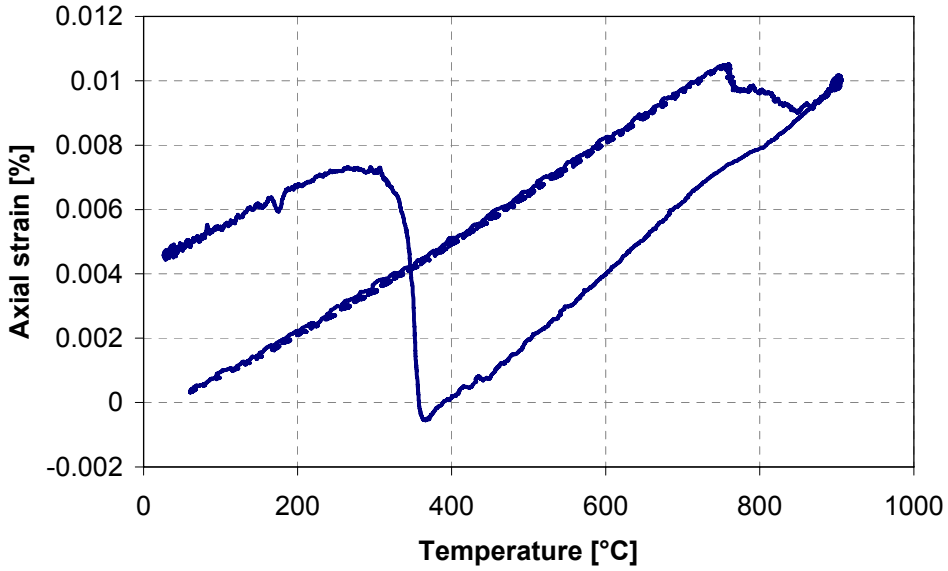

Figure A.12 Martensitic t transformation plasticity test curve at 50 MPa

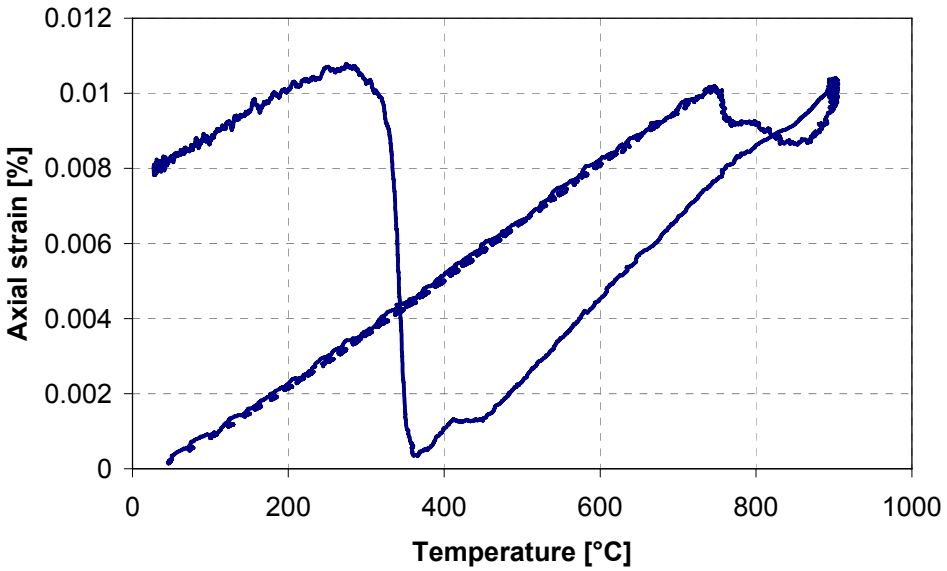

Figure A.13 Martensitic t transformation plasticity test curve at 75 MPa

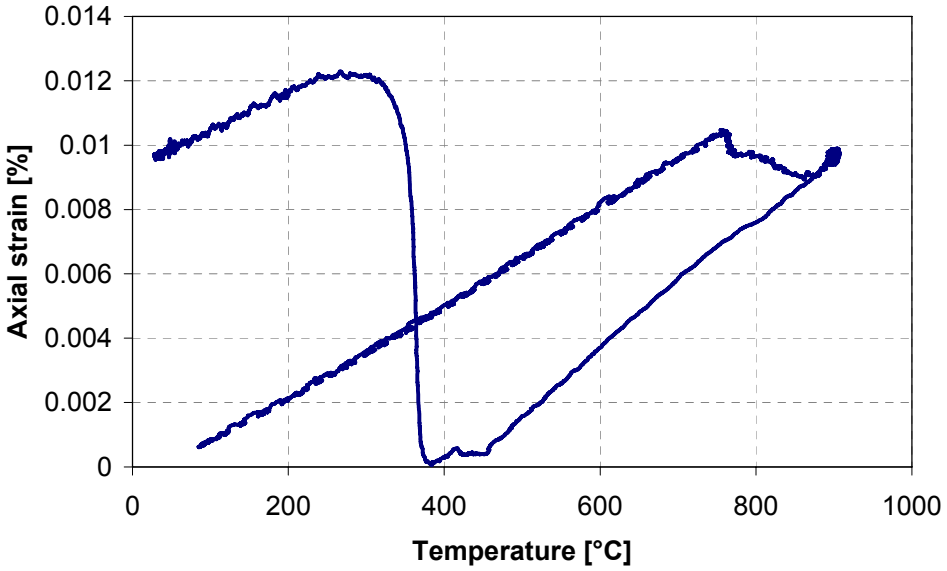

Figure A.14 Martensitic t transformation plasticity test curve at 100 MPa

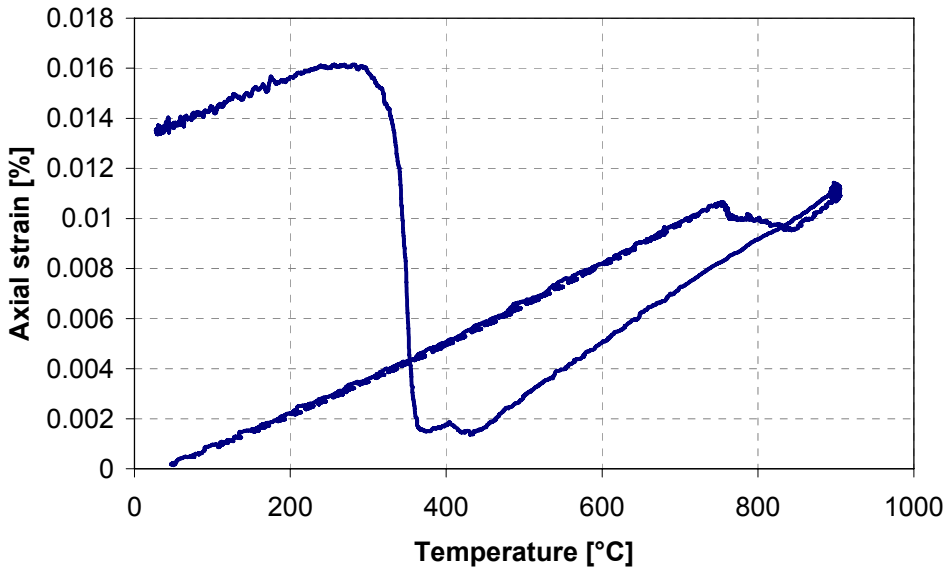

Figure A.15 Martensitic t transformation plasticity test curve at 125 MPa

APPENDIX B

Experimental and numerical temperature profiles

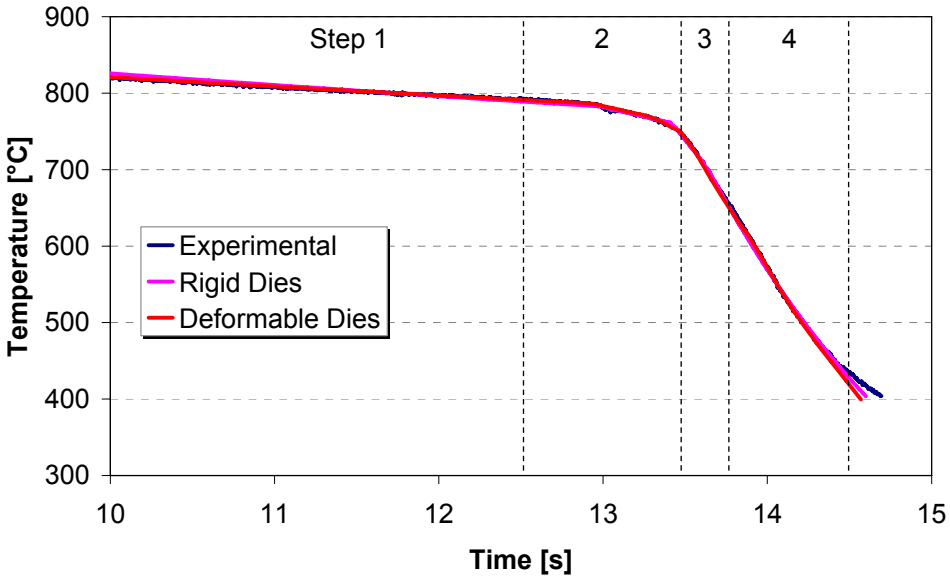

Figure B.1 Comparison between experimental and numerical temperature evolutions with a contact pressure of 5MPa

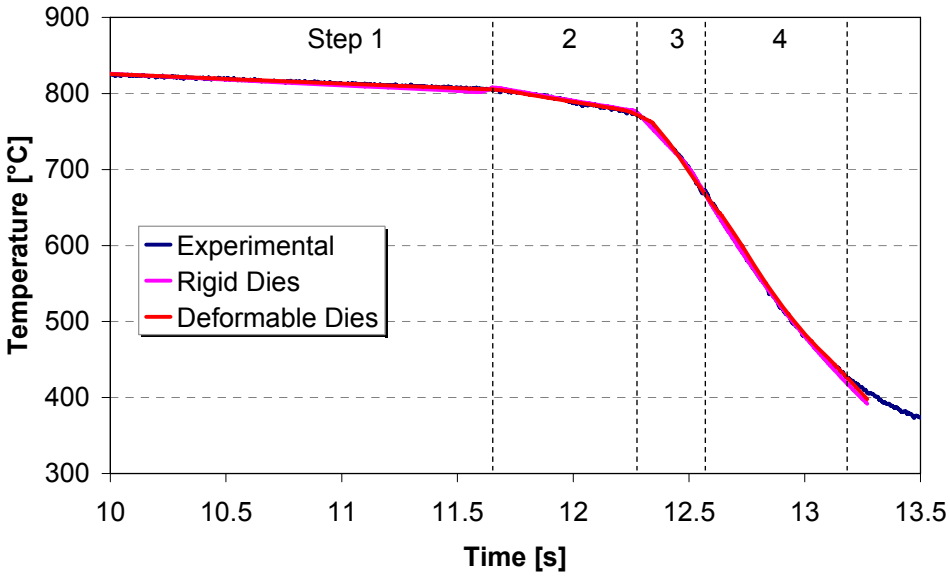

Figure B.2 Comparison between experimental and numerical temperature evolutions with a contact pressure of 10MPa

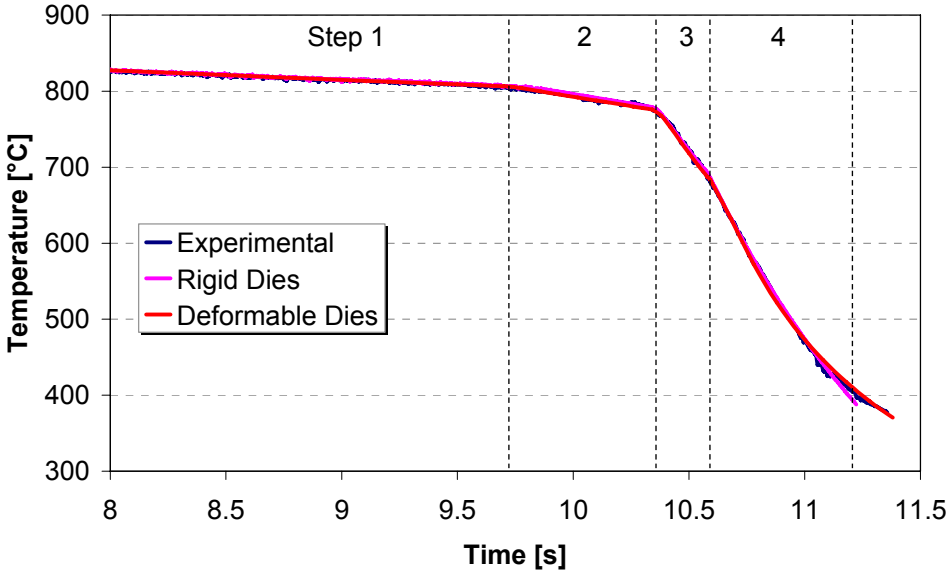

Figure B.3 Comparison between experimental and numerical temperature evolutions with a contact pressure of 20MPa

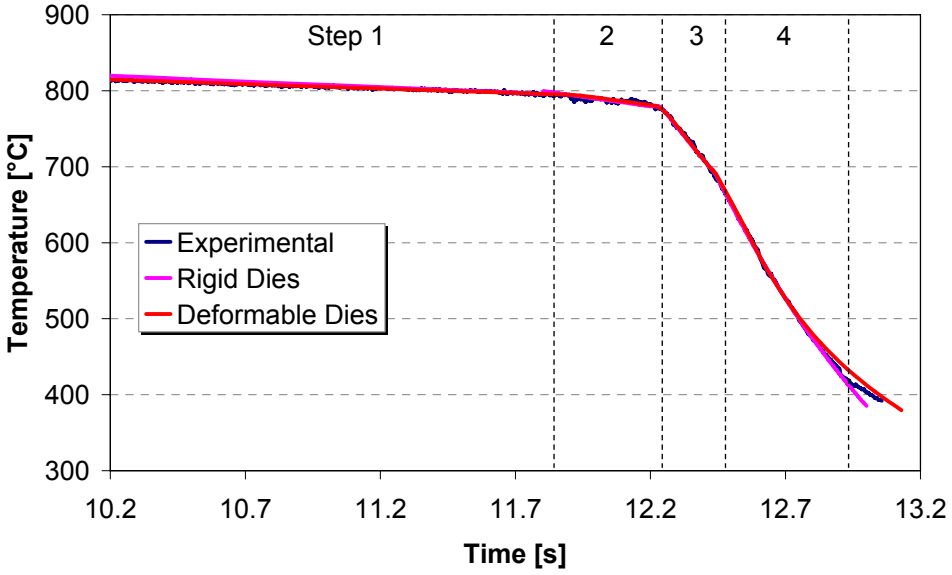

Figure B.4 Comparison between experimental and numerical temperature evolutions with a contact pressure of 30MPa

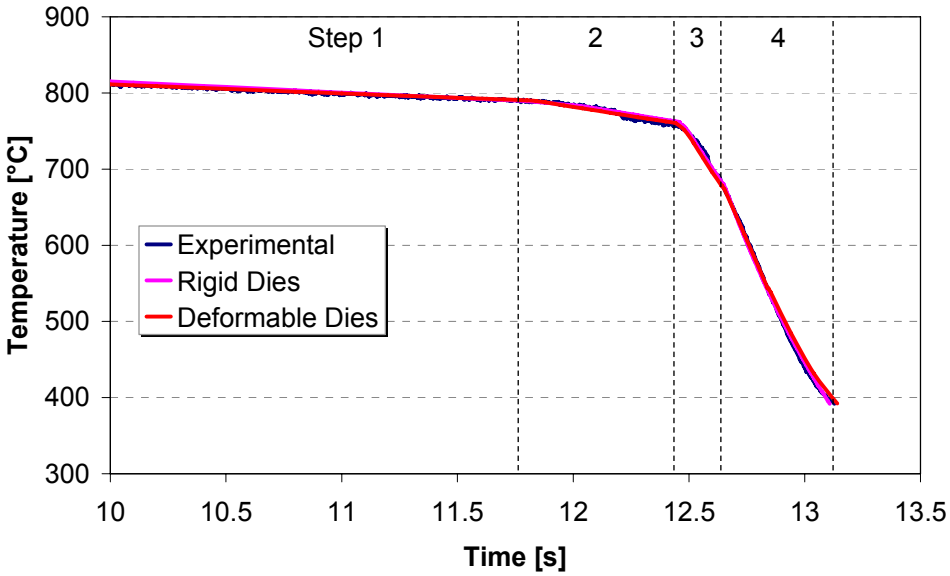

Figure B.5 Comparison between experimental and numerical temperature evolutions with a contact pressure of 40MPa

REFERENCES

[1] M.Merklein and J. Lechler, "Determination of Influencing Parameters of the Hot Stamping Process," presented at Proceedings Asia Steel Conference 2006.

[2] D.Lorenz and K. Roll, "Modelling and Analysis of Integrated Hot forming and quenching Processes," *Sheet Metal 2005 Conf.,Proc. (2005)*, pp. 787-794, 2005.

[3] *International Iron and Steel Institute, UltraLight Steel Auto Body - Advanced Vehicle Concepts (ULSAB-AVC) Overview Report (2002)*.

[4] J.Wilsius, P. Hein, and R. Kefferstein, "Status and future trends of hot stamping of USIBOR 1500 P," presented at Erlangen Workshop 2006.

[5] P.Hein, "A Global Approach of the Finite Element Simulation of Hot Stamping," *Sheet Metal 2005 Conf.,Proc. (2005)*, pp. 763-770, 2005.

[6] D.Lorenz and K. Roll, "Simulation of Hot Stamping and Quenching of Boron alloyed Steel.," presented at 7th Int. ESAFORM Conf. on Mat. Forming, Trondheim, Norway, 2004.

[7] P.F.Bariani, T. D. Negro, and S. Bruschi, "Testing and Modelling of Material Response to Deformation in Bulk Metal Forming," *Annals of the CIRP Vol. 53/2/2004 573-598*.

[8] R.Neugebauer, T. Altan, M. Geiger, M. Kleiner, and A. Sterzing, "Sheet metal forming at elevated temperature," *Annals of the CIRP*, vol. 55/2/2006, pp. 793-8166.

[9] "http://www.arcelor.com/."

[10] M.Merklein, J. Lechler, and M. Geiger, "Determination of Thermal and Mechanical Material Properties for Hot Stamping Processes of Ultra High Strength Steels," presented at Proceedings of the 2007 SAE International World Conference.

[11] L.G.Aranda, P. Ravier, and Y. Chastel, "Hot Stamping of Quenchable Steels: Material Data and process Simulations," *IDDRG 2003 Conf., Proc. (2003)*, pp. 166-164, 2003.

[12] P.Akerstrom, "Austenite decomposition during press hardening of a boron steel - Computer simulation test," *Journal of Materials Processing Technology*, vol. 174, pp. 399-406, 2006.

[13] H. S. H. Kim, S. Kang, S. Park, "Thermal-Mechanical coupled simulation of the forming of hot press formed part," presented at Proceedings of the IDDRG 2006 Conference.

[14] P.Akerstrom, G. Bergman, and M. Oldenburg, "Numerical implementation of a constitutive model for simulation of hot stamping," *Modelling and Simulation in Materials Science and Engineering*, vol. 15/2, pp. 105-119, 2007.

[15] M.Coret and A. Combescure, "A mesomodel for the numerical simulation of the multiphasic behavior of materials under anisothermal loading (application to two low-carbon steels)," *International Journal of Mechanical Sciences*, vol. 44/9, pp. 1947-1963, 2002.

[16] P.Akerstrom, B. Wikman, and M. Oldenburg, "Material parameter estimation for boron steel from simultaneous cooling and compression experiments," *Modelling and Simulation in Materials Science and Engineering*, vol. 13, pp. 1291-1308, 2005.

[17] L.G.Aranda, P. Ravier, and Y. Chastel, "Experimental, material data and numerical model for hot stamping of quenchable steels," *6th ESAFORM Conference on Material Forming*, 2003.

[18] M.Merklein and L. Lechler, "Investigation of the thermo-mechanical properties of hot stamping steels," *Journal of Materials Processing Technology*, vol. 117 (2006), pp. 452-455.

[19] L.Burkhardt and B. Oberpriller, "Sensitivity analysis of process and material parameters for the efficient simulation of hot forming," presented at Forming Technology Forum 2007, Zurich (Switzerland).

[20] J.G.Lenard, *Modeling hot deformation of steels*: Springer-Verlag, 1989.

[21] L.Anand, "Constitutive equations for the rate□dependent deformation of metals at elevated temperatures," *Journal of engineering materials and technology*, pp. 104/13, 1982.

[22] C.S.Hartley and R. Srinivasan, "Constitutive equations for large plastic deformation of metals," *Journal of engineering materials and technology*, vol. 105, pp. 162-167, 1983.

[23] J.C.Fisher and J. H. Hollomon, "Dislocation glide as an aid to precipitation at low temperatures," *Acta metallurgica*, vol. 3/6:608, 1955.

[24] E.Voce, "A practical strain-hardening function," *Acta metallurgica*, vol. 51, pp. 219-226, 1948.

[25] M.A.Meyers and K. K. Chawla, *Mechanical metallurgy □ Principles and applications*: Prentice-Hall, 1984.

[26] C.Aliaga, "Simulation numérique par éléments finis en 3D du comportment thermomécanique au couer du traitment thermique d'aciers: application à la trempe de pièces forgées ou coulées," in *L'école nationale supérieure des mines de Paris*, 2000.

[27] M.C.Somani, L. P. Karjalainen, M. Eriksson, and M. Oldenburg, "Dimensional Changes and Microstructural Evolution in a B-bearing Steel in the Simulated Forming and Quenching Process," *ISIL International*, vol. 41, pp. 361-367, 2001.

[28] S.H.Kang and Y. T. Im, "Three-dimensional thermal-elastic-plastic finite element modeling of quenching process of plain-carbon steel in couple with phase transformation," *International Journal of Mechanical Sciences*, vol. 49 (2007), pp. 423-439.

[29] M.Merklein, J. Lechler, and M. Geiger, "Characterisation of the Flow Properties of the Quenchenable Ultra High Strength Steel 22MnB5," presented at Annals of the CIRP Vol. 55/1/2006.

[30] W.Avrami, "Kinetics of Phase Change," *Journal of chem Physics*, vol. 7, pp. 1103-1112, 1939.

[31] W.A.Johnson and R. F. Mehl, "Reaction kinetics in process of nuceation and growth," *Trans. AIME*, vol. 135, pp. 416-458, 1939.

[32] E.Sheil, "Arch. Eisenhuttenwesen," vol. 12, 1935.

[33] D. P. Koinstinem and R. E. Marburger, "A general equation prescribing the extend of the austenite-martensite transformation and temperature evolution during quenching of steels," *Acta metallurgica*, vol. 7, pp. 59-60, 1950.

[34] B.A.Behrens, P. Olle, F. Schafer, and C. Schaffner, "Numerical simulation of microstructure evolution during the hot stamping process," presented at Proceedings of the IDDRG 2007 International Conference.

[35] C.L.Magee, "Transformation kinetics, microplasticity and agening of martensite in Fe-31-Ni." Pittsburgh: Carnegie Institute of Technologie University, 1966.

[36] G.W.Greenwoog and R.H.Johnson, "The deformation of metal under small stresses during phase transformations," *Proc. Royal Society*, vol. 283, pp. 403-422, 1965.

[37] S.Petit-Grostabussiat, L. Taleb, and J. F. Jullien, "Experimental Results on Classical plasticity of steels subjected to structural transformation," *Journal of Materials Processing Technology*, vol. 20 (2004), pp. 1371-1386, 2003.

[38] L.Taleb, N. Cavallo, and F. Waeckel, "Experimental analysis of transformation plasticity," *International Journal of Plasticity*, vol. 17, pp. 1-20, 2001.

[39] E.Gautier, A. Simon, and G. Beck, "Plasticite de transformation durant le transformation perlitique d'un acier eutectoide," *Acta metallurgica*, vol. 35, pp. 1367-1375, 1987.

[40] P.Akerstrom, "Modelling and Simulation of Hot Stamping," Lulea University of Technology, 2006.

[41] Z.Malinowsky, J. G. Lenards, and M. E. Davies, "A Study of the Heat Transfer Coefficient as a Function of Temperature and Pressure," *Journal of Materials Processing Technology*, vol. 42, pp. 125-142, 1994.

[42] P. R. Burte, Y. T. Im, T. Altan, and S. L. Semiation, "Measurement and Analysis of Heat Transfer and Friction during Hot Forging," *J. of Eng. for Ind.*, vol. 112, pp. 332-339.

[43] K.Lange, *Handbook of Metal Forming*: Mc Graw Hill.

[44] C.V.Madhusudana, *Thermal contact conductance*. Berlin: Springer.

[45] M.Croin, "MODELLING INTERACTIONS AMONG PRESS, TOOLS AND WORKPIECE IN HOT FORGING OPERATIONS," 2006.

[46] M.Geiger, M. Merklein, and C. Hoff, "Basic Investigation on the Hot Stamping Steel 22MnB5," *Sheet Metal 2005 Conference Proceedings (2005)*, pp. 795-802, 2005.

[47] K.Forstner, S. Strobich, and B. Buchmayr, "Heat transfer during press hardening," presented at Proceedings of the IDDRG 2007 International Conference.

[48] A.Tarantola, *Inverse problem theory*: Elsevier, 1987.

[49] J.P.Norton, *An introduction to Identification*. London: Ed. Academy Press, 1986.

[50] J.D.Coolins, G. C. Hart, T. K. Hassleman, and B. Kennedy, "Statistical identification of structures," *AAIA Joutnal*, vol. 12, pp. 185-190, 1974.

[51] J. V. Beck and K. J. Arnold, *Parameter estimation in Engineering and Science*: John Wiley & Sons, 1986.

[52] R.C.Mehta and T. Jayachandran, "Determination of Heat Transfer Coefficient using transient temperature response chart," *Warme und Stoffubertrangung*, vol. 26, pp. 1-5, 1990.

[53] A.Badrinarayanan, A. Constantinescu, and N. Zabras, "Preform in metal forming," presented at Proceedings of the 1995 Numiform Conference (Balkema).

[54] L.Fourment, T. Balan, and J. L. Chenot, "Shape optimal design in metal forming," presented at Proceeding of the 1995 Numiform Conference (Balkema).

[55] D.S.Schnur and N. Zabras, "An inverse method for determining elastic material properties and a material interface," *International Journal for Numerical Methods in Engineering*, vol. 33, pp. 2039-2057, 1992.

[56] C.Caillateaud and P. Pilvin, "Identification and inverse problem: a modular approach," presented at Winter annual meeting symposium on material parameter estimation for modern constructive equations, New Orleans, 1993.

[57] D.M.Bates and D. G. Watts, *Nonlinear regression Analysis and its Application*, 1988.

[58] P.E.Gill, W. Murray, and M. H. Wright, *Pratical Optimization*. London, 1981.

[59] W.J.Minkowycz, E. M. Sparrow, and G. E. Schneider, *Handbook of heat transfer*, 1988.

[60] D.A.Tortorelli and P. Michaleris, "Design sensiticity analysis: overview and review," *Inverse problem in Engineering 1*, pp. 71-105, 1991.

[61] S.P.Keller, "Circular grid system: A valuable aid for evaluation sheet forming," *Sheet Met. Ind.*, vol. 45, pp. 633-640, 1969.

[62] G.M.Goodwin, "Application of strin analysis to sheet metal forming problems," *Metall, Ital.*, vol. 60, pp. 767-771, 1968.

[63] R.Arrieux, J. M. Chalons, J. M. Bedrin, and M. Bovin, "Computer aided method for the determination of the FLD at necking," *Annals of the CIRP*, vol. 33/1, pp. 171-174, 1984.

[64] H.W.Swift, "Plastic instability under plane stress," *J. Mech. Phys. Solids 1*, pp. 1-18, 1952.

[65] R.Hill, "On discontinuus plastic states with special reference to localized neking in thin sheets," *J. Mech. Phys. Solids 1*, pp. 19-30, 1952.

[66] D.Banabic, H.-J. Bunge, K. Pohlandt, and A. E. Tekkaya, *Formability of Metallic Materials*: Berlin: Springer, 2000.

[67] D.Banabic, "Anisotropy and formability of AA5182-0 aluminium alloy sheets," presented at Annals of CIRP, 53, pp. 219-222, 2004.

[68] M.Geiger, G. V. d. Heyd, M. Merklein, and W. Hußnätter, "Novel concept of Experimental Setup for Characterisation of Plastic Yielding of Sheet Metal at Elevated Temperatures," *Advanced Materials Research*, vol. 6-8, pp. 657-664, 2005.

[69] Q.Q.Nie, D. Lee, and J. Matter, "The effect of strain rate sensitivity on history dependent forming limits of anisotropic sheet metals," *Journal of Material Shaping Technology*, vol. 9, pp. 233-240, 1991.

[70] Q.Situ, M. Bruhis, and M. Jain, "Obtaining Formability Characteristics Of Automotive Materials Using On-line Strain Imaging System," presented at Proceedings of the 6th International NUMISHEET Conference (2005).

[71] F.Barlat and A. B. D. Rocha, "Influence of danage on the plastic instability of sheet metals under complex strain paths," *J. Mater. Sci.*, vol. 19, pp. 4133-4137, 1984.

[72] V.Uthainsangsuk, U. Prahl, S. Munstermann, and W. Bleck, "Experimental and numerical failure criterion for formability prediction in sheet metal forming," *Computational Material Science*, 2007.

[73] W.Thomas, T. Oenoki, and T. Altan, "Process simulation in stamping - recent applications for product and process design," *International Journal of Materials Processing Technology*, vol. 98 (2000), pp. 232-243.

[74] M.Tolazzi and M. Merklein, "Inlfuence of Pre-forming on the Forming Limit Diagram of Aluminum and Steel Sheets," presented at Proceedings of the 2007 SHEMET Conference.

[75] M.Merklein and S. Beccari, "Influence of predeformation on the formability of aluminium alloys," presented at Proceeding of the 8th International Confernce on Technology of Plasticity, 2005, Verona (Italy).

[76] "Standard ISO 12004-2:1997, TC 164/SC 2."

[77] M.Geiger and M. Merklein, "Determination of forming limit diagrams – a new analysis method for characterization of materials´ formability," *Annals of the CIRP 52/1, 213*, 2003.

[78] H.Liebertz, A. Duwel, R. Illig, W. Hotz, S. Keller, A. Koehler, A. Kroeff, M. Merklein, J. Rauer, L. Staubwasser, G. Steinbeck, and H. Vegter, "Guideline for the determination of forming linit curves," presented at Proceedings of the IDDRG 2004 Conference.

[79] P.Hora, M. Merklein, L. Tong, and J. Lechler, "Numerical and experimental evaluation of thermal dependent FLC (FLC-T)," presented at Proceedings of the IDDRG 2007 International Conference.

[80] Y.Dahan, Y. Chastel, P. Duroux, P. Hein, E. Massoni, and J. Wilsius, "Formability investigations fot the hot stamping process," presented at Proceedings of the IDDRG 2006 International Conference.

[81] Y.Dahan, Y. Chastel, P. Duroux, J. Wlsius, P. Hein, and E. Massoni, "Procedure for the experimental determination of a forming limit curve for USIBOR 1500 P," presented at Proceedings of the IDDRG 2007 International Conference.

[82] "N.N.; ASTM 03.01."

[83] S.Petit-Grostabussiat, L. Taleb, and J. F. Jullien, "Experimental Results on Classical plasticity of steels subjected to structural transformation," *Journal of Materials Processing Technology*, vol. 20 (2004), pp. 1371-1386, 2004.

[84] A.S.Judlin-Denis, "Modèlisation des interactions contrainte-transformation de phase et calcul par èlèments finis de la gènère des contraintes internes au cours de la tempre des aciers," in *Institut National Polytechnique de Lorraine, France*, 2004.

[85] M.Coret, S. Calloch, and A. Combescure, "Experimental study of the phase transformation plasticity of 16MND5 low carbon steel induced by proportional and nonproportional biaxial loading paths," *European Journal of Mechanics A\Solid*, vol. 23 (2004), pp. 823-842, 2002.

[86] E.Lamm, "Advanced Steel Solutions for Automotive Lightweighting," *Windsor Workshop June 5, 2005*.

[87] S.Kobayashi, S. I. Oh, and T. Altan, *Metal Forming and Finite Element method*, 1989.